Final Report

Marshall-plan Stipendium

09.01.2018-15.08.2018

Vertragsnummer: 850

Supported Lipid Bilayer: A Novel Tool to Characterize the Plant Plasma Membrane

School of Chemical and Biomolecular Engineering, Cornell University, Ithaca, NY 14853, United States

Department for Nano biotechnology, University of Natural Resources and Life Sciences, Vienna, 1180, Austria

Stipendiant: Martin Stübler, MA. BSc

Cornell Betreuer: Univ. Prof. Dr. Susan Daniel

BOKU Betreuer: Univ. Prof. Dr. Erik Reimhult

Table of Content

..... - 2 -

1 Introduction ..... - 4 -

1.1 Background ..... - 4 -

1.2 Aim of this work ..... - 10 -

1.3 The proteolipid system ..... - 17 -

1.4 Characterization tools for SLBs ..... - 20 -

2 Materials and methods ..... - 22 -

2.1 Preparation of Protoplasts ..... - 22 -

2.1.1 Protoplast transformation of mesophyll cells ..... - 23 -

2.1.2 Transformation of Tobacco protoplasts ..... - 23 -

2.1.3 Transformation of *Arabidopsis thaliana* protoplasts ..... - 24 -

2.2 Production of Plasma membrane vesicles ..... - 24 -

2.2.1 Production of plasma membrane bubbles ..... - 24 -

2.2.2 Preparation of plasma membrane blebs ..... - 25 -

2.2.3 Production of membrane fraction ..... - 26 -

2.3 Characterization of plasma membrane vesicles ..... - 27 -

2.3.1 Characterization of bleb concentration size and charge ..... - 27 -

2.3.2 Cryo SEM Characterization ..... - 27 -

2.3.3 Characterization of protein expression by confocal microscopy ..... - 28 -

2.3.4 Protein expression in vesicles ..... - 28 -

2.3.5 Quartz crystal micro balance QCM-D ..... - 29 -

2.4 Formation of SLB's ..... - 30 -

2.4.1 Chip preparation ..... - 30 -

2.4.2 Preparation of liposomes ..... - 30 -

2.4.3 Supported lipid bilayer formation ..... - 31 -

2.5 Characterization of plant supported lipid bilayers (SLB's) ..... - 31 -

2.5.1 Fluorescent Recovery after Photo bleaching FRAP ..... - 31 -

2.5.2 Single protein tracking in SLB ..... - 32 -

2.5.3 Plants and growth conditions: ..... - 33 -

3 Results and discussion ..... - 34 -
3.1 Protoplast generation ..... - 34 -
3.2 Production of Bubbles ..... - 35 -
3.3 Production of Blebs ..... - 37 -
3.4 Production of membrane fraction ..... - 38 -
3.5 Characterization of PM-vesicles ..... - 38 -
3.6 Scanning electron microscopy (SEM) ..... - 41 -
3.6.1 BUBBLES: ..... - 41 -
3.6.2 BLEBS: ..... - 42 -
3.7 Characterization of protein expression in cells ..... - 43 -
3.8 Quartz crystal microbalance ..... - 45 -
3.9 Characterization of SLBs using FRAP ..... - 49 -
3.10 Characterization of protein orientation in SLB ..... - 56 -
3.11 Single protein tracking in SLBs ..... - 60 -
4 Conclusions and Implications ..... - 67 -
4.1 Future perspective: ..... - 69 -
4.2 Acknowledgements ..... - 70 -
5 References ..... - 71 -
6 APPENDIX A: LIST OF ACRONYMS ..... - 82 -
7 List of figures ..... - 83 -
8 List of tables ..... - 86 -

1 Introduction

1.1 Background

Plants as sessile phototropic organisms have provided humans with food, shelter, clothing and beneficial substances for many centuries (Petrovska, 2012). The oldest written evidence of medicinal plants usage for preparation of drugs has been found on a Sumerian clay slab from Nagpur, approximately 5000 years old (Kelly, 2009). The Neolithic revolution featured by a transition from hunting and gathering to farming approximately 10 000 years ago (Svizzero & Tisdell 2014) changed the livelihood of mankind forever, as well as landscape of our planet. Plants have undergone a coevolution with humanity since the domestication of the first einkorn 12 000 years ago (Harlan 1971) and since then provided the material surplus to allow a diversification into different Neolithic social institutions necessary for the development of culture (Fuller & Grandjean 2001).

Agriculture is still the major impact factor on livelihood-systems in developing countries with a high socioeconomic-impact of harvest loss or droughts. Especially in the Middle East, Southeast Asia and Sub-Saharan-Africa (SSA) where livelihood systems are often built upon agriculture. In these countries the improvement of agriculture is directly affecting the lives of millions of people. Almost three quarters of a century ago, the League of Nations recognized the importance of agricultural development for dietary diversification for developing countries to improve nutritional benefits (Jones & Ejeta 2016).

One important step towards this goal was achieved by patent 235.421 which was filed by Fritz Haber more than a century ago. He developed a process for ammonia fixation from its components (Smil 1999). This process also known as the Haber&Bosch process used to produce ammonia a nitrogen fertilizer essential for plant growth had the biggest influence on human agriculture since the Neolithic revolution and lead to a global population explosion at the beginning of the 20th century (Erisman et al. 2008). As this rapid development is exclusively based on nonrenewable resources it should be our common interest to transition into a sustainable agriculture able to feed the world without wearing out our resources. But not only nitrogen also phosphorus and potassium are considered macronutrients for plant development and as such almost directly proportional to crop yield and harvestable biomass.

Developed countries with access to oil resources have improved yields for staple crops by 50% and therefore solved most of their agricultural problems at the beginning of last centuries whereas countries with less access to resources were almost excluded from this development.
To improve agriculture and quality of life in these areas it is essential to deal with multi-factorial aspects of plant resistance against biotic and abiotic factors, plant nutrient uptake efficiency and post-harvest stability. Plants as sessile organisms, need to adapt constantly to a dynamic environment in order to supply their needs and fend off pathogens and pests. To understand these complex signaling cascades in biological membranes, *in vivo* assays have been predominantly used (Martiniere et al. 2012).

At the beginning of the green revolution, crop yield and pest resistance was improved by the application of genetic engineering to major cash crops, such as soy bean, corn, cotton and canola (Tilman 1998). Most of these improvements can be attributed to the insertion of a resistance gene and the availability of high-throughput screening for genetic markers. Whereas plant genomic technologies have seen rapid development over the past two decades a lack of access to plant phenotyping techniques limits our abilities of analyze the effects of genetic changes on phenotypical traits (Li et al. 2014). Analysis and quantification of macroscopic traits via image analysis and machine learning has seen big improvements over the last decade. Nowadays multiple traits such as height, dry mass, growth type as well as nutrient content, level of secondary plant components can be analyzed via high-throughput screening and image analysis (Li et al. 2014). These traits are essential for plant breeding and provide important insights for choosing crossing partners and selecting for specific breeding goals. The availability of these detection methods has major influence on the selection process as it is only possible to select for quantifiable breeding goals. Especially on the microscopic level breeders as well as biologists are simply lacking options to quantify results. Plant biology has made big leaps forward by the improvement of optical microscopy, e.g. fluorescence microscopy, essential to unveil the complex hierarchical structure of plant organs. Microscopy offers fundamental insights into plant physiological aspects such as the development of new shoots, root growth, pathogen entry and the veins system containing xylem and phloem.
Additional insights can be gained when looking deeper into the sub-cellular processes of plant cells. Observations at the sub-cellular level can help answer various

biologically relevant questions such as transport phenomena, protein modifications, cell growth and recycling processes. Another very interesting topic are all the different biological membranes present in a cell.

As almost every biological process aims to produce a gradient across a membrane, it is not surprising that the examination of membranes was always a central aspect of biology. The cell plasma membrane (PM) as the most diverse and multifunctional membrane (Simons & Toomre 2000; Gamper & Shapiro 2007) encapsulates the cell cytosol and organelles and plays a crucial role in all interactions with the external environment. The native lipid-to-protein mass ratio for the plant PM is approximately 1:1 (Angus S. Murphy, Wendy Peer 2011). However, taking into account that the molar mass of a lipid molecule is far below the average protein molecular mass, the lipid-to-protein molar ratio in the plant PM ranges around 75:1. The lipid-to-protein molar ratio is influencing protein function and influencing signal transduction as well as membrane-bound enzyme activities (Hsia et al. 2015) which makes it an interesting target to study.
This semipermeable barrier is involved in signal recognition and transduction, intracellular responses as well as environmental responses and developmental signaling (Simons & Toomre 2000; Gamper & Shapiro 2007). But also the selectively permeable barrier for the specific uptake of required macromolecules and solutes and the blocking of other unwanted components (Mengel & Kirkby 2001). The study of mammalian membranes is facilitated by the fact that they are not covered by a peptidoglycan cell wall (CW) like plant cells are. The existence of the CW poses a big challenge for all surface based characterization techniques. Surface based characterization techniques developed rapidly over the last. Traditional characterization techniques for lipid-protein interaction are often using detergents to extract membrane proteins, protein function as well as the native lipid-protein association (Seddon et al. 2004; Helenius & Simons 1975). Or they suffer from difficulties to isolate single events from background events in the surrounding structure (Martiniere et al. 2012). Proteins are regulated by a complex cascade of protein – protein and lipid – protein interactions in various ways (Rajendran 2005; Lee 2004).

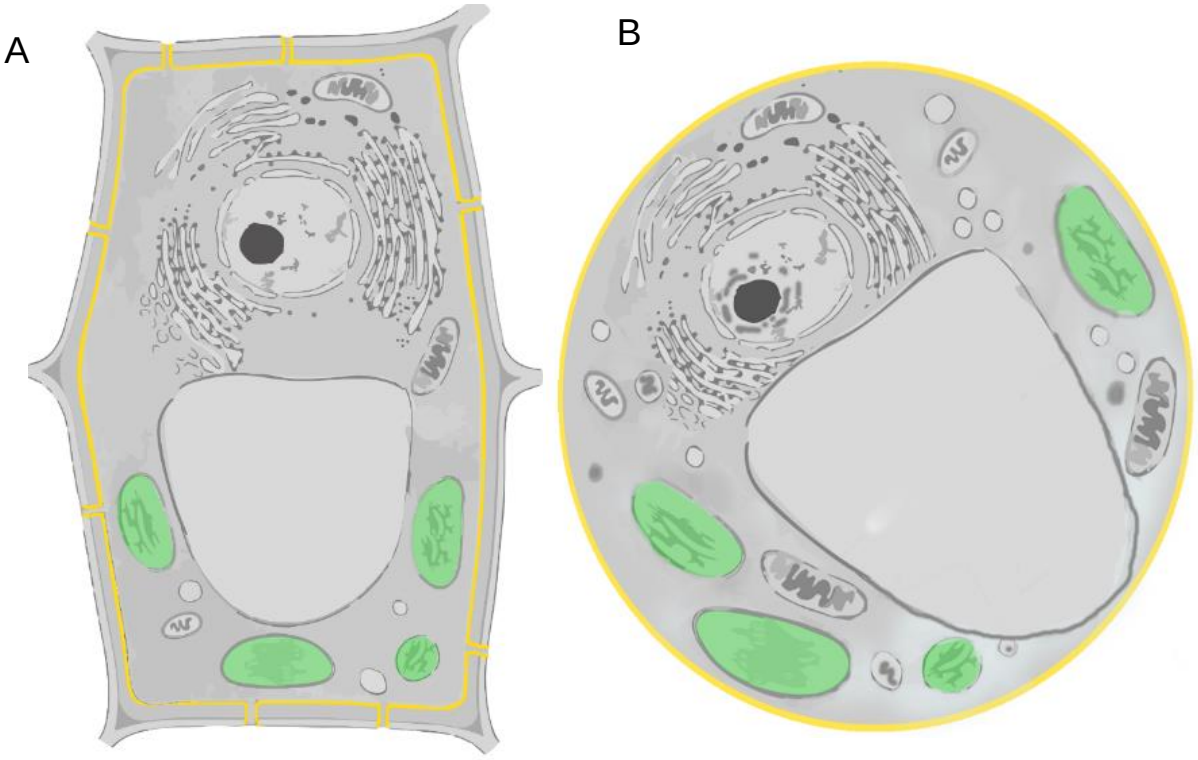

Figure 1: (A) plant cell with CW showing the membrane of interest in false color yellow and the chloroplasts in green. The ducts interconnecting all cytoplasts are shown in yellow. There are several thousand such ducts interconnecting all individual cells. (B) Healthy chloroplast after cell wall digestion and closing of the plasmodesmata. Depicted right after the digestion and before the centrifugation step. The chloroplasts are moved to one side of the cell during centrifugation due to the centrifugal force.

A lot of emphasis was put on the physiological characterization of plant membranes as the main gates of entrance for nutrients. Plants naturally grow in a suboptimal environment providing excess of some nutrients that negatively affect the plant growth (Al, Fe, Se) and a short supply for other nutrients that are usually the growth limiting factors called macro nutrients (N, P, K). Until now many relevant transporters and ion channels responsible to take up or block the entrance of wanted nutrients and unwanted toxins have been identified. But despite the fact, that these protein families are known for decades we are still unable to understand their function to the extent that we could improve plant yields based on their subcellular properties. Actions have been taken to monitor these structures in their native environment: the whole cell. The clear advantage of these cell-based assays is the preservation of the native structures such as the presence of the cell wall and structural hierarchy; however, this advantage when working with total cells is also its biggest disadvantage. The isolation and measurement of individual factors in a system of still unknown complexity and dynamism makes such assays inconvenient, error prone

and often not reproducible. Also the accessibility with electrophysiological characterization tools is very limited for whole plant experiments whereas the accessibility of a planar platform could solve this problem by simply placing a membrane on a solid conductive surface and measuring the changes based on the ion channel activity.

The plants ability to adapt to different environmental temperatures also involves major changes in the PM structure. Warm-blooded animals such as mammals are operating at a constant temperature not requiring specific adaptations to the changing environment. Plants as a species on the other hand are surviving temperature fluctuations of almost 100° C ranging from -40° C in the Siberian tundra to + 60° C for desert areas which is only possible for full plants and not isolated cells. Especially well known is the adaptability of succulents to tolerate extreme temperature. These plants have developed fascinating ways to adapt their lipid composition according to the environmental conditions to maintain perfect membrane fluidity. Understanding temperature impact on plant growth can only be partially achieved by analyzing membrane fractions for their total lipid composition. A new tool is needed to monitor the behavior and hierarchy of temperature effects directly at the plant PM.

Besides harsh abiotic environmental conditions multiple pathogens such as enveloped plant viruses are also targeting plants through the PM. Fusion studies for Ebola and H3N2 viruses have unveiled important insights into the function of the spike protein during the process of entrance (Hsu et al. 2016). Due to the lack of an appropriate platform it has never been tried to study the fusion behavior of plant viruses with plant membranes despite its economic importance. Such investigations could help breed more resistant crop plants by gaining a deeper understanding for the entrance mechanism of each virus.

Another interesting field would be the host-pathogen membrane fusion studies. For human pathogens (Ebola and Zika virus) microfluidic devices combined with SLBs and TIRF microscopy were providing a powerful tool to capture the complexity of the cell membrane with the reproducibility of a microfluidic device (Costello et al. 2013). This study focused on human viruses but the method is applicable to all enveloped viruses, such as the Tomato spotted wilt virus ranked as the second most important plant virus (Scholthof et al. 2011).

Tomato spotted wilt virus (TSWV) (Zhang et al. 2012) and Tospoviruses for example are enveloped virions that encapsulates ssRNA genome segments that have helical symmetry and are covered in nucleocapsid protein. All enveloped plant viruses are transmitted in a circulative, persistent-propagative manner by small pests such as trips, aphids or other insects (Whitfield et al. 2005). The molecular plant pathology review determined the 10 most important plant viruses based on scientific/ Economic importance. Ranked number one the Tobacco mosaic virus a non-enveloped virus and the most important plant virus followed by the Tomato spotted wilt virus ranked two which is therefore the most important enveloped plant virus (Scholthof et al. 2011). Despite its economic importance there has never been a fusion study of virions and plant membrane. For fusion studies of these enveloped plant viruses a plant SLB would provide a useful tool. SLBs could provide the first opportunity to conduct host-pathogen fusion studies to better understand this important plant virus strain. But to understand the interaction between enveloped plant viruses and the plant PM better it is important to take a look at the composition of the plant-PM (PPM). Even more importantly for plant physiology is the characterization of proteins for signaling and transport such as Ion channels this field of the electrochemical is currently rapidly developing. Ion channels are transmembrane proteins embedded in the PPM see *Figure 2* and responsible for transmembrane transport. The latest field is especially successful in providing a platform for studying transport phenomena of ion channels during nutrient uptake. Environmental stresses can cause significant subcellular restructuring of plant cell organelles and a better knowledge of the PM would help in developing strategies to increase plants' natural defense mechanisms (Komatsu et al. 2007).
Despite the importance of the PM various factors are disadvantageous when studying the PM directly in its native state. First, the signal to noise ratio is not good enough due to its limited accessibility from the exoplasmic space. Second, the curved geometry is unfavorable for planar surface characterization techniques that require precise control over the surface geometry. Finally, the composition can't be controlled; it varies both as consequence of the fluctuating conditions during reconstitution processes and by the biological variance when directly expressed in the host cell. The reconstitution process refers to the artificial integrating a certain compound, usually a polypeptide into a membrane. Therefore several systems have been developed and optimized over the past decades to investigate the cell PM.

1.2 Aim of this work

To fill this vacuum regarding methods to properly address important plant biology questions on the sub-cellular level, with the aim also to further improve life-sustaining plant breeding, the aim of this thesis is to develop a novel platform by which the properties of the plant plasma membrane can be studied in detail. This platform should allow for investigations of membrane processes using surface-sensitive and optical microscopy techniques without the impeding influence of the cell wall or reconstitution agents. These aims imply that the missing link is the creation of a supported lipid bilayer version of the plant PM, through which plant membrane processes can be investigated on the level of molecular interactions in membranes derived from native plant plasma membranes in a defined geometry.

Several steps need to be achieved to obtain a fully functional plant PM mimetic platform for cell-free membrane characterization. First and foremost the plant cell is enclosed by the cell wall, which has to be removed. After this step the generated cell wall free plant cells, so called protoplasts should be purified from the cell wall debris. Thereafter we aim to produce PM-proteoliposomes representing miniature versions of plant cells. These vesicles will be used for self-assembly on a glass (silicon oxide) slide on which lipid vesicles are known to rupture them to form a supported lipid bilayer (SLB) by addition of fusogenic rupture vesicles. Such SLB derived from plant PM constituents will combine the two sought after major advantages of being as close to the native plant PM as currently possible while providing a planar 2D geometry accessible with standard state-of-the-art surface characterization tools. Finally, the functionality of the plant PM-SLB will be tested by surface characterization tools on transmembrane proteins RCI2A, Pin1, Pip2A and SbMATE proteins which are involved in a variety of biological process such as Auxin signaling (Leyser 2017) aluminum transport and cold response.

Nowadays the urge to understand these subcellular transport and response processes is more pressing than ever. As these processes can lead to important insights into nutrient uptake and stress response. The interest in the function of membrane proteins has grown rapidly to bridge the gap between structure and gene. Neher and Sakmann developed the patch clamp technique in the 1970s and early 1980s to study the function of ion channels for the first time. This novel approach lead to the Nobel Prize in Physiology and Medicine in 1991. A patch clamp set up is trying to isolate a single

membrane protein and measure its electrophysiological properties. This set up involves a hollow glass tube (patch pipette, reference electrode a working electrode and counter electrode connected to an amplifier. The patch electrode and the recording electrode are brought into contact with an isolated cell whereas the ground electrode is placed in the surrounding buffer. The patch pipette is put under negative pressure to gently attach to the cell and create an electrical circuit between the recording and reference electrode with the cell of interest in between. The cell membrane creates a high resistant seal between them. The pipette tip is used to enclose or “patch” a PM surface area that should contain only one or a few transport proteins. This very tedious setup could be substituted by a SLB on a conductive polymer measuring two important properties simultaneously. First the movement of the ion channel in the 2D plane and secondly the transport activity. The transport of ions is measured by amplifying the change of the electromagnetic potential above and below the membrane.

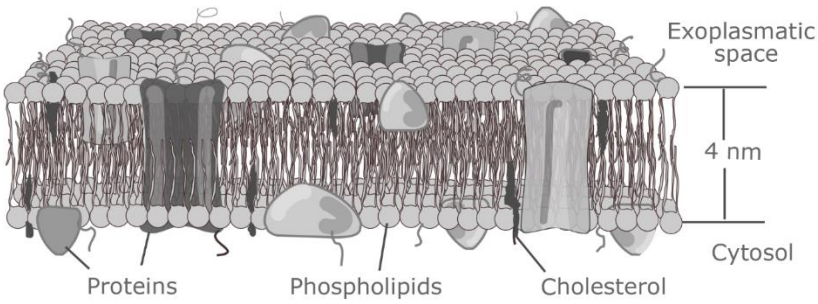

Figure 2: Native plant lipid bilayer including membrnae proteins, transmembrnae proteins, spingolipids, sterolipids, cholesterol shielding their hydrophobic parts in the inside of the about 4 nm thick lipid doublelayer.

It is therefore helpful to take a closer look at the plant plasma membrane (PPM). The lipid and protein composition of the PM is highly heterogeneous and arranged in lipid rafts and lipid shells (Angus S. Murphy, Wendy Peer 2011). The lipid-to-protein mass ratio in the native plant PM is approximately 1:1. These highly complex assemblies, only about 4 nm thick, consist of two main components: a self-assembled sheet of lipid molecules held together by hydrophobic interactions and proteins attached to or embedded within the membrane.

The self-assembly of lipid and protein into a membrane is energetically favored by increasing the overall entropy of the aqueous phase. This is achieved by that lipid membranes are able to shield their hydrophobic fatty acid parts from the bulk water by

exposing only their hydrophilic head groups to the water. This entropy driven self-assembly of membranes is the most fundamental aspect of life as we know it today. This self-assembly is independent of any cellular processes and also taking place when the lipids are exposed to a hydrophilic environment or a solid support see (Figure 3) This properties can be used to create cell-free platforms. The plant PM is clearly the most diverse membrane of a plant cell. Its composition of lipids and associate proteins is dynamic and varies with cell type, developmental stage and environmental conditions.

Our current knowledge about biological membranes and of all the relevant molecular processes occurring at biological membranes is mainly based on experiments performed on membrane models e.g. liposomes (Figure 3, A), lipid monolayers (Figure 3, B), black lipid films (Figure 3, C), membrane patches at pipettes, or solid-supported membranes (Figure 3, G) (McConnell et al. 1986). In this work we have only used SLBs as the currently most used platform next to liposomes to study membrane processes in biophysics. The other techniques are only mentioned for completeness due to their role in the development of our understanding of membrane assembly and membrane biophysical processes. Solid SLBs can provide a powerful platform to analyze functional and structural areas, transport and catalytic properties of membrane proteins simultaneously. Optical and electrophysiological data can be obtained in parallel in one simple but effective 2D plane with strongly reduced background noise and in a controlled environment.

Following the pioneering work of McConnell and collaborators (Brian & McConnell 1984) who first utilized unilamellar liposomes to form SLBs on hydrophilic (glass) [1]solid supports, this approach has become very popular for studying basic membrane processes (Hsia et al. 2015).

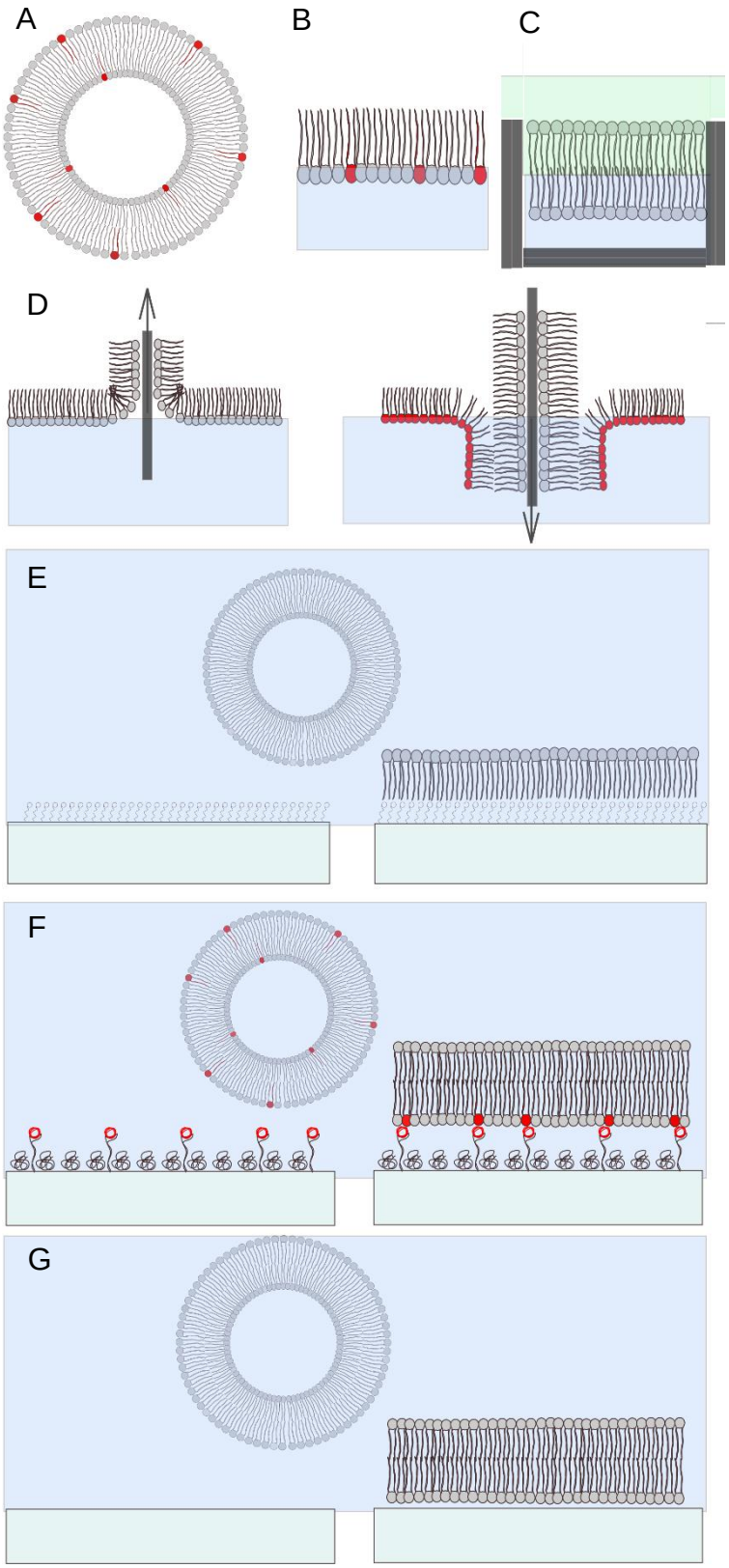

Figure 3: Cell plasma membrane mimicking models

(A) Liposomes (25 nm to 100 µm in diameter) enveloped by a lipid bilayer;

(B) Monolayer at the air-water interface;

(C) Lipid bilayer suspended over an aperture between two aqueous phases (black lipid);

(D) Langmuir-Blodgett method, transfer of initially a lipid mono-layer followed by adding a second layer from the air-water interface to a solid object;

(E) Self-assembled monolayers (SAMs, e.g. Au or thiols), a lipid monolayer can be deposited on the SAM;

(F) Polymer coating with tethers followed by spontaneous rupture of liposomes, to create a SLB on a cushion;

(G) Direct rupture of liposomes on glass or silica.

As already previously mentioned, the single lipid molecules are arranging in solution in spherical structures. This process is entropy driven and aims to minimize the entropy of the water molecules surrounding the hydrophobic tails of the phospholipids. On the other hand is the Self-assembly at the interface driven by various other factors. The most dominant intramolecular force driving the attachment and rearrangement at the silica substrate is the Van-der-Waals-force. The distance of about 1 nm between the silica substrate and the vesicle is enough to cause self-assembly at the surface. The surface tension due to the vesicle curvature is neglect able due to the average size of several hundred nanometer in diameter. After deposition of the unilamellar vesicles they stay intact but are deformed at all coverages. After the fusogenic vesicles are injected they are rupturing individually or after interaction with other vesicles causing the formation of bilayer patches. The herefore critical surface coverage is estimated to be approximately 30% of the total surface area covered by deformed vesicles at 295 K (Reimhult et al. 2003) this number is probably too low to enable a direct physical interaction between the vesicles. After the initialization of rupture the single bilayer patches have a very high line-tension causing single water molecules to infiltrate the hydrophobic lipid tails creating an unfavorable but reactive edge of the unfolding lipid sheet.

In order to study PM proteins it is necessary to study their function and properties in a native membrane system without altering its structure and function.

Membrane proteins can be integrated into synthetic membranes and studied without having the hassle of expressing the protein *in vivo* in exactly this system. Usually a bacterial expression system is chosen to achieve high yields of the protein of interest. These host systems (e.g. *E. coli*) are able to produce very high titers in very short time periods, unfortunately the posttranslational modifications necessary for structure and function are not possible in a bacterial system due to its prokaryotic nature. Even if expressed in eukaryotic hosts such as CHO cells or oocytes, the post translational modifications are taking place but without the plant specific quality control systems such as check for correct conformation and folding, correct glycosylation and assembly of dimers or trimers present only in the genuine host. These proteins are then undergoing at least 3 major procedures such as (i) extraction from the host (ii) purification from the cell lysate or the supernatant via precipitation, affinity sorting or chromatographic steps such as size exclusion, ion exchange or hydrophobic interaction chromatography and (iii) reconstituted into a synthetic membrane. All these

steps can alter the protein unfavorable for a subsequent analysis of function. In the last 40 years many reconstitution processes based on reconstitution agents such as sodium dodecyl sulfate (SDS), TritonX-100 or CHAPS have been developed and optimized (Wang & Tonggu 2015). Such reconstituted proteins integrated in liposomes can be ruptured to SLBs and analyzed. An example of such reconstituted proteins are the malate transporters of the ALMT1 family of *A. thaliana*. The transporters which were expressed in frog oocytes and then reconstituted into synthetic membranes by (Hoekenga et al. 2006).

But there are drawbacks for these conventional reconstitution processes. Despite the simplicity and low cost “there exist a few significant disadvantages for reconstituted proteins: (i) uncontrolled detergent removal rate, thus poor reproducibility, (ii) unknown final sample concentration as the volume changes due to the osmotic pressure differences, (iii) long duration of dialysis due to the number of changes of buffer” (Wang & Tonggu 2015). And even if the reconstitution process worked as intended, protein orientation and protein function might be altered and will not represent the native system. This is especially true for complex structures that are assembled from monomers. “Therefore, to expand our current knowledge of how plant membrane proteins function and are regulated, membrane platforms must be further developed to expand the characterization of lipid–protein interactions and minimize possible artifacts” (Hsia et al. 2015).

To increase our structural and functional understanding of essential membrane proteins various approaches are used. As of this writing more than a thousand membrane proteins have been structurally solved. The majority by X-ray crystallography which represents the most robust way of determining the structure of a protein at an atomic level. Unfortunately important integral membrane proteins have been shown to be very difficult to crystallize by X-ray crystallography due to the large percentage of non-polar amino acids (AA) present within the primary structure (Delmar et al. 2015). During the extraction and reconstitution process it is essential to keep the proteins stable and folded correctly a challenge that is not easily achieved and also the explanation why membrane protein crystal structure are only representing less than 1% of the total protein structure database (Parker & Newstead 2016). The crystal structure can offer revealing insights into the secondary structure of the protein. But only limited assumptions can be drawn from it when it comes to function or mechanism of action.

Our current knowledge about biological membranes and of all the relevant molecular processes occurring at biological membranes is mainly based on experiments performed on membrane models e.g. liposomes (Figure 3, A), lipid monolayers (Figure 3, B), black lipid films (Figure 3, C), membrane patches at pipettes, or solid-supported membranes (Figure 3, G) (McConnell et al. 1986). Solid SLBs can provide a powerful platform to analyze functional and structural areas, transport and catalytic properties of membrane proteins simultaneously. Combining optical and electrophysiological data in one simple but effective 2D plane without background noise distortion and fluctuating environment.

To form a supported SLB two factors are of importance, the substrate and the vesicles. The vesicles are interacting with the substrate to rupture and transform into a bilayer disk together with neighboring vesicles they fuse into membrane patches triggering the rupture of additional adsorbed vesicles. This formation is governed by the interplay of solid support, inter- vesicle, and intra-membrane forces. The relative contribution is depending on the physiological properties of the supporting surface such as charge, structure, and roughness. As well as the fusogenic vesicle itself and their composition, surface charge, vesicle size (Erik Reimhult et al. 2002), temperature (E. Reimhult et al. 2002), and osmotic pressure (Reimhult et al. 2003) have been shown to influence the rupture process. Ultimately the pH and ionic strength of the aqueous environment plays a significant role (Richter et al. 2003). Other factors such as the Calcium concentration in the aqueous environment, which is a well-known promoter of the formation of SLBs (Ekeroth et al. 2002). Large continuous supported lipid bilayers are formed by the fusion of single patches, resulting from the rupture of several neighboring vesicles till the SLB finally covers the whole surface. The supporting material plays a critical role for the formation of an SLB e.g. it is possible to form SLBs on silica, glass not on Au or TiO2 under identical conditions (Erik Reimhult et al. 2002). Based on these findings, it can be assumed, that hydrophilicity of the supporting material is important but cannot explain the SLB formation on its own (Silin et al. 2002).
The fact that SLBs allow free diffusion of proteins in translation and rotation of lipid molecules makes them well a suited platform to analyze membrane processes such as protein adsorption (Andree et al. 1992), protein self-assembly (Yip et al. 2002),

protein localization at lipid phase boundaries (Milhiet et al. 2002), and protein function (Grandbois et al. 1998). The formation of two-dimensional ordered protein arrays depends on the presence and relative positioning of favorable inter-molecular interaction sites and is, thus, protein-dependent (Richter et al. 2003). Whereas SLBs are a highly useful tool for microscopy the necessity to reconstitute proteins with all the disadvantages mentioned above is a hassle. It should be possible to produce cell derived vesicles which are maintaining the native lipid environment and correct protein orientation. When these native vesicles are ruptured into SLBs they combine all advantages of a 2D planar layer together with the native membrane environment. In contrast to previous techniques (Steinem et al. 1996) which are based on commercially available lipids, these membrane platforms bridge in-vivo and in-vitro assays, as well as increase robustness and compatibility with a wide variety of surface characterization tools.

1.3 The proteolipid system

One of the major difficulties with SLBs is the confinement of larger proteins protruding from the SLBs and getting into contact with the glass followed by a partial denaturation and rearrangement on the silica resulting in an immobilization of the specific protein. To increase protein mobility it is also good to know, that silica substrates are inflexible, brittle, optically transparent and electrically insulating whereas on other substrates better mobility could be achieved. Especially for protein tracking it can be a major obstacle, that all the fluorophore domains are designed to face the cytosol when incorporated into the membrane. This is a very good decision when observing the plant membrane protein in a full cell enclosed by a CW. If the fluorophore domain would be located in the apoplastic space it would be into contact with the cell wall, which leads especially under high turgor conditions as present in well-watered and healthy plants to an immobilization of most PM-proteins (Martiniere et al. 2012). To obtain any protein mobility small constructs were chosen which are well known to have only one transmembrane loop and a high mobility. These constructs such as PIP2A or RCI2A are designed as membrane marker (Thompson & Wolniak 2008) and used for fluorescence microscopy. If the cytosolic part is in contact with and underlying solid substrate such as a microscopy slide it is likely to resulting in immobilization of the protein.

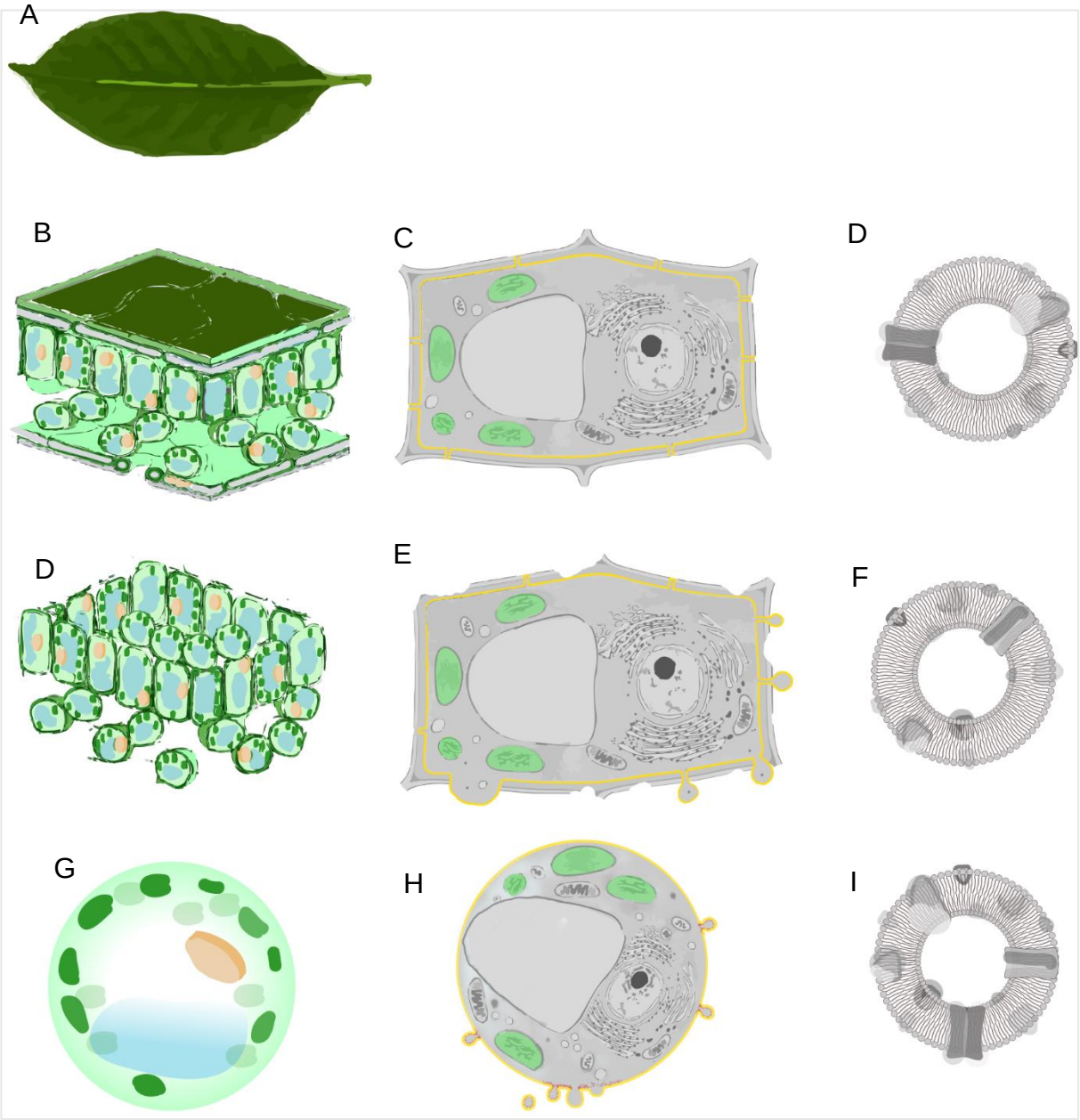

Figure 4: Production of PM-vesicles: (A) plant material, (B) Cross section of an undigested leaf, (C) Extraction of a MF from the whole leaf material, (D) Cross section of the leaf material after digestion with enzymes, ((E) plant cell during the digestion process, partially digested CW with emanating cytosol after the plasmodesmata channels have been closed, (F) Bubble after cytosolic budding, (G) Final healthy protoplast only encapsulated by the PM, (H) protoplast during blebbing and vesicle budding, (I) Plant PM-bleb.

Many techniques are already well known and established to produce proteoliposomes from the cell plasma membrane of mammalian cells. They can be induced either by chemical reagents, French-press or blebbing inducing proteins. These proteoliposomes retain the host specific lipid and protein diversity. But this

has never been tried for plant cells. In the following text the term PM-vesicle is used as a generalization for all types of PM derived liposomes independent of the method of production. If not further specified all vesicle types are addressed as PM-vesicle. The term bubble was chosen based on the mechanism of formation which was initially imagined to be similar to the formation of soap-bubbles.

In order to create host specific proteoliposomes, henceforth referred to as blebs the two most commonly used methods are serum starving and chemical blebbing. The first process is characterized by the removal of all serum, an essential component of a mammalian cell culture, followed by a cascade of stress responses by the mammalian cell (Charras 2008; Fackler & Grosse 2008). Whereas formaldehyde (FA) and dithiothreitol (DTT) are commonly used for the chemical blebbing procedure. The complete process was first described as cytoplasmic protrusions during mitosis by the Strangeways research laboratory (Boss 1955). For the chemically induced blebbing process the DTT reduces disulfide bonds and cysteines, which is effecting lipid phase partitioning (Fraenkel-Conrat & Olcott 1948; Sezgin et al. 2012; Levental et al. 2010). FA is facilitating the local anomalies in the PM by functioning as a protein cross-linking agent resulting in protrusions of the PM (Hopwood 1969)

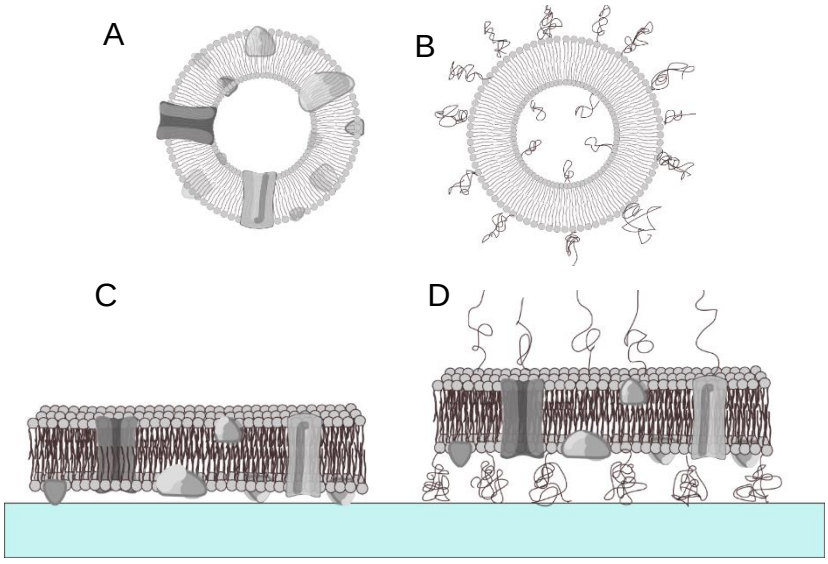

Figure 5: (A) Vesicle derived from the plant PM with native lipid and protein ratio and orientation. (B) Fusogenic vesicle equippe dwith PEG-5000 in a molar ratio of 0,5%. (C) SLB after rupture and spred out, leaving most of the proteins sitting on the glass substrate. (D) SLB with included PEG-5000 brushes fused with the bilayer during the rupture process and supporting the SLB at a hight of about 5 nm above the glass substrate.

The extraction of membrane fractions is a commonly performed procedure and used for various experiments such as the extraction of membrane proteins, lipid fractions for their analysis and evaluation of enzyme activities PM-microsomal chimeric vesicle isolation was carried out in *Arabidopsis thaliana* and *Nicotiana benthamiana* mesophyll leaf tissue by an adopted procedure from (Abas & Luschnig 2010; Yoo et al. 2007). Briefly,

The extraction of membrane fractions is a commonly performed procedure and used for various experiments such as the extraction of membrane proteins, lipid fractions, enzyme activities and the isolation of subcellular enzymes like microsomal fragments (Abas & Luschnig 2010) or nuclei, mitochondria and lysosomes (Storrie & Madden 1990). Plasma membrane fractions have first been isolated around 1960, due to the complexities inherent in working with membranes it was not shown that purifications were not rigorous enough to avoid contamination with other subcellular particles (DePierre, J. W., Karnovsky 1973). The isolation of Membrane fractions provided a simple tool to increase protein concentration for subsequent TIRF studies and despite the drawback of uncontrolled orientation during formation, this method provided a valuable method to study mobile protein.

1.4 Characterization tools for SLBs

To monitor the formation and investigate the properties of PM-SLBs a wide variety of optical and surface based characterization tools are already available such as total internal reflection microscopy (TIRFM)(Watts et al. 1986), atomic force microscopy (AFM) (Chiantia et al. 2006) , quartz crystal microbalance (QCM) (Cho et al. 2010) , and surface plasmon resonance (SPR) (Mengel & Kirkby 2001)(Terrettaz et al. 1993)**,** super-resolution Imaging (Henriques & Mhlanga 2009), such as photo activation localization microscopy (PALM) (Owen et al. 2010), stochastic optical reconstruction microscopy (STORM), (Wu et al. 2013) and classical fluorescence microscopy (Mueller et al. 2011; Kellner et al. 2007). These techniques have revealed complementary insights into the properties of mammalian and prokaryote membrane mimic SLBs, their organization and interactions. They would likewise be the tools to perform equivalent studies on plant PM mimic SLBs.

To study the successful formation of SLBs two techniques have been particularly important and often used: fluorescent recovery after photobleaching (FRAP) and quartz crystal microbalance with dissipation monitoring (QCM-D). FRAP is a photo bleaching-based microscopy technique which was developed in the mid-1970s by (Axelrod et al. 1976) as a technique to study protein mobility in membranes of living cells by bleaching a defined spot and measuring the rate of fluorescence recovery. The technique pioneered at Cornell (Koppel et al. 1976) was utilized as a method to measure diffusion coefficients in cellular membranes by staining them with fluorescent dyes.

QCM-D is a valuable tool used to quantify bilayer deposition as well as binding kinetics to this membrane. It can be used to study adsorption of very small masses onto a sensor substrate of any surface composition. It is particularly useful to study macromolecular interfacial self-assembly due to its sensitivity to water content and viscosity of the self-assembled interfacial layer. The measurement principle for QCM is a change in resonance frequency (Δ_f) and energy dissipation (Δ_D) of a piezoelectric quartz crystal which is stimulated by an alternating current (AC) to oscillating at its resonance frequency. Every change in frequency (Δ_f) is proportional to the adsorbed mass on the sensor surface. Simultaneously, changes of energy dissipation per oscillation cycle (Δ_D) were recorded to characterize the viscoelastic properties of the attached material.

2 Materials and methods

2.1 Preparation of Protoplasts

The protoplasts used in our work were obtained from *Arabidopsis thaliana*, *Zea mays* or *Nicotiana benthamiana* and isolated following a standard protocol for *A. thaliana* (Columbia) (Yoo et al. 2007), *N. Benthamiana* (Waadt & Kudla 2008) and *Z. Mays* (Richter et al. 2016). GPMV

Protoplasts were prepared from 4-week-old *A. thaliana* plants, 4-week-old N. tabacum plants or 3-week-old *Z. mays* plants by enzymatic digestion of leaf mesophyll tissue. Additionally for *Z. mays* the plant material was bleached for 2 days, by turning off the light in the growth chambers, to reduce the chloroplast content which is interfering with the purification procedures. For all stable transformed monocot *Z. mays*, the central section of each leave was harvested. For dicots (*N. Benthamiana, A. thaliana*) the mid rib was removed, and cut into 1 mm stick striped with a new razorblade whereas only the middle part of the monocot (*Z. mays*) leaves was used to achieve more homogeneous protoplast results.

For Z. mays (Inbred line B73, ZmPIN1a-YFP from D. Jackson (Cold Spring Harbor Laboratory). protoplasts, plant material was harvested and processed in the dark, to prevent bleaching of the expressed transporter. The plant material was cut as shown in Figure 7 with a new razorblade and a pull-trough chopping action to keep the cut surface as clean as possible. The stripes should not exceed 1 mm in width and should be cut as homogeneous as possible. After each cut, the material was put into the 50 mL tubes filled with 20 mL digestion buffer see Table 2: Digestion buffer for *Arabidopsis* thaliana protoplasts (20 mL buffer per 0.5g tissue) and submerge the stripes in digestion buffer. The transfer should be accomplished within 30 seconds to avoid oxidation and wound closure actions to taking place, which prevents the digestion buffer from entering the extracellular space. To speed up the digestion process, a vacuum was applied to move the digestion buffer into the intercellular spaces.

The vacuum was slowly applied over 3 min till reaching 80 kPa the air bubbles emerging at the plant material surface should be detached by gently bumping the vacuum chamber on the bench. Once the bubbles were detached, the pressure inside the chamber was slowly raised to the environmental level. This step should be

performed slowly to help the stripes take up the surrounding buffer which will result in darker colored tissue see Figure 8. The step can be repeated two to three times till to the submerged material was of homogeneous dark color and then kept constant at 80 kPa for 3 hours at room temperature (23ø C, 74ø F)..

After 3 hours, the pressure was increased to the surrounding pressure and the tissue is gently swirled with a spatula to release the protoplasts from the cell debris.. The protoplasts were then cleared from the buffer by a centrifugation step at 250 rcf for 3 minutes. The supernatant containing the bubbles was transferred to a new 15 mL tube and spun at 2000 rcf for 5 minutes to clear the buffer from cell debris. The clear supernatant containing g the bubbles is transferred to a new 15 mL tube and stored at 4° C for up to 2 weeks.

The protoplast pellet was resuspended in 5 mL filtered GPMV buffer as the digestion buffer by gently swirling the mixture and after resuspension the tube was filled up to 20 mL with GPMV buffer and afterwards centrifuged at 250 rcf for 3 min. This step was repeated one more time and the final protoplast pellet resuspended in 4 mL of blebbing buffer (see Table 5). The chemical induction of cell blebs was performed for 2 hours at room temperature (23° C, 74° F) while inverting the closed 15 mL tube containing protoplasts in blebbing buffer see Table 3: Blebbing buffer every 30 minutes very gently. The mixture was then cleared at 200 rcf for 5 minutes to pellet the intact protoplasts without bursting them. The supernatant was then transferred to a new 15 mL tube and spun at 2000 rcf for 10 min. The plant cell PM blebs in the supernatant were then transferred to a new 15 mL tube and stored at 4°C for up to a week.

2.1.1 Protoplast transformation of mesophyll cells

2.1.2 Transformation of Tobacco protoplasts

The coding region of the proteins of interest (SbMATE, PIP2A) were cloned into plant binary expression vectors pGreen mCherry and pK7m34GW respectively, and transformed into Agrobacterium strain GV3101. The expression assays in *N. benthamiana* were carried out according to (Waadt & Kudla 2008) but briefly, *Agrobacterium* cultures were grown overnight at 30° C. These were mixed in ratios of 1 part expression vector to 3 parts p19 vector (common suppressor of post-transcriptional gene silencing). This mixture was spun down, the supernatant removed and the pellet was mixed with the activation buffer (200 mM MES at pH 5.6, 150 mM

MgCl2 and 150 mM Acetosyringone). This was left at room temperature for at least two hours. The *Agrobacterium* solution was injected into the abaxial side of *Nicotiana benthamiana* leaves that were at least 4 cm (1.5 “) across. The plants were left to grow for 3 to 5 days to allow for transient expression of the gene of interest.

2.1.3 Transformation of *Arabidopsis thaliana* protoplasts

The coding region of AtALMT1, TaALMT1 (Ligaba et al. 2013) and SbMATE1 were subcloned into the expression vectors pSAT6-EYFP-C1. Transient expression was carried out in *Arabidopsis thaliana* (Columbia) mesophyll protoplasts as described by (Yoo et al. 2007). Briefly, *Arabidopsis* protoplasts were isolated from 4-week-old plants, grown under 13 hour light at 23°C and 11 hour dark at 20°C cycles, by digestion in a digestion buffer (see Table 2). Protoplasts were transiently transformed with 10 to20 µg of plasmid DNA via polyethylene-glycol (PEG)-mediated transformation, and were incubated in the dark at room temperature overnight in a buffer of 2 mM MES (pH 5.7) containing 154 mM NaCl, 125 mM $CaCl_2$ and 5 mM KCl.

2.2 Production of Plasma membrane vesicles

2.2.1 Production of plasma membrane bubbles

This procedure was used when producing bubbles during the protoplast digestion. The digestion buffer (Table 2: Digestion buffer for *Arabidopsis* thaliana protoplasts) was prepared fresh from stock solutions as shown in Table 4 and heated to 55° C and afterwards filtered through a 0.45 µm filter.

Table 1: Osmotic conditions for protoplast and bubble generation

Species	protoplast generation [Mol/L]	bubble generation [Mol/L]
Arabidopsis thaliana	0.5	0.4
Nicotiana benthamiana	0.5	0.4
Zea Mays	0.6	0.5

Table 2: Digestion buffer for *Arabidopsis thaliana* protoplasts

Reagent for 10 mL buffer	Mass [mg]	Final concentration [mM] or [%] v/v
Cellulase R10	150	25%
Maceroenzyme R10	50	5%
Mannitol	1,2	100
MES	0,5	20
CaCl	0,04	5
2-Mercaptoethanol 0.0105	0,0015	2
Bovine serum albumin fraction V	0.01	0.001%

Table 3: Blebbing buffer

Reagent for 4 mL buffer	Volume added [µ]	Final concentration [Mol/L]
GPMV buffer	1600 - 2300	
Formaldehyde	9	234
DTT	8	234
Mannitol, stock solution 1M	1600 - 2400	0.4 – 0.6

2.2.2 Preparation of plasma membrane blebs

Protoplasts were prepared from transgenic or transiently expressing leaf tissue as explained above and pelleted at 250 rcf for 2 minutes at 18°C and afterwards resuspended in 4 mL blebbing buffer consisting of GPMV buffer (2 mM $CaCl_2$, 10 mM HEPES, 150 mM NaCl, 0.5 M Mannitol at pH 6) with 25 mM formaldehyde and 2 mM dithiothreitol was used to induce the cell blebs subsequently. The cells were incubated in the blebbing solution for 2 hours at 23° C. The blebbing solution containing cells and blebs was centrifuged first for 2 minutes at 200 rcf to pellet the protoplasts without rupturing them. This was followed by a centrifugation of 5 minute at 2000 rcf to clear

other impurities from the supernatant. Cell blebs were collected from the supernatant and stored at 4° C.

2.2.3 Production of membrane fraction

Leaf tissue was submerged in liquid nitrogen and homogenized manually with a precooled mortar and pestle. Every subsequent step was performed on ice. Cell material was mixed 1:2 with basic extraction buffer (EB) consisting of 100mM Tris–HCl, 25% (w/w, 0.81 M) sucrose, 5% (v/v) glycerol, 10mM ethylenediaminetetraacetic acid, 5mM KCl, and 2mM 1,4-dithiothreitol adjusted to 7 pH.

Table 4: Membrane fraction extraction buffer

Reagent for 100 mL buffer	Mass [g]	Final concentration [mM] or [%] v/v
Sucrose	25	25%
Glycerol	6,3	5%
Tris-HCL	1,2	100
Ethylenediaminetetraacetic (EDTA)	0,5	20
KCl	0,04	5
1,4-dithiothreitol	0,0015	2

For each gram plant material (fresh weight), 0.05 g of PVPP (dry weight) was used and added in dry form directly into the buffer before use. Mixture was sonicated with a tip solicitor (80% max. power) for 5 minutes in 10 seconds on and 10 seconds off intervals and afterwards spun down at 600 g for 5 minutes. The pellet containing the cell wall debris and chloroplasts was discarded and the supernatant filtered through a 100 µL nylon filter. Another clearing centrifugation step at 2000 g for 5 min was performed and the cleared supernatant was collected and stored. The supernatant was diluted 1:1 with GPMV buffer and centrifuged in an ultra-centrifuge at 50,000 g for 2 hours. The supernatant was discarded and the pellet was resuspended with 1 mL GPMV buffer (pH7) per 1 g fresh material. The membrane fraction usually showed Nanodrop concentrations of around 800 mg/mL. Concentrations above 2000 mg/mL were prone to precipitation of membrane proteins and thus not used. The membrane fraction stored at 4° C for up to one week. This protocol yields a mixed fraction of

probably microsomal, vacuolar and PM membranes. This enabled the highest yield of transmembrane protein.

2.3 Characterization of plasma membrane vesicles

2.3.1 Characterization of bleb concentration size and charge

To evaluate and compare the efficiency of the different production methods, nanoparticle concentration was measured and analyzed with the Malvern internal algorithm, NanoSight NS300, Malvern. Vesicle size distribution and surface charge (zeta potential) dynamic light scattering, Zetasizer Nano ZS, Malvern was used. All measurements were performed in GPMV puffer at pH 7 at 23° C. For the NanoSight measurements all videos were analyzed using a detection threshold of 12 units and a screen gain of 24 units. They were performed according to the manufacturer's directions (NanoSight, Malvern Instruments Ltd, Malvern, UK).

The Zetasizer Nano ZS was operated on a standard operation procedure for size measurement for liposomes in aquatic buffers according to manufacturer's directions. Samples were by default diluted 1:10 with GPMV buffer prior to measurement. The zeta potential was determined with a standard extension module for electrophoretic measurements. Raw data from both systems was exported into an excel file and further analyzed in R studio (Version 1.1.447).

2.3.2 Cryo SEM Characterization

Imaging conditions were used as reported by (Champion-Lapalu et al. 2002) to generate the images of the vesicles. The sample was kept in the sublimation chamber for 5 minutes at 2 * 10^6 torr and -100° C and afterwards coated with a 2nm thick gold-palladium layer at 10 mA for 10s. This step was necessary for biological samples in order to avoid charging of the surface and further on imaging artifacts. Images were obtained by detecting secondary electrons at 1 * 10^6 torr and -165° C using 5kV electron beam currency. As the sample surface at 10k magnification was eroded already after one second, most of the images were obtained in blind-zoom mode using a new spot for every image. After obtaining the primary image (shown in this work) a second image was generated (data not shown) using a much higher exposure time to observe the sample erosion patterns. This method was useful to distinguish between physical samples (which remained unchanged after longer exposure to the

E-beam) and imaging artefacts (which vanished after less than 1 second). Only those pictures were used that showed an unspoiled surface after the longer beam bombardment.

The cryo scanning electron microscopy (SEM) utilized for our approach was used to visualize the blebbing and bubbling process.
The 100 µL of sample was spread out in a thin layer on the metal carrier and plunged frozen in liquid nitrogen to avoid ice crystal formation. The following sublimation step at -100° C for 5 min at $1*10^{-6}$ tor was performed on the cryo stage of the microscope and is intended to remove all the water from the sample by avoiding the liquid stage and transferring it directly transferring into the gaseous stage, which was removed by the vacuum pump from the specimen. To avoid surface charging and sample damage biological samples were commonly sputter coated with a thin layer of gold. We chose to apply a 1 nm thick layer of gold-palladium at 10 mA for exactly 10s. The sample was introduced to the specimen chamber operated at -165 C and $2*10^{-6}$ tor and scanned using low voltage scanning electron beam at 5 kV to avoid sample damage.

2.3.3 Characterization of protein expression by confocal microscopy

Confocal imaging was performed using a Leica TCS SP5 confocal laser scanning microscope at excitation and emission wavelengths of 514 nm and 525–550 nm (YFP) and 561 nm and 673-726 nm (chlorophyll) to check for successful transformation and health of the cells. Tissue of *Z. mays* and *N. tabacum* was excised from the leaves and the abaxial side was imaged, as well as protoplasts after the second purification step. This two-stage approach confirmed the integrity of the PM proteins after the digestion step and removal of the cell wall.

2.3.4 Protein expression in vesicles

The presence of the protein of interest in the PM vesicles was determined by coomassie staining of the membrane protein. In preparation 10-20 mL of vesicle-containing buffer was spun by an ultracentrifugation step (50 000×g for 1 h) and the pellet resuspended in 200 µL of GPMV buffer. The bleb concentration was measured by Nanosight (Malvern Instruments Ltd, Malvern, UK) before and after the ultracentrifugation step to make sure that the sample was intact and showed

approximately 10^8 particles/mL prior and 10^9 particle/mL post centrifugation. The resuspended pellet was mixed with 4x Laemmli sample buffer (Bio-Rad) plus 10% DTT and incubated at 70°C for 10 min. This step was followed by a separation on a premade 10% SDS-PAGE (Invitrogen) and stained by a fast staining procedure according to (Dong et al. 2011) and (Májek et al. 2013) without heating for distaining but at room temperature and overnight.

2.3.5 Quartz crystal micro balance QCM-D

Prior to the experiments sensors (Q-Sense, glass SiO_2) were sonicated in a 3% [w/v] SDS solution for 30 minutes, cleaned with Milli-Q water and dried under nitrogen gas. The clean sensors were then treated in an UV-Ozone Procleaner (Bioforce, USA) for 10 minutes to remove any organic contamination and to reduce the surface of the silicon dioxide. For these measurements, all 9 overtones were recorded but only the third overtone frequency ($F_3 = 15\,MHz$) and dissipation (D_3) was used for an estimation. Lower overtones were from the data as they were unstable due to edge effects (Hsia et al. 2016). Measurements were performed under constant flow conditions of 500 µL/min by Peristaltic pump (Ismatec Reglo Digital M2-2/12, Q-Sense). The QCM sensor was equilibrated with the buffer solution for 1 minute to determine the baseline (i.e.$\Delta_f = \Delta_D = 0$) of the sensor. Then the POPC-PEG (5 k) at a molar concentration of 0.5% liposomes were pumped into the chamber for about 3 minutes until a bilayer was formed and the values for Δ_f and Δ_D stabilized. The system was rinsed with GPMV buffer for 1 minute to wash out excess liposomes and to determine the final frequency and dissipation shifts Δ.

The QCM sensor was equilibrated with the buffer solution for 1 minute to determine the baseline (i.e.$\Delta_f = \Delta_D = 0$) of the clean sensor. Then the cell derived vesicles, either blebs or bubbles were sent into the chamber and continuously circulated in the tubing system (about 1 mL total volume) for about 3 minutes to attach to the sensor. Then the system was rinsed with GPMVM buffer for 1 minute to wash out excess of fusogenic vesicles which were pumped into the chamber for about 3 minutes until a stable supported lipid bilayer was formed and the values for Δ_f and Δ_D reached a stable level. Finally the system was rinsed with GPMVM buffer for 60 seconds to wash out excess of liposomes and determine the final values of frequency and dissipation. All experiments were recorded using Qsoft (version 1.1.28.4) and normalized changes of frequency and dissipation of the third overtone were monitored (1) and fit

to a Sauerbrey model (Kankare 2002) Using the third overtone (n=3) and the following sensor parameter (C= 17,7 ng * Hz^{-1}*cm^{-2}) to calculate the mass deposition on the quartz sensor.

$$\Delta m = -\frac{C * \Delta f}{n}$$

2.4 Formation of SLB's

2.4.1 Chip preparation

All used glass slides (25×25 mm No.1.5, VWR) were pretreated with a piranha solution (70% (v/v) H_2SO_4 (BDH) and 30% (v/v) H_2O_2 (Sigma 50 wt %)) for 10 minutes and rinsed by flushing deionized water for 20 minutes continuously. To hold the sample, polydimethylsiloxane (PDMS) wells were made by mixing 10:1 elastomer: cross linker mixture of Sylgard 184 (Robert McKeown Company) and were baked for 2 hours at 80°C. The blebs were labeled with Octadecyl Rhodamine B Chloride (R18) at a concentration of 4uL [1mg/mL] per 1 mL vesicles and sonicated for 30 minutes at room temperature. After sonication, the excess R18 was removed by a size exclusion chromatography step, performed in a MicroSpin G-25 Columns (GE Healthcare) at 300 rcf for 3 minutes.

2.4.2 Preparation of liposomes

Fusogenic unilamellar liposomes were prepared via extrusion using the following synthetic lipids: 1-oleoyl-2-palmitoyl-sn-glycero-3-phosphocholine (POPC) and 1-oleoyl-2-palmitoyl-sn-glycero-3-phosphocholine-polyethylene glycol (POPC-PEG-5000) (Avanti Polar Lipids). The liposomes were prepared by mixing the individual components in chloroform (Sigma) in a molar ratio of 99.5:0.5 in a 50 mL glass vial which was pre rinsed with ethanol and double desalted water (ddH_2O), and afterwards dried for 30 minutes to remove residual water. The mixtures were combined from chloroform stock solutions and the chloroform was gently evaporated using a stream of nitrogen followed by a vacuum drying process under deep vacuum (0.05 mbar) for 3 hours to remove residual chloroform. To create liposomes, the dried lipid films were resuspended in GPMV buffer to reach a final concentration of 2 mg/ml. Single unilamellar liposomes were prepared by high pressure extrusion (500 kPa, manufacturer) using a 100 nm membrane with a home made one-way extruder and

completing at least 10 passes. The 99.5% w/v POPC, 0.5% POPC-PEG liposomes (henceforth referred to as fusogenic vesicles) were used to rupture the plant PM vesicles after attaching the latest to the piranha cleaned glass slides to form a continuous supported lipid bilayer. The fusogenic liposomes were used without labeling whereas the plant vesicles were labeled with R18. The POPC-PEG liposomes functioned rupture inducing and when injecting into the system after the native PM-vesicles.

2.4.3 Supported lipid bilayer formation

After the PDMS well was attached to the glass slide, 100 µL of size exclusion chromatographically purified native PM-vesicle solution containing labeled vesicles at approximately 5×10^8 vesicles/mL was added to the well and incubated for 20 min static at room temperature. After incubation, the well was gently rinsed with GPMV buffer pH 7 to remove all unattached blebs. 50 µL of fusogenic vesicles (POPC-PEG 5000) at a concentration of 2 mg/mL was added into the well and incubated static for 30 minutes to 3 hours to form the supported lipid bilayer. After the bilayer was formed, the glass slides were scratched with a glass fragment to facilitate finding the focal plane at the surface during the microscopy measurements and rinsed again with GPMV buffer pH 7 to remove the excess liposomes. The scratch was used later on during microscopy to confirm the right focus layer.

2.5 Characterization of plant supported lipid bilayers (SLB's)

2.5.1 Fluorescent Recovery after Photo bleaching FRAP

After completing the rupture and bilayer formation, the experiments were carried out on a Zeiss Axio observer Z1 equipped with an argon/krypton ion-laser. Samples were irradiated for 200 ms with 4.7 mW at 568.2 nm with an argon/krypton laser (CVI Melles Griot, Model 643-AP-A01) and the emission recorded at 578 nm. Two scans of the field of view were made prior to bleaching, followed by a circular laser bleaching of a circular region of interest (ROI) of approximately 450 µm2 (radius 12 µm). The bleach spot was created by focusing the light through a 20× objective onto the bilayer and the fluorescence recovery was recorded for approximately 15-30 minutes in incrementing intervals from 0.5 seconds to 10 seconds between the individual frames using AxioVision software. Autophotobleaching of the recording laser was taken into account by recording a separate control region in a distance of approximately two times ROI

radius to avoid bleached lipids affect the control region. This was a good estimate as the expected diffusion was expected on the order of less than 1 µm/s^2. The signal intensity was normalized as follows.

$$I_n = \frac{I_t - I_{post}}{\mathrm{I_{pre}} - \mathrm{I_{post}}}$$

Where I_n is the normalized intensity used for the curve fitting, It is the intensity of the bleach spot at any time t, I_{post} is the lowest post-photo bleaching intensity, and I_{pre} is the mean intensity before photobleaching. The recovery curves were fit using a Bessel function according to (Soumpasis 1983). Diffusion coefficient of the mobile fraction of labeled lipids (R18) was calculated using a simplified Soumpasis equation (Diaz et al. 2008),where w is the width at half maximum of the Gaussian circular bleached profile at any time td.

$$D = \frac{w^2}{4 * td}$$

2.5.2 Single protein tracking in SLB

Fluorescently labeled transmembrane proteins from various plant-derived vesicles were imaged using total internal reflection microscopy (TIRF). The formed PM derived bilayer which is incorporating the native proteins of interest (PIN1::YFP, SbMate::YFP, PIP2A::MCherry and RCI2A::Citrin) were recorded by the settings described below. Various methods for single particle tracking (SPT) have already been described in previous literature (Kusumi et al. 2005; Sonnleitner et al. 1999; Ferrari et al. 2001). To enable accurate tracking, all trajectories were calculated using the method reported by (Richards et al. 2016). In order to calculate the trajectory of a migrating particle in a supported lipid bilayer (simplified as an infinite 2D plane) the SPT algorithm is using various sets of information gained from image analysis such as intensity, displacement and variability of intensity throughout multiple frames (Smith et al. 2011). For a particle, three different kinds of motion are possible: confined motion, 2D planar motion and 3D motion. If the particle is mobile in an area smaller than the maximum observed displacement for an equivalent immobile fluorescent bead then the system is regarded as immobile (Sbalzarini & Koumoutsakos 2005). To deal with this heterogeneous system, the single particle tracking algorithm uses the slope of the mean squared displacement (MSD) of the first three frames to determine the local “homogenous”

diffusion coefficient (Kusumi et al. 1993; Smith et al. 1999). By doing so the heterogeneity of the different domains of the bilayer does not strongly influence the initial diffusion coefficient of the natural membrane heterogeneity (Ferrari et al. 2001; Sbalzarini & Koumoutsakos 2005). They employed moment scaling spectrum (MSS) analysis. This method is utilizing a parameter β to characterize the motion of a molecule as one of three states, $\beta < 0.4$ is confined diffusion $0.4 \leqslant \beta \leqslant 0.6$ is quasi-free diffusion and $\beta > 0.6$ is convective diffusion. All the data was analyzed with MATLAB and ImageJ (FIJI).

2.5.3 Plants and growth conditions:

Arabidopsis thaliana:

Arabidopsis protoplasts (Colorado Colombia? wild type, pLH13 35S::RCI2A) were isolated from 4 week-old plants, grown in 13 hour light at 22-23°C and 11 hour dark at 20°C cycles with 100 µmol light intensity. For the temperature experiments the p2 weeks old plants were moved to (i) Four-degree cold room with just the cold room light and (ii) Day 28° C and night 23° C with light 5 AM - 9 PM (250 µmol light).

Nicotiana benthamiana:

Transiently transformed *N. benthamiana* plants were cultivated at 23 °C, 50% rel. humidity and 12h light/dark cycle's pre and post infiltration. The SbMate::mCherry constructs were produced by the Piñeros Labs as well as PIP2A::mCherry which was a generous gift from Maria Harrison lab at the Boyce Thompson Institute (Ithaca, NY). All constructs were used for transient expression in *N. Benthamiana* after syringe infiltration in 4-week-old-plants. *Nicotiana* protoplasts were isolated from 4 week-old plants four days post infiltration.

Zea mays:

The stable transformed 35S::PIN1::YFP *Z. Mays* lines were obtained from the Jander research group at the Boyce Thompson Institute. Plants were cultured for

4 weeks and only the second biggest leaf used for the protoplast isolation. Prior to harvest, the plants were put into 48 h darkness to reduce to chloroplast content and facilitate the protoplast purification steps.

3 Results and discussion

3.1 Protoplast generation

Protoplasts were generated according to the above mentioned procedure. Final isolate protoplasts were purified with two washing steps. The yield of the washing procedure was determined by simple counting of intact protoplasts in the appropriate-sized squares in a hemocytometer (data not shown). And was approximately 80% for *A. thaliana and N. benthamiana* protoplasts and 60% for *Z. mays* protoplasts. This can be explained by observing the supernatant and finding predominantly protoplasts with a lower total density than chloroplast rich protoplasts.

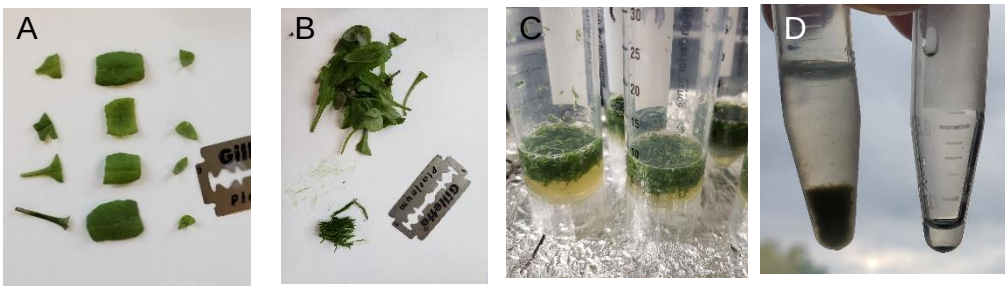

Figure 6: Material preparation for protoplast digestion: (A) Middle section is used for the digestion. Leaf tip and base are removed from the whole plant, (B) Plant material removed from the leafs and the cut leaf stripes of about 1 mm, (C) Leaf material in digestion buffer after the application of the vacuum when the leaf stripes appear darker, (D) Protoplast after the first washing step and spin down.

Also size distribution plays a major role. Smaller chloroplasts were more likely to end up in the supernatant and get discarded than bigger protoplasts. The washing steps altered the collected protoplast size and physiology. The overall yield for protoplast extraction is hard to determine. It is certain that not all cells survive the digestion process, especially old and young cells are prone to rupture due to osmotic shock (Yoo et al. 2007). It is assumed, that the average osmotic potential is either too low or too high for them. Assumptions based on volumetric comparison of a stacked leaf staple and a pellet volume which is only a very inadequate estimation indicates a total protoplast yield between 10% for *Z. mays* and 50% for *A. thaliana*.

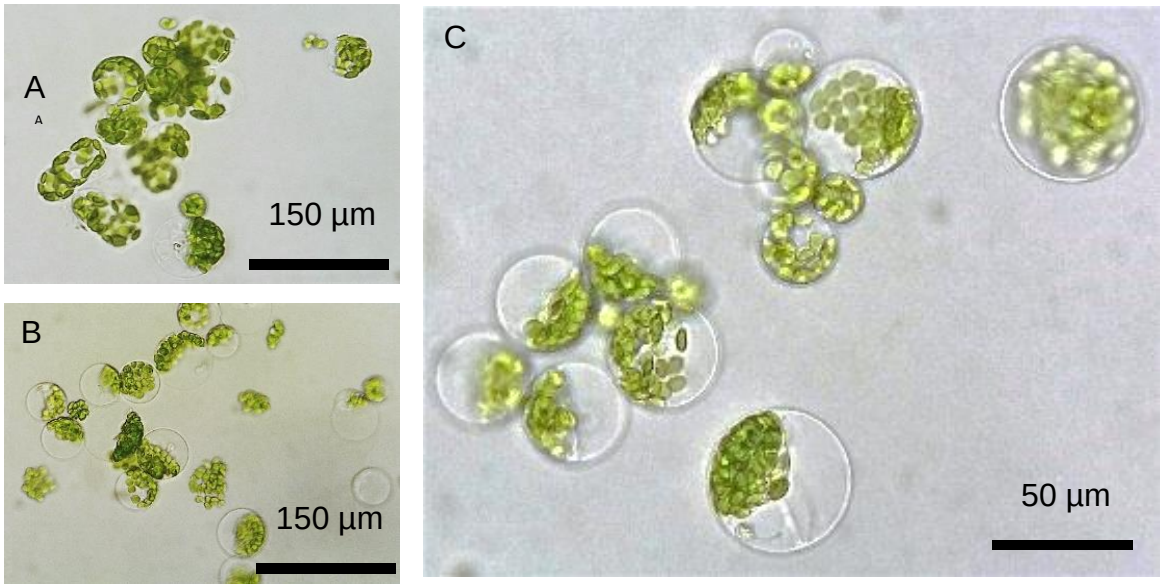

Figure 7: Protoplasts: (A) Arabidopsis thaliana protoplasts after the second washing step. Visible in the upper right corner are free Chloroplasts which are removed after the washing steps, (B), N. benthamiana protoplasts after the first washing step. Visible is already the clear shift of chloroplasts to one side (lowest protoplast in figure C) by the centrifugal forces (C) Zea mays protoplasts after the second washing step. Compared to unwashed protoplasts the size distribution is much more homogeneous and all protoplasts with a higher or lower relative density are removed. The relative density is predominantly determined by the chloroplast content. One reason why the Zea Mays plants yielded more protoplasts after two days in the dark prior to the digestion process, which leads to a degradation of excessive chloroplasts.

3.2 Production of Bubbles

These spherical cell wall free plant cell are extremely susceptible especially to shear forces and osmotic shocks. This fragility is one of the major obstacles when handling protoplasts and but on the other hand a big advantage for the bubble production. Plant PM Bubbles are spherical vesicles that pinch off the protoplast during the enzymatic digestion process. They are generated passively during the early stages of the digestion process. The plant cell is naturally under positive pressure which pushes the PM against the CW. This pressure is usually referred as turgor and responsible for nutrient transport and essential for cell maintenance. The turgor is caused by the osmotic influx of water through the PM resulting in a hypotonic milieu inside the plant cell. When first holes are appearing in the plant cell wall or natural holes such as plasmodesma channels are freely exposed to the osmotic pressure the swelling of the cytosolic part is probably driving the formation of vesicles through these open holes.

The turgor pushes parts of the PM into the exoplasmic space, followed by a separation due to surface tension to pinch off the vesicle from the main PM. This process is genuine to plant cells due to the cell walls. Crucial parameters for a successful formation of bubbles is the osmotic potential of the digestion buffer Table 1 displays optimal osmotic conditions for protoplast and bubble formation based on the mannitol concentration. Mannitol is a sugar alcohol which is structurally derived from mannose and naturally present in fruits and halophytes used as an osmotic diuretic. As shown below, the osmotic conditions of the digestion buffer for bubble production are always slightly lower than for protoplast generation to increases the influx of water. Too low mannitol concentrations in the digestion buffer have not been shown to improve the production of bubbles but rather the opposite effect as the cells are put under too much osmotic stress resulting in a hypotonic shock and subsequent bursting of the protoplast before forming bubbles. Special care was taken about using the middle section of very similarly sized leafs as well as an unused razor blade. Leafs were cut according to Figure 6. Usually 10 cuts of approximately 1 mm width were performed before the freshly cut leaf tissue was submerged in digestion buffer. This step was performed so quick to avoid oxidation at the rim of cut surface and subsequent wound closure. This wound closure is limiting the infiltration with digestion buffer. After vacuum application the leaf striped should appear dark green, this is a good indicator for a buffer filled apoplastic space and therefore a fast and homogeneous digestion.

The formation of bubbles was first hypothesized after observing the digestion process in closer detail under the microscope. During the approximately 3 hours of digestion the cell wall is loosened and falls partially apart by small movements of the buffer. Almost always is one part of the cell wall more prone to degradation and thus the place of first exit for the protoplasts. This observation was leading to the basic idea of bubble formation. If it is possible for a full protoplast to break in half then it is probably also possible for smaller fragments. The self-healing ability of the plant PM is already proven by the fact that it is possible to produce protoplasts although all the individual cytosols of a plant are interconnected via plasmodesmata (Faulkner 2013). Plasmodesmata ducts generate continuity between individual plant cells via the cytoplasm, endoplasmic reticulum (ER) and PM. These ducts 50-60 nm in diameter are in control of the symplastic transport in plants allowing movement of molecules between cells. There are several thousand individual so called plasma membrane

sleeves between the cytoplasm of two cells, depending on the plant and tissue. All these sleeves need to detach in order to form a protoplast resulting in the detachment of the PM at the plasmodesmata to form a spherical protoplast.

3.3 Production of Blebs

The second method used to produce PM-vesicles is chemical induction with a blebbing buffer to induce blebbing of the protoplasts for 2 h. Multiple different experiments covering a wide range of blebbing durations from 3 min up to 24 h were tested and showed that the formation and budding of blebs happens primarily within the first two hours and was not significantly higher after 24 h (data not shown). The particle concentration was determined by nanoparticle tracking analysis (NTA) using a NanoSight NS300. The obtained data must be taken with a grain of salt, as the particle density is naturally slightly rising the longer the blebbing process takes. Possible explanation for this is the rupturing of protoplasts and subsequently release of their cell content into the buffer resulting in more individual particles. But the rise in particle concentration was insignificant for a control group which was kept in simple GPMV buffer with the correct mannitol concentration. This leads to the conclusion, that the conditions are favorable for protoplasts which can usually survive intact with good osmotic conditions for more than 12 h. According to literature, chemically induced blebbing was never observed before but when looking at data obtained from mammalian experiments the average blebbing time is around 30 s for the inflation process and about 2 minutes for the retraction (Charras 2008) and might be a rough indicator for plant cells. All factors significant for blebbing are present in plant cells as well such as actomyosin in the cortex, actin membrane-linker proteins, actin-bundling proteins as well as myosin motor proteins. It is therefore assumed that the plant cells are also capable of forming blebs when freed from the CW.

3.4 Production of membrane fraction

The production of a membrane fraction, which is an isolation of the lipid enriched phase of a crude cell lysate was considerably easier than the production of bubbles and blebs. The remaining leaf tissue was treated as described above and stored away. Special care was taken to avoid too high protein concentrations above 1000 mg/mL and subsequent precipitation of proteins. The pH was therefore raised to pH 7 to avoid the precipitation of the majority of cytosolic soluble protein.

3.5 Characterization of PM-vesicles

To investigate the properties of each method, both techniques were tested on a monocotyledon (*Zea mays*) and dicotyledonous plant species (*Arabidopsis thaliana, Nicotiana benthamiana*), as shown in figure 9. In parallel the resulting blebs were characterized in size, charge, and concentration. SLPs formed with each fraction were characterized for diffusivity, confinement, protein orientation, protein mobility, and activity.
Although this vesicle based transporter method allows the incorporation of membrane protein into SLBs, there are key features that need to be addressed before this platform can be applied to study various plant molecular phenomena. Especially regarding the protein and lipid orientation, mobility, level and activity.

All three vesicle types were analyzed for concentration, size distribution and zeta potential. All samples were analyzed in GPMV (pH 7) buffer except the bubbles which remained in digestion buffer (GPMV + enzymes pH 7). It was tried to purify the bubbles from the digestion buffer but recovery yield after ultracentrifugation was not satisfying. The pH and salt concentration was equalized in both buffers prior to analysis. All three PM-vesicles were spun in a centrifuge at 2000 rcf for 3 min to get rid of potential precipitates or cell debris prior to measurement.

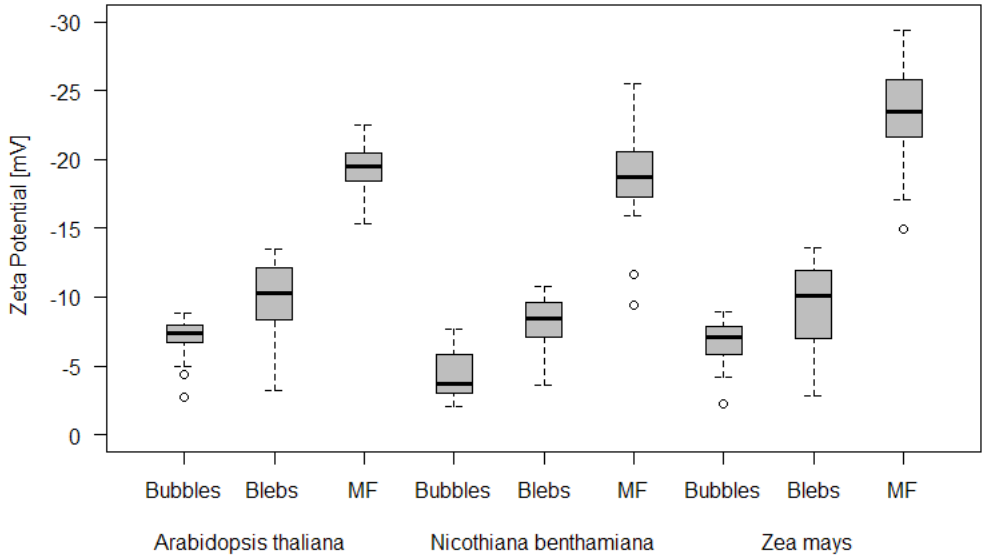

Figure 8: Zeta potential of all the plants and all vesicle types: The data was obtained from more than 30 individual measurements from six independent isolation experiment shows the zeta potential (ZP) for three plants and three different types of vesicles. The surface charge density is similar for all three plants with no significant difference between bubbles and blebs ranging from -10 mV to -5 mV. And a significantly higher charge for the MF around -20 mV. These results indicate that the origin of plant material has less influence on the zeta potential than the method of production. Impact on the surface charge density by the blebbing buffer and the associated chemicals seems to influence on the charge of the particles raising the average ZP between 25% for A. thaliana and 50% for N. benthamiana.

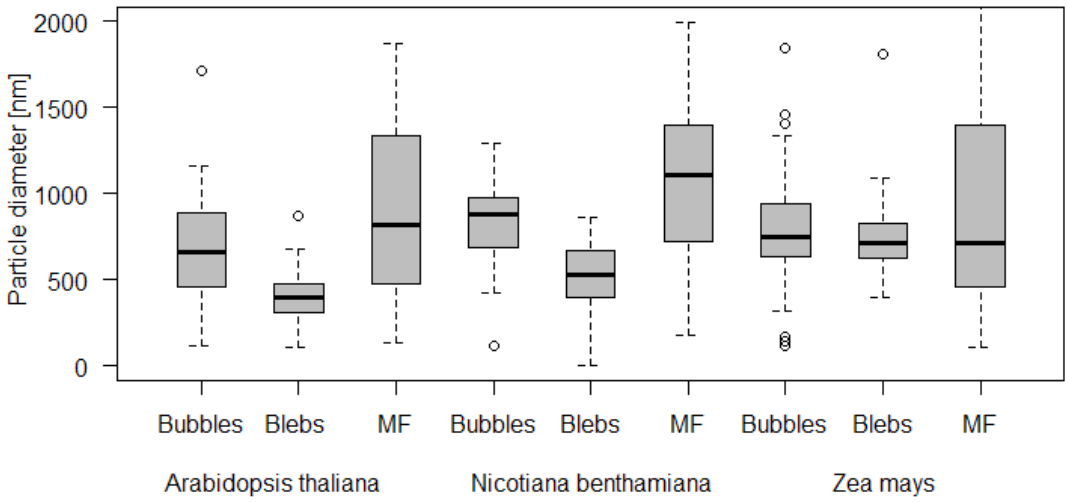

Figure 9: Particle size distribution: The size distribution obtained from more than 30 individual measurements from six independent isolation experiment shows the vesicle size distribution for three plants. Differences for vesicle types between the plant species are not significant. As the 95% quantile whiskers indicate, there is no significant difference between the individual vesicles with blebs (average 500 nm) as the smallest fraction. Bubbles (average 750 nm) as the second smallest fraction but a much higher dispersity grade which can be explained by the uncontrolled inflation during the osmotically driven production of vesicles. Membrane fraction (average 1000 nm) was produced the biggest vesicles with the highest heterogeneity.

As visible in Figure 10 the biggest influence on vesicle size was the centrifugal force which showed a negative correlation between relative centrifugal force/time and size/density of the individual particles. Hence bigger particles got cleared faster than small particles. The heterogeneity of the MF can be explained by the difficulty to suspending the ultracentrifugation pellet, which was done by pipetting and sonication (5 min, 80% in 10s intervals) but might still have left some vesicles agglomerated. The more homogeneous size distribution for blebs might be an indicator for the actomyosin contractions of the cortex, resulting in transient detachment of the bleb from the actin cortex of the mother cell (Charras 2008). The typical size range of cell blebs is between 100 - 500 nm with an upper maximum of up to 5000 nm (Charras 2008).

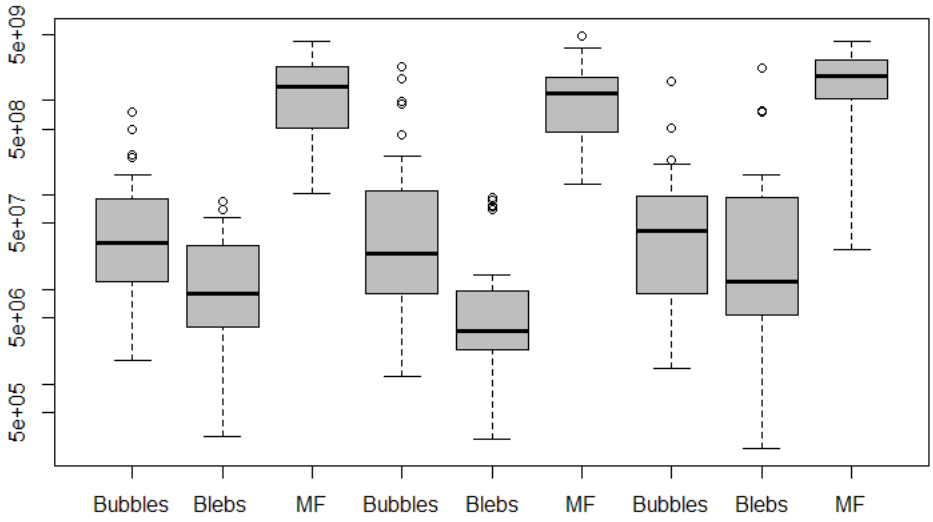

*Figure 10: Particle concentration: The concentrations of PM-vesicles isolated from blebs and bubbles was constantly around 5*10^{7} vesicles/ml. Due to the ultracentrifugation concentration step the particle concentration was considerably higher for the MF. Blank experiments showed a buffer concentration of 2* 10^{5} for the GPMV buffer. Particle concentration for blebs was significantly lower from blebs for mammalian cells 1*10^{9} (Liu et al. 2017) which was only achieved for plant vesicles with a MF isolation.:*

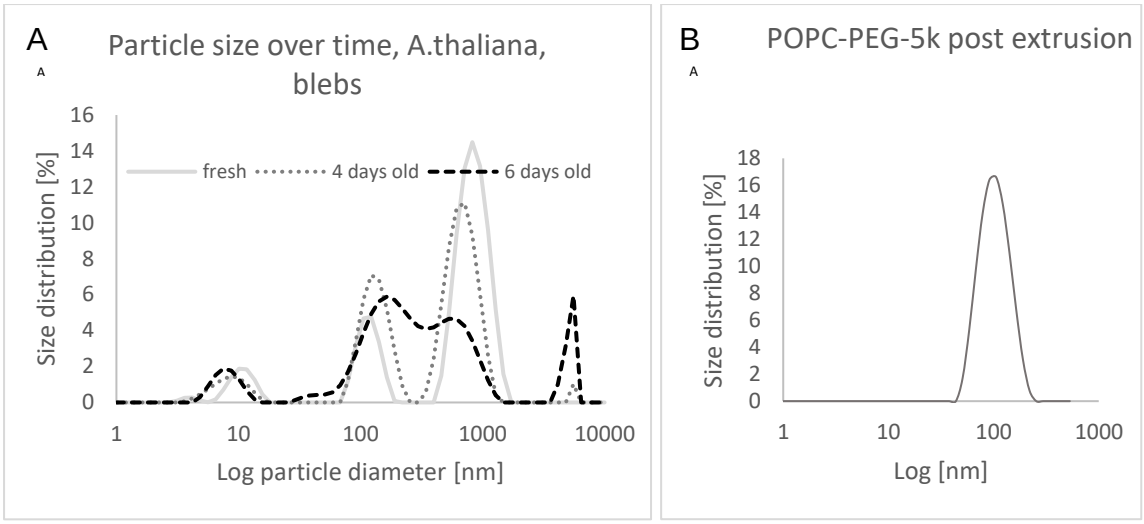

Figure 11: Intensity weighted particle size distribution over time: (A) The fresh bleb sample showed three peaks at 10nm, 200nm and 800nm. The smallest peak bight be cell debris which couldn't be cleared from the buffer due to its relative density. The other two peaks are probably cell blebs, it couldn't be clarified if both peaks are cell blebs. Over time the article distribution shifts towards a medium fraction around 400 nm and a big fraction of around 8000 nm which might be explained by auto vesicle fusion. (B) To evaluate the accuracy of the dynamic light scattering measurements of the Zetasizer the fusogenic liposomes extruded with a 100 nm nylon membrane were measured and showed the expected Gaussian distribution profile around 100nm.

Due to the complete lack of information on plant blebs, which was already stated by (Charras 2008) storage conditions were monitored over the bleb lifetime, while the ZP stayed constant over two weeks (data not shown) the particle size distribution was subject to change. This change was monitored for 6 days showing a clear shift in size distribution.

3.6 Scanning electron microscopy (SEM)

3.6.1 BUBBLES:

Due to the crude cell lysate for the bubble production the imaging was mainly performed in native cracks (Figure 13) that were obtained by the freezing process. We were able to capture the full digestion process, starting at full cell wall fragments as shown in Figure13 showing two empty neighboring cells. Down to 400nm small spherical structures further addressed as bubbles shown in Figure 14. The plasmodesmata channels are clearly visible in Figure13 showing the abundance of these communication and transport pipes between two cells. According to my bubble hypothesis these plasmodesmata play a crucial role in dispersing the cytoplasm filled PM into the exoplasmic space producing bubbles.

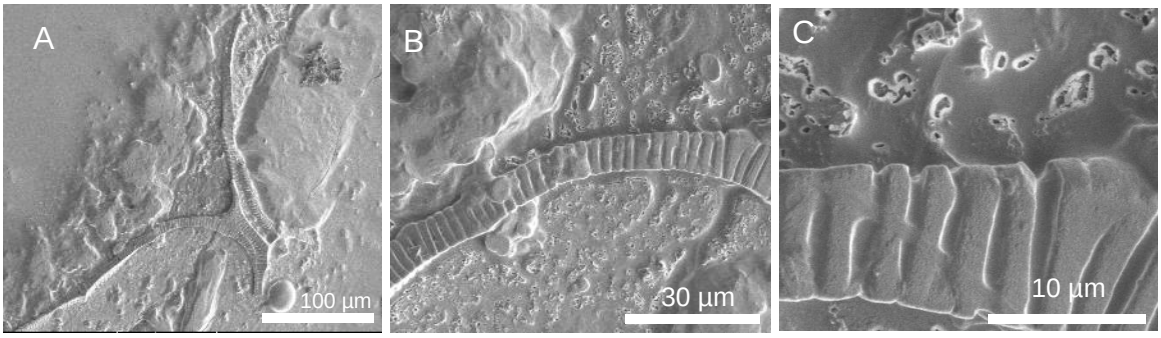

Figure 12: Cryo SEM images of whole plant cells during digestion: (A) Two semi digested parenchyma cell walls bordering each other with the lumen already released, next there is an intact spherical chloroplast. This picture was taken 30 min post digestion start. (B) Detail of the secondary cell wall with clearly visible plasmodesmata channels. The CW is already empty as there is no protoplast inside the cell. (C) Detail of the plasmodesmata tubes connecting the individual plant cells.

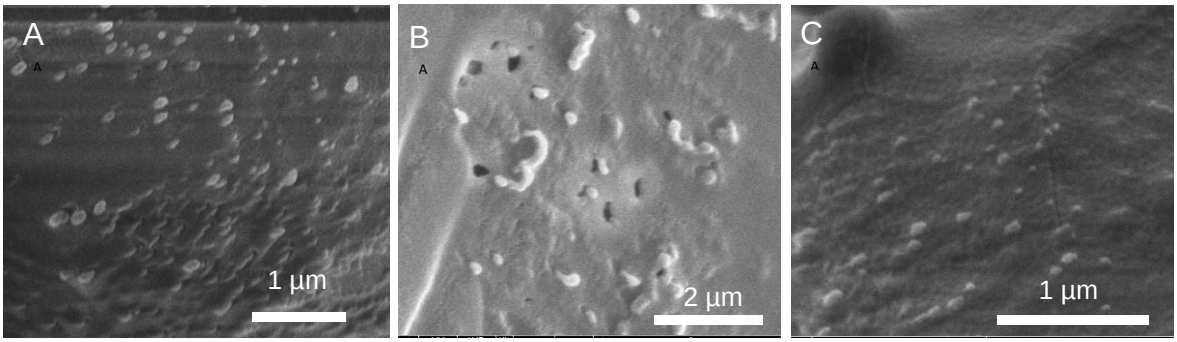

Figure 13: SEM images of spherical objects addressed in the following as bubbles: (A) Bubbles images in a natural crack next to a Chloroplast. The majority of spherical objects seems to be around 200nm to 400nm. (B) Bubbles on the cell surface next to holes where they might have been produced (C) Bubbles imaged here show a slightly deformed structure which could be explained by the cryo conservation process. Although the size distribution is very broad as visible in Figure 13 the majority of spheres ranges from 200 - 2000 nm in diameter, which is the average size of bubbles supported by light scattering measurements on the Zeta-sizer.

3.6.2 BLEBS**:**

The formation of blebs was also observed 20 min after transferring the purified protoplasts into the blebbing solution. Due to the higher dilution of protoplasts in the blebbing buffer it was not possible to capture the abundance of images as for the bubble procedure. Never the less we are able to show that blebs are produced already after 20 min and bud off the protoplasts see Figure 14. The blebbing conditions were optimized by (Liu et al. 2017) for mammalian cells. Starting off with this protocol we optimized the conditions for plant cells using dynamic light scattering and maximizing the fraction between 200 nm and 800 nm.

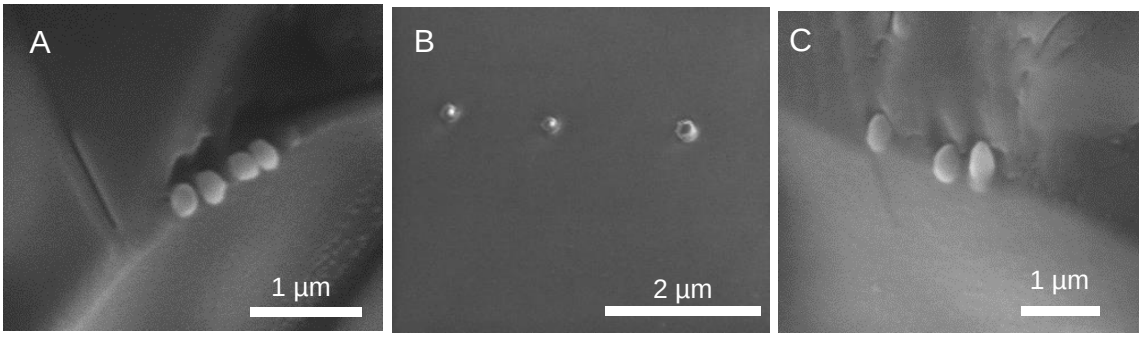

Figure 14 Cryo SEM images of spherical objects addressed in the following as blebs: (A) Four blebs of about 400 nm diameter next to each other monitored in a crack, (B) Blebs on the surface of the cryo sample, (C) Blebs imaged in a crack where they seem to peel out of the fractionated sample.

3.7 Characterization of protein expression in cells

Protein expression was first qualitatively confirmed by confocal microscopy. As all target proteins had fluorescent protein linked to them the protein was observed under the according emission spectra. This was done at the macroscopic level of full and intact leaf tissue to see where the protein is located after expression.

Due to the lack of site specific monoclonal antibodies for most of the target proteins the fluorescent tag (GFP, YFP or RFP) was detected under the TIRF microscope and the presence of the full construct was confirmed by a coomassie blot see Figure 16. The last confirmation step was performed on a TIRF microscope with a laser excitation of the fluorescent tag at the appropriate excitation wave length.

Protein concentration was low compared to mammalian cell culture determined by nanodrop measurements, which is well-known for plant expression systems. Especially for transgenic hosts the protein expression can be up to 100x lower than for transient expression (Melnik et al. 2018). Expression of fluorescent protein was qualitatively checked with a confocal microscope and coomassie staining for all three constructs.

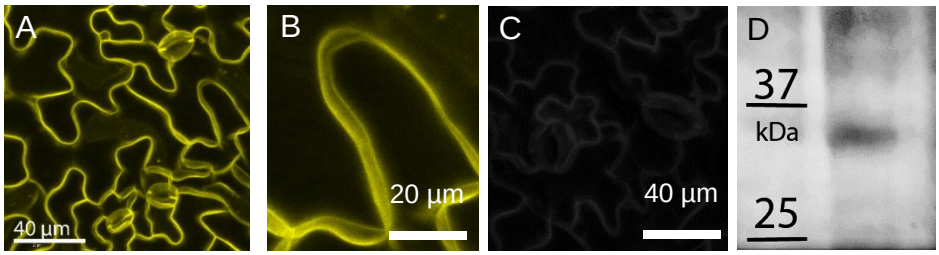

Figure 15: Characterization of RCI2A protein from Arabidopsis thaliana: (A) The RCI2A::YFP (~34 kDa) construct stably expressed in Arabidopsis showing a homogeneous and very strong expression all over the PM. (B) Detail of the CW shows a clear separation of the two PM's and indicates that the construct doesn't get secreted into the apoplastic space and is detached from the PM. (C) Negative control (D) Coomassie staining showing a band at around 34 kDa which is the molecular weight of RCI2A.

The SbMate::YFP (~55 kDa) construct was transiently expressed in N. benthamiana using initially a leaf infiltration and protoplast transformation approach. Later experiments reached transformation rates up to 80% using a protoplast transformation approach. The expressing protoplasts were checked under a confocal microscope as shown in Figure 17 showing a clear illumination at the protoplast PM (yellow). Negative control groups didn't show any expression at the PM. Only the chloroplasts Figure 17C, which are shown in in red. A coomassie blot was used to double check for the presence of a construct of the right size.

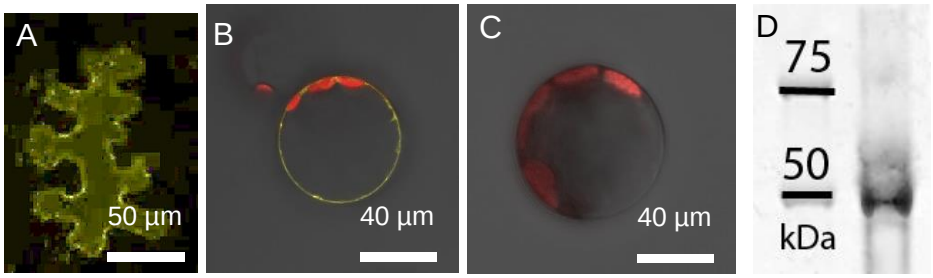

Figure 16: Characterization of SbMate protein from Arabidopsis thaliana: (A) The SbMate::GFP (~55 kDa) construct transiently expressed in Nicotiana benthamiana protoplasts (B) strong expression of SbMate after the protoplast digestion visible around the PM (C) Negative control with an untransformed protoplasts. (D) Coomassie staining showing a band at around 55 kDa which is the molecular weight of SbMate.

The PIN1::YFP (~19 kDa) construct was stably expressed in Z. mays showing a clear expression all over the PM. A coomassie blot was used additionally to confirm the presence of a construct of the right size via a full plant lysate shown in Figure 18. Expression of Pin1 was lower than the other two constructs. This is commonly observed for stable expression systems and can be explained by the fact that a

D

transgenic protein Pin1 stable expressed represents a metabolic burden for the plant.

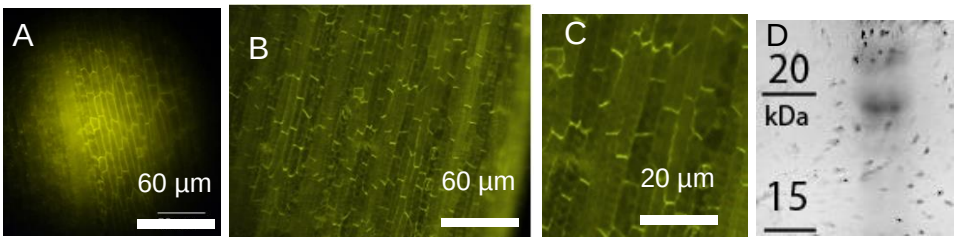

Figure 17: Characterization of Pin1 protein in Zea mays: (A) The Pin1::YFP (~18 kDa) construct stable expressed in Zea mays (B) strong expression of Pin1::YFP in the leaf tissue (C) Closer look at the abaxial side of the Zea mays leaf (D) Coomassie staining showing a band at around 18 kDa which is the molecular weight of Pin1::YFP.

3.8 Quartz crystal microbalance

QCM-D was used to monitor the formation of SLBs from plant PM-derived vesicles on silicon oxide surfaces. The QCM-D profiles of a *N. benthamiana* blebs shown in Figure 19 as well as for *N. benthamiana* bubbles shown in Figure 20 are showing a successful deposition of vesicles and rupture to a SLB. First 50 s are used for equilibration of the sensor to the buffer followed by the flow in of blebs leading to an upshift in mass on the QCM sensor which is saturated after ~200 s. One minute to determine the baseline for Δ_F and Δ_D is a bit short but the data was reproducible and stabilized usually within this timeframe. Additionally, the measurement was started one minute prior to the first vesicle inflow to confirm the stable baseline. If the baseline of the third overtone showed changes of more than 5 Hz the recording was stopped and started over again after another minute. If the baseline was still not stable the sensor was removed from the chamber and a new sensor installed. All overtones were recorded but only overtone 3 of the frequency and dissipation was used for analysisIn the next step the fusogenic liposomes are introduced leading first to a mass upshift followed by the characteristic rupture curve when water is released and mass attached to the sensor is removed resulting in a frequency upshift. The rupture profile after injection of fusogenic vesicles should give a good indicator for a formed bilayer. But it is difficult to evaluate the formation of a continuous SLB or just individual bilayer discs on the sensor. The excess of fusogenic liposomes (2mg/mL) should provide enough material to form a continuous SLB sheet. But QCM-D is not the right tool and other tools were chosen to do so.

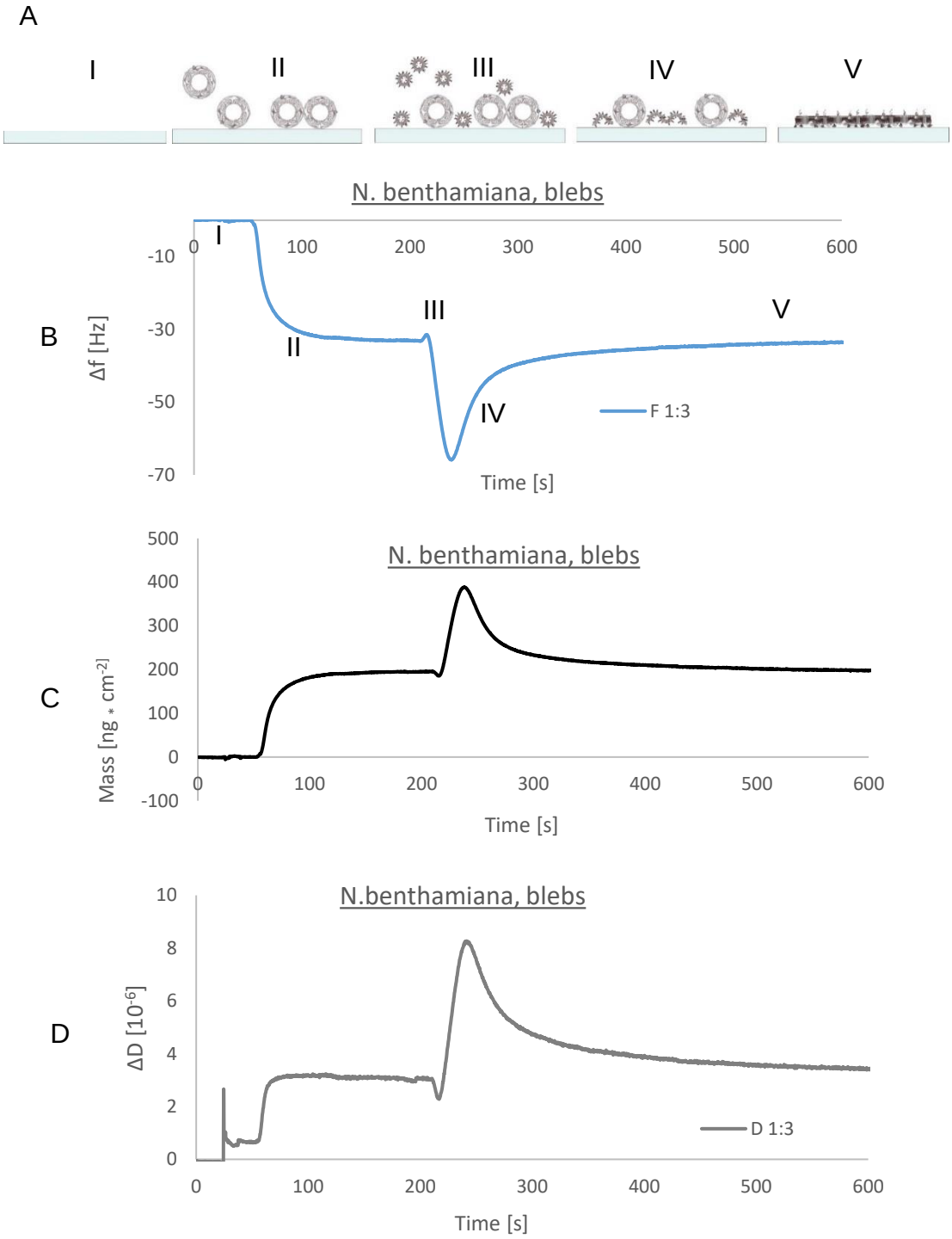

*Figure 18: QCM profile of Nicotiana benthamiana blebs: (A) show the supported lipid bilayer formations of pure fusogenic vesicles in GPMV buffer pH 5.5. For the control experiments, pure fusogenic rupture vesicles (99.5% [w/v] POPC, 0.5% [w/v] POPC-PEG-5000) were used to form a bilayer. Depiction of QCM workflow (I) Injection of PM-vesicles, (II) Injection of rupture vesicles (III) Injection of the fusogenic rupture vesicles, (IV) Self-assembly of SLB, (B) Change in the third frequency overtone (C) Calculated mass deposition on the quartz sensor, as the upshift is only 50 ng * cm-2 from deposition to final rupture the blebs might have been ruptured or not, but when looking at the dissipation a clear tendency towards successful rupture is shown (D) Dissipation profile during the rupture process shows an upshift in ΔD which vanishes later to almost the same level as during the vesicle attachment phase from 80 s to 220 s.*

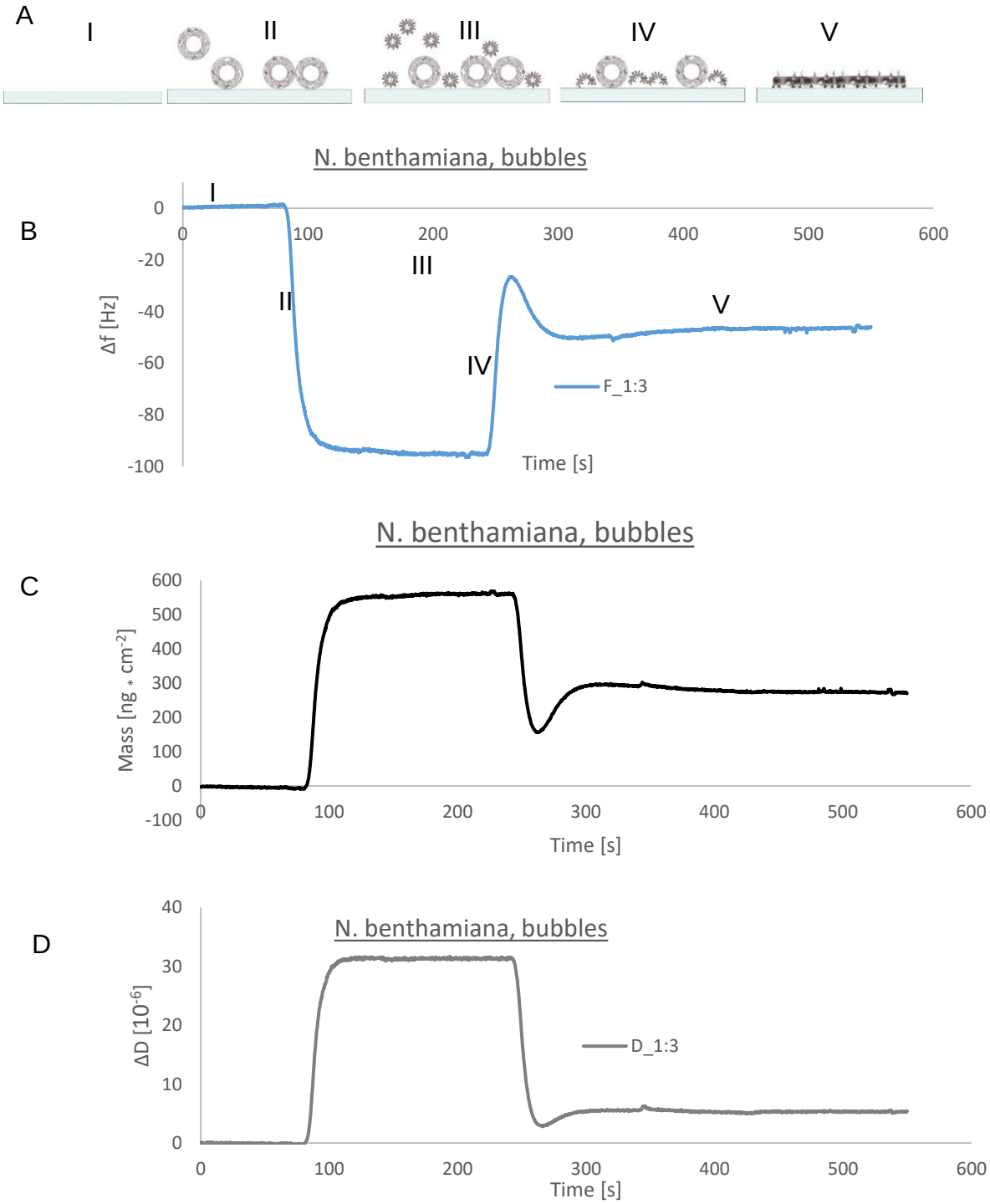

*Figure 19: QCM profile of: QCM profile of Nicotiana benthamiana blebs: (A) Depiction of QCM workflow (I) flow in on PM-vesicles, (II) Injection of fusogenic vesicles (III) Auto rupture of fusogenic vesicles, (IV) Self assembled SLB, (B) Change in the third frequency overtone indicating a mass deposition (C) Calculated mass deposition on the quartz sensor, as the upshift is about 400 ng * cm-2 less than the pure vesicles themselves. This downshift in mass can be explained by the release of water from the vesicles into the buffer. When looking at the dissipation a clear tendency towards successful rupture is shown (D) Dissipation profile during the rupture process shows a slightly higher upshift than for the blebs. This indicates, that something has bound to the sensor and then become more compact probably due to the release of water.*

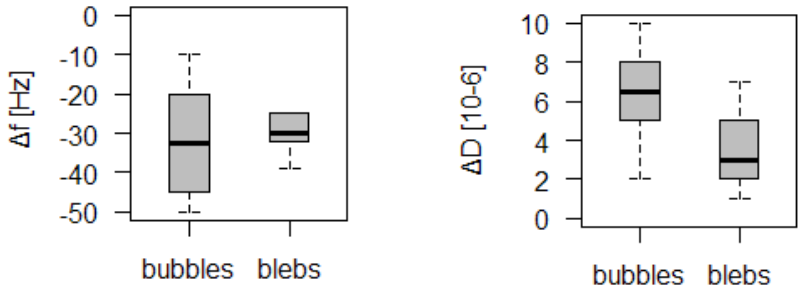

Figure 20: Summarized changes in frequency and dissipation after 600 s: (A) Total change in frequency of (N=6) experiments, (B) Total change in dissipation (N=6) indicating that bubbles lead to a bigger mass deposition than blebs.

The dissipation change in figure 19D is not indicating a successful rupture when compared to 20D. One possible explanation for this observation could be the material of the QCM sensors were composed. Although they were composed of glass (silicon oxide) such as the cover slips used in the microscopic experiments the comparison is difficult. The difference in elemental composition is probably the minor influence but the surface texture is probably the major influence on the bilayer formation. As shown in figure 20D is the final ΔD bigger for the bubbles than for the blebs. One possible explanation would be a deposition onto the sensor which is less than just pure PM-vesicles but more than the empty sensor. From this data is is also hard to conclude that the fusogenic vesicles are replacing the PM-vesicles or if they are rupturing. At this point FRAP experiments can offer important insights intot the rupture and formation of the bilayer.

3.9 Characterization of SLBs using FRAP

Figure 22 shows rupture processes for vesicles of three plants and different production processes. The non-fluorescent structure in the corner of figure 22 B-C is a scratch used as a reference to focus. As the rupture process is starting dark, than getting blurry and finally ending bright white it is not possible to check if the picture is taken in focus without a scratch mark. The pictures are taken at irregular time intervals for the first picture showing the R18 PM-vesicles attached to the glass slide. The vesicles are labeled with R-18 dye but quenched by the proximity of the neighboring rhodamine fluorophores. One fluorophore is emitting a virtual photon which is instantly absorbed by the neighboring fluorophore.

Picture one shows the rupture process about 2 s – 5 s after adding the fusogenic vesicles. Picture three is taken about 5 s – 10 s after the initial rupture process started. The irregularities in the fourth picture are due to time of exposure which ranges for the fourth picture from 1 min post fusion up to 30 min post fusion. A homogeneous layer of fluorophore is indicating that the formation of a continuous bilayer is completed. Rupture was observed for all labeled PM-vesicles and can be found in Appendix A, displayed here are bubbles of all three plants. The fusogenic vesicles are not labeled and do not contribute to the fluorescence signal when they rupture.

The final image obtained 30 min post-rupture is displaying sometimes brighter domains as in Figure 22 subsection D location IV. The small bright spots can be explained by unruptured vesicles. The brighter bigger domains are always vanishing after a while and can be understood as a snap shot of the spreading process. They are indicative of long range mobility of the lipid dye.

After the homogenization is completed the bilayer showed an evenly distributed fluorescence. All FRAP-images were obtained by using R18 incorporated into the native cell vesicles. No fluorescent proteins were used for the FRAP experiments.

A

Arabidopsis thaliana: Bubbles + POPC-PEG-5000

B

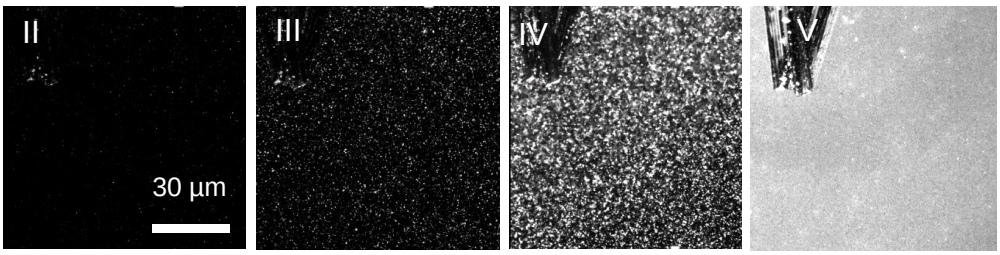

Nicotiana benthamiana: Bubbles + POPC-PEG-5000

C

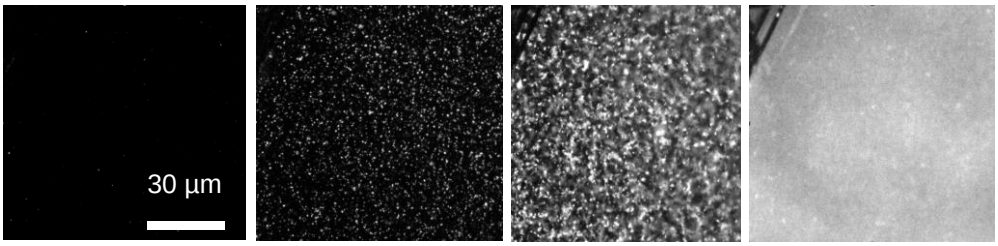

Zea mays: Bubbles + POPC-PEG-5000

D

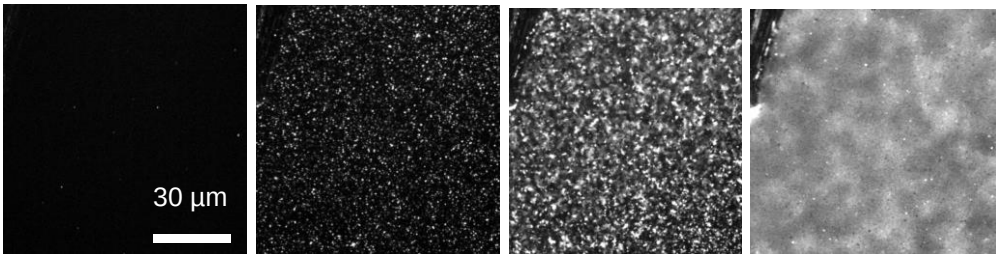

Figure 21: Rupture process induced by fusogenic vesicles at bubbles from three different plants. Blebs and MF ruptured identical and was put into the supplemental Appendix A: (A) Simplified rupture comic, (B) Rupture and dequenching of Arabidopsis bubbles, (C) Rupture and dequenching of Nicotiana benthamiana bubbles, (D) Rupture and dequenching of Zea mays bubbles.

The observed rupture process was similar for the vesicles of all three plants and similar for all three vesicle types. As shown in figure 22 / B / V most even rupture and highest recovery was observed with bubbles. This was true independent of the plant species. For the membrane fraction dye impurities in the bilayer were very common due to the very crude production process. It couldn't be confirmed, if the data is showing reliable results due to impurities. The big variability in diffusion coefficient D was observed with the diffusion coefficient of the membrane fraction ranging from 0.15 $\mu m^2/s$ to 0.44 $\mu m^2/s$. N. benthamiana bubbles were used fresh and stored at 4° C for about a week. This ripening process seemed to precipitate some of the soluble

protein and the secondary plant components which are otherwise remaining in solution. The ripened bubbles produced the most homogeneous bilayers with the least impurities.

To evaluate the recovery of the R18 dye in the bilayer a laser spot was bleached after incubating the chip for at least 15 min. The raw data shown as dotted line was fitted with a simplified Soumpasis equation to calculate the fluorescently labeled lipid diffusion coefficient. The images shown in figure 23 were taken at 5% laser power and exposed for 100 ms per image. Pictures were taken at time point A right after the laser bleaching, image B shows the same bleach spot after about 30 s – 60 s with image C showing the full recovery after about 20 min to 35 min post bleaching showing full recovery. The mobility of the eighteen carbon chain of R-18 inserted into the lipid bilayer is showing a continuously formed bilayer. The diffusion coefficient was measured to confirm the consistency and repeatability of the data. The membrane mobility as well as the lipid diffusion coefficient although proportionally related to the diffusion coefficient of R-18 can't be determined by this procedure. But the long range mobility and mobile fraction wan be used to indicate that a continuous SLB was formed.

The factor t_d as calculated from formula (3) is conditional on the diffusion coefficient and marks the point in time when half of the FRAP spot is recovered. With the mobile fraction (MF) showing the level of recovery ranging from 93% to 98%. This factor is influenced by multiple factors such as sample purity, formation of immobile micro domains, protein content, as well as smoothness of the silica surface. These values are comparable to diffusion coefficient values observed in other systems such as bacterial outer membrane vesicles (OMVs) being in the same order of magnitude (Hsia et al. 2016). Figure 23BII shows a darker semi-circle in the lower part of the FRAP spot, this is a speckle pattern produced by interference of the laser beam. The asymmetry of the bleach-spot which can be observed in some images is due to the mirror and lens arrangement. The lens system was fine-tuned every week to try to achieve a circular bleach spot.

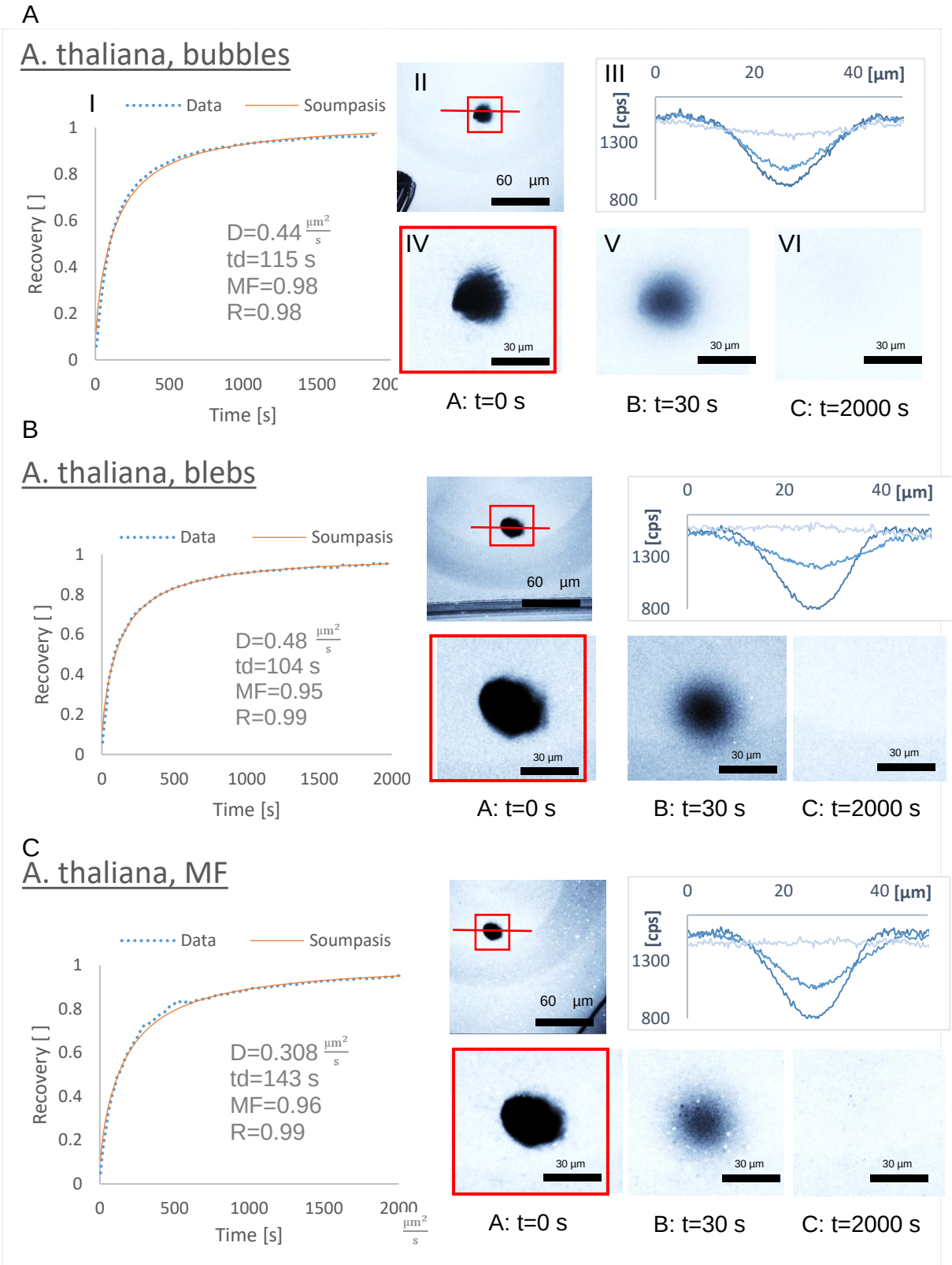

Figure 22: FRAP profile of bubbles, blebs and MF: (A) Bubbles, Arabidopsis thaliana, (I) raw data and Soumpasis fit to calculate the diffusivity, (II) Area of interest (AOI) with the scratch mark in the corner, (III) cross section of the recovery profile to demonstrate recovery due to mobility and not by photo bleaching, (IV) Close up of the frap spot at time zero, (V) Close up of the FRAP spot after 30 seconds, (VI) Close up of the FRAP spot after 2000s showing a complete recovery (B) Blebs, Arabidopsis thaliana (C) MF, Arabidopsis thaliana.

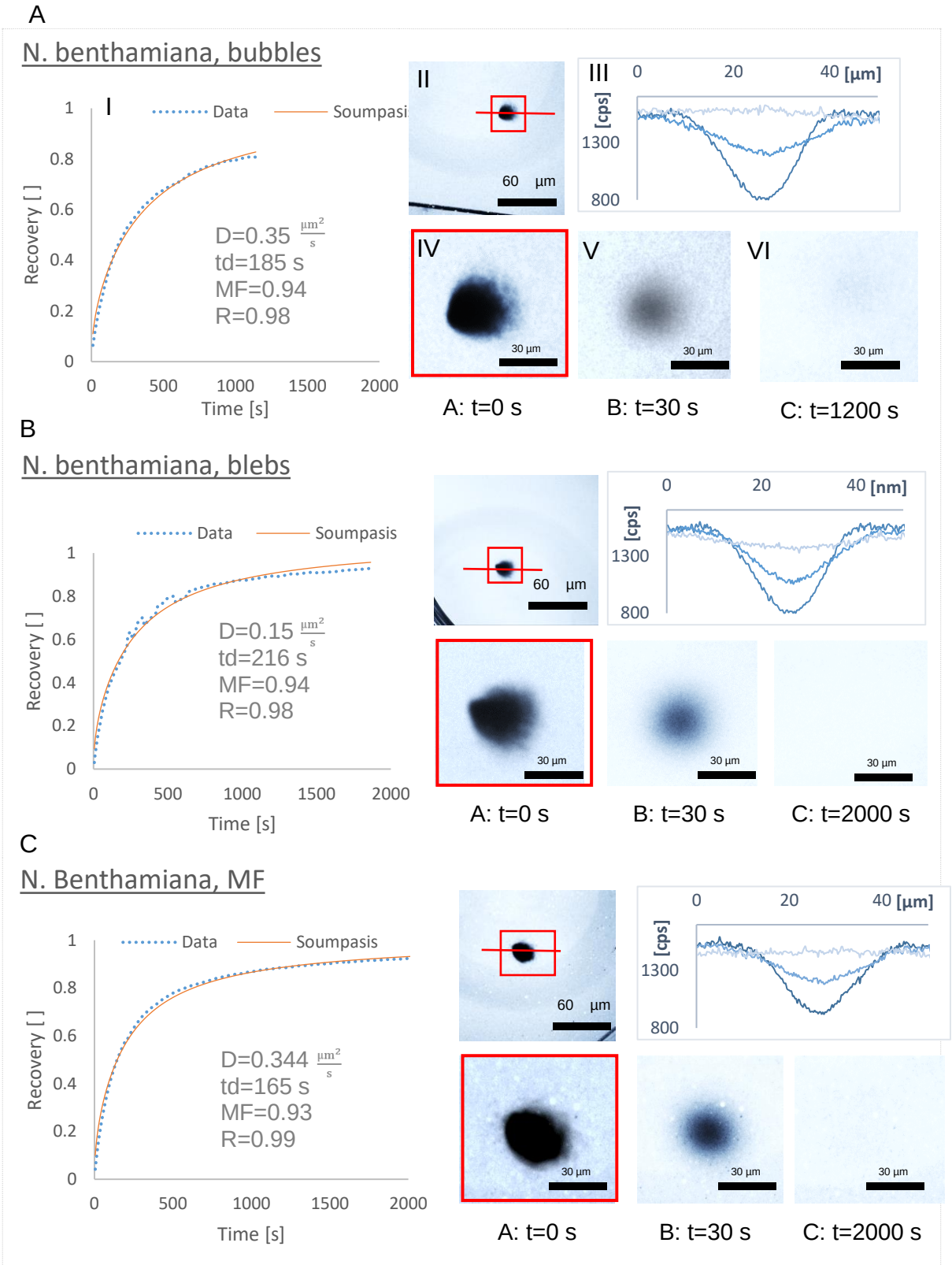

Figure 23: FRAP profile of bubbles, blebs and MF: (A) Bubbles, Nicotiana Benthamiana, (I) raw data and Soumpasis fit to calculate the diffusivity, (II) Area of interest (AOI) with the scratch mark in the corner, (III) cross section of the recovery profile to demonstrate recovery due to mobility and not by photo bleaching, (IV) Close up of the frap spot at time zero, (V) Close up of the FRAP spot after 30 seconds, (VI) Close up of the FRAP spot after 2000s showing a complete recovery (B) Blebs, Nicotiana Benthamiana (C) MF, Nicotiana Benthamiana.

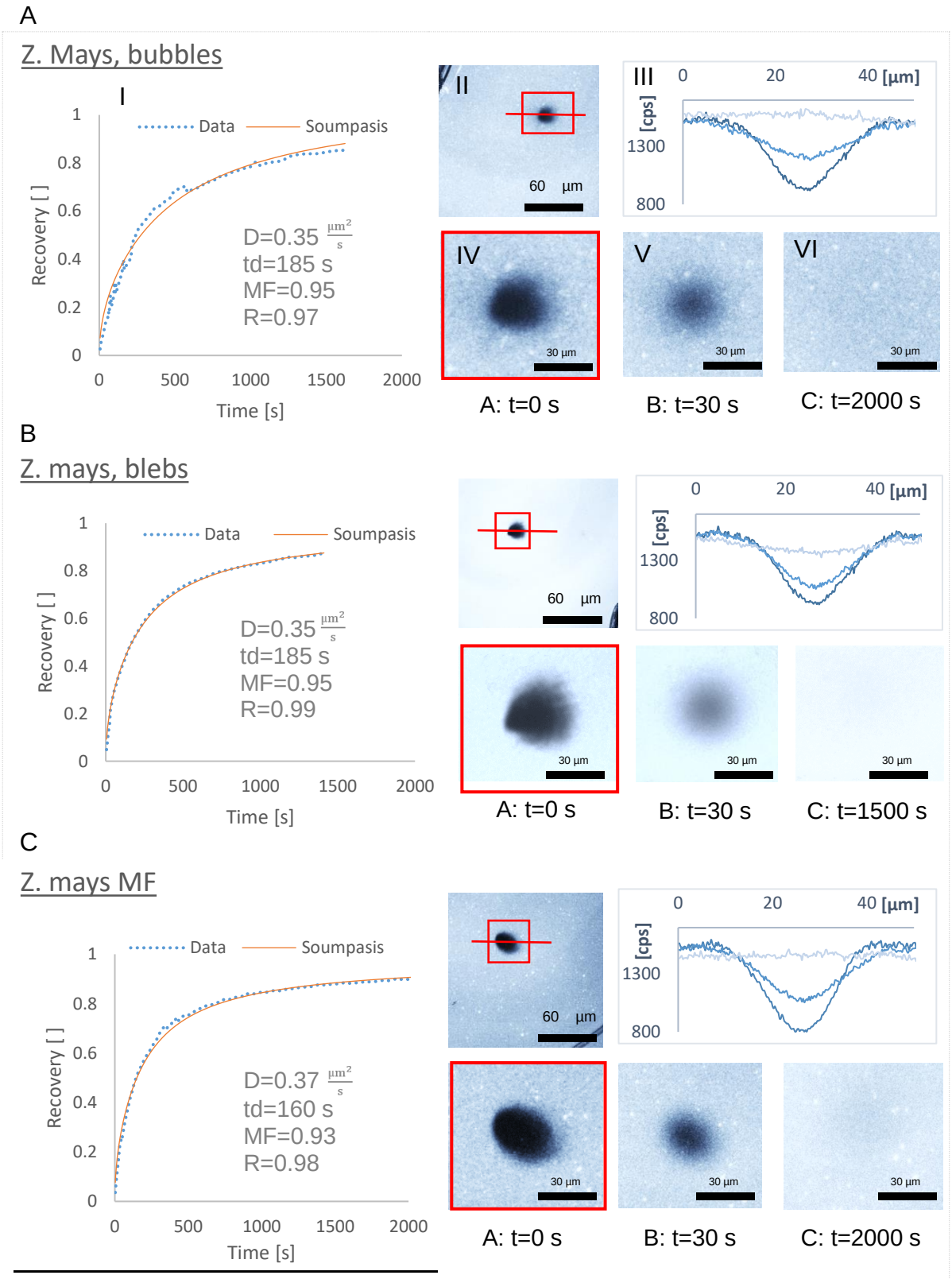

Figure 24: FRAP profile of bubbles, blebs and MF of Zea mays: (A) Bubbles, Zea mays, (I) raw data and Soumpasis fit to calculate the diffusivity, (II) Area of interest (AOI) with the scratch mark in the corner, (III) cross section of the recovery profile to demonstrate recovery due to mobility and not by photo bleaching, (IV) Close up of the frap spot at time zero, (V) Close up of the FRAP spot after 30 seconds, (VI) Close up of the FRAP spot after 2000s showing a complete recovery (B) Blebs, Zea mays (C) MF, Zea mays.

To confirm that the recovery of the bleached spot is due to diffusion of unbleached R18 fluorophores into the bleached spot and not by homogeneous photobleaching of the surrounding area, we analyzed the recovery of each bleach spot. As shown in each graph above, the slope of the Bessel function of the bleach spot is not staying constant, which would be an indicator for photobleaching but rather changing constantly throughout recovery. All experiments are summarized in Figure 26A values for Diffusivity ranged from 0.17 $\mu m^2/s$ to 0.44 $\mu m^2/s$ with no significant difference between the different PM-vesicles nor the three plant types. This is as expected as only the diffusivity of the R18 fluorophore is measured within the bilayer. The consistency of the results ranging around 0.30 ± 5 $\mu m^2/s$ is a good indicator for a stable system. All boxplots display the 50% quantile in the box as well as the 95% confidence intervals with the whiskers whereas outliers are marked as circle.

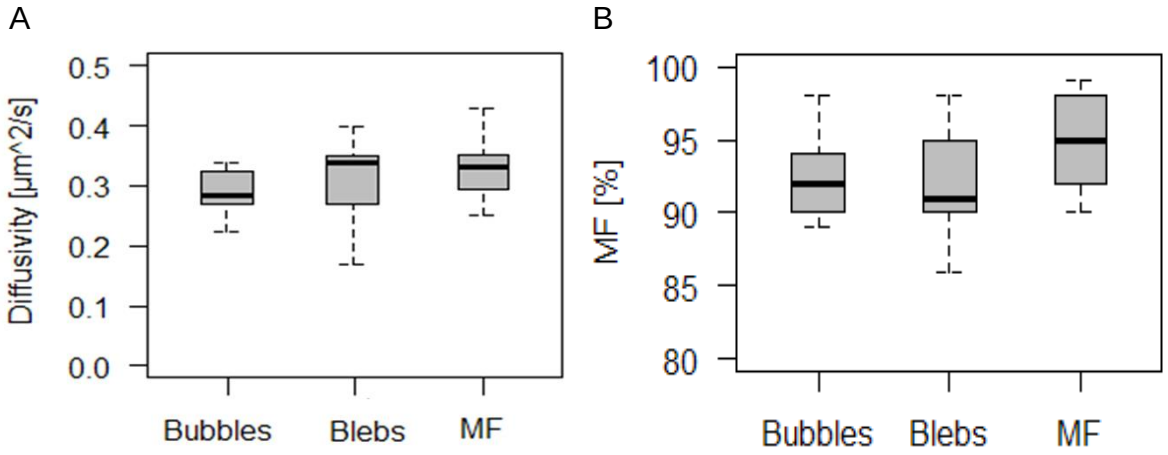

Figure 25: Summary of Diffusivity and Mobile fraction of all FRAP experiments (N=30): (A) Total diffusivity ranges around 0.3 for all three fractions with a broader distribution for the blebs and MF (B) Summarized MF for all three fractions showing an average mobile fraction between 90% and 95%. The best recovery was obtained using the MF.

The differences in diffusivity can be explained by the laser bleached spot. Over the time of 6 months the laser lenses had to be adjusted several times resulting in slightly changed structures for the bleach spot. The used Soumpasis equation is optimized for a circular and homogeneous bleached spot. Any divergence from this optimal conditions was already leading to major changes in diffusivity up to 100% leading to the exclusion of some experiments from the displayed graphs. The summary of all results is summarized in Figure 26B including all experiments for diffusivity and mobile fraction. The results obtained from the FRAP experiment show only the unrestricted short range diffusion. It is only partially informative to draw conclusions about the long range diffusivity.

3.10 Characterization of protein orientation in SLB

When producing a SLB the membrane is undergoing two major transformations. The first is initiated at the cell and leads to the vesicle formation and budding off the plasma membrane. This process is considered to lead to apoplastic out structures that maintain the native cell structure just as a miniature version. The second big transformation happens after the vesicles have adhered to substrate followed by a rupture step induced my fusogenic vesicles injected into the system. PM- vesicles are attached to the hydrophilic glass substrate surrounded by fusogenic vesicles. These PM-vesicles attach to the silica substrate and remain in vesicular shape whereas the fusogenic vesicles are inherently less stable and auto rupture as soon as they get into contact with the surface triggering also the rupture of the PM-vesicles. The unfolding process of liposomes was already investigated by (Reimhult et al. 2009) and shows a clear tendency towards parachute rupture for smaller vesicles as well with a much smaller fraction (especially bigger vesicles) collapsing chaotically and rearranging again on the surface.

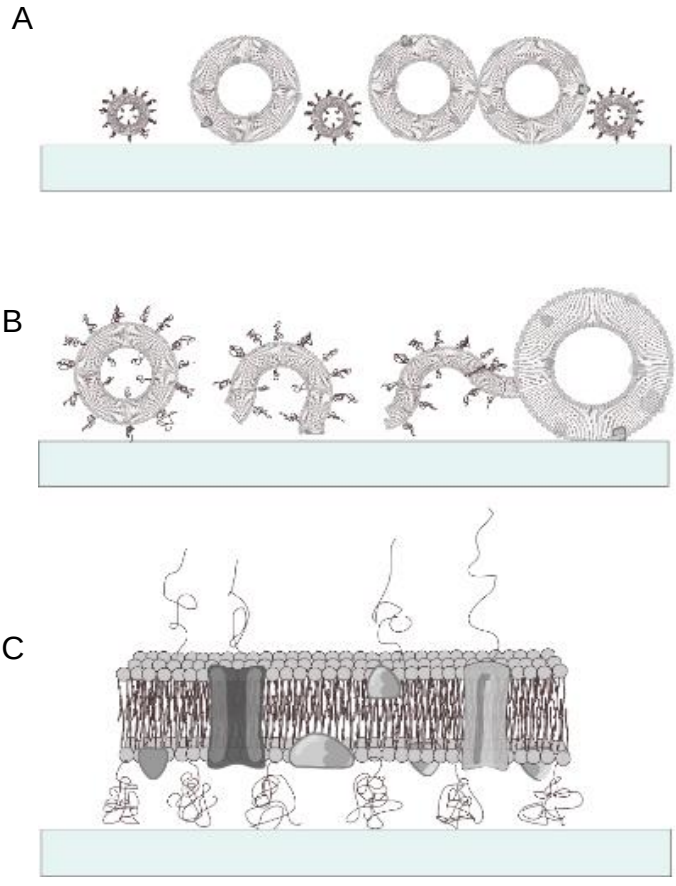

Figure 26: Overview rupture process of plant PM-vesicles by fusogenic vesicles.

(A) Attached PM-vesicles on silica substrate in GPMV buffer. The smaller vesicles are fusogenic vesicles made of POPC-PEG-5000 to form a cushion.

(B) Auto rupture of fusogenic vesicles as soon as they get into contact with the silica substrate triggering the rupture of PM-vesicles.

(C) Fully ruptured SLB after about 30 min. The Peg-5000 is functioning as cushion providing a 4-5 nm space between the silica substrate and the SLB.

During the vesicle rupture process the main driving forces arise from the van der Waals interactions.. The 1 nm gap between the vesicles and the silica substrate is small enough to bind the vesicles non-covalently to the silica and deform them. During the rupture and the following spreading of the SLB disc, the reduction of “line tension” at the edge of the SLB islands is triggering the fusion with the next neighboring vesicle. Once the next vesicle is touched by the edge of the SLB island the van der Waals forces are pulling the vesicle in a planar configuration facilitated by the self-arrangement of the phospholipid tails towards the hydrophilic phase. For mammalian blebs it was found by lipid orientation and protein orientation assays that they rupture primarily in a parachute mode (Liu et al. 2017) and rearrange again in an apoplastic up 2D planar sheet. This supported lipid bilayer can be used as biomimetic platform as the protein orientation is the same as in a native plant cells.

Due to the lack of data on orientation for plant PM-vesicle a protease cleavage assay was carried out. The *Arabidopsis thaliana* stable expressed protein RCI2A was used for this assay to compare a protein with the fluorescent tag in the outer leaflet and the fluorescent domain buried underneath the supported lipid bilayer.

According to our hypothesis of “inside down” or “parachute” rupture the protein of RCI2A should not be cleaved by protease whereas the fluorescent domain of the extruded sample with has a 50% distribution of the protein in the outer and inner leaflet should be cleaved if exposed to the protease. Two possible scenarios can be imagined if the fluorescent domain is exposed to the protease. First, the protease is cutting at the linker region resulting in the cleaved portion of the fluorescent signal floats out of the evanescent field generated during TIRFM. Second the exposed fluorescent domain is directly degraded by the protease resulting in a defunct fluorescent domain and therefore loss of signal. Additional control cases without proteinase K treatment were set up, where the fluorescent signals remained unchanged over time experiencing only collective photo bleaching. Monomeric yellow fluorescent protein (mCitrine) was N-terminally fused to a small (approximately 6 kD) membrane protein (AtRCI2A) and stably expressed in *Arabidopsis thaliana* (Columbia-0 ecotype) (Thompson & Wolniak 2008). Whereas those experiments with proteinase K treatment showed prominent drops in RCI2A-YFP signals as shown in Figure 27D. The results indicate that the mCitrine is located in the inner leaflet hence below the SLB and cannot be be reached by protease. This

shows that in bleb bilayers, the GPI-YFP protein orientation is maintained as in live cells. These results show, that blebs rupture as a “parachute,” while keeping luminal sides downward facing the glass slide when the bilayer forms(Hsia et al. 2016; Fuhrmans & Mueller 2013), and that this mechanism seems to be preserved regardless of the chemical blebbing agent or other method used to generate the blebs.

The negative control group showed no fluorescent activity, indicating that the plant lines used for the transfection were wild type and therefore not containing any fluorescently active domains.

To avoid photobleaching an experiment was set up to determine the photo-stability of the fluorophore. The photo bleached sample showed a different change than the protease cleaved one, reducing the contrast between fluorescence signal and background. Extrusion through a one-way membrane composed of Polyhexamethylenadipinacideamid was used to disrupt the vesicles resulting in a mixed orientation. Unfortunately was the protein yield for extrusion was about 50% per passage resulting in less protein to track. The untreated native vesicles showed no effect upon protease treatment within the first 30 min. Loss of fluorophore function was the inevitable effect after about an hour which can be explained by defects in the SLB or the entrance underneath the SLB via holes.

The extrusion experiment was repeated 10 times with an average protease cleavage rate of 50% ± 10% relative error.

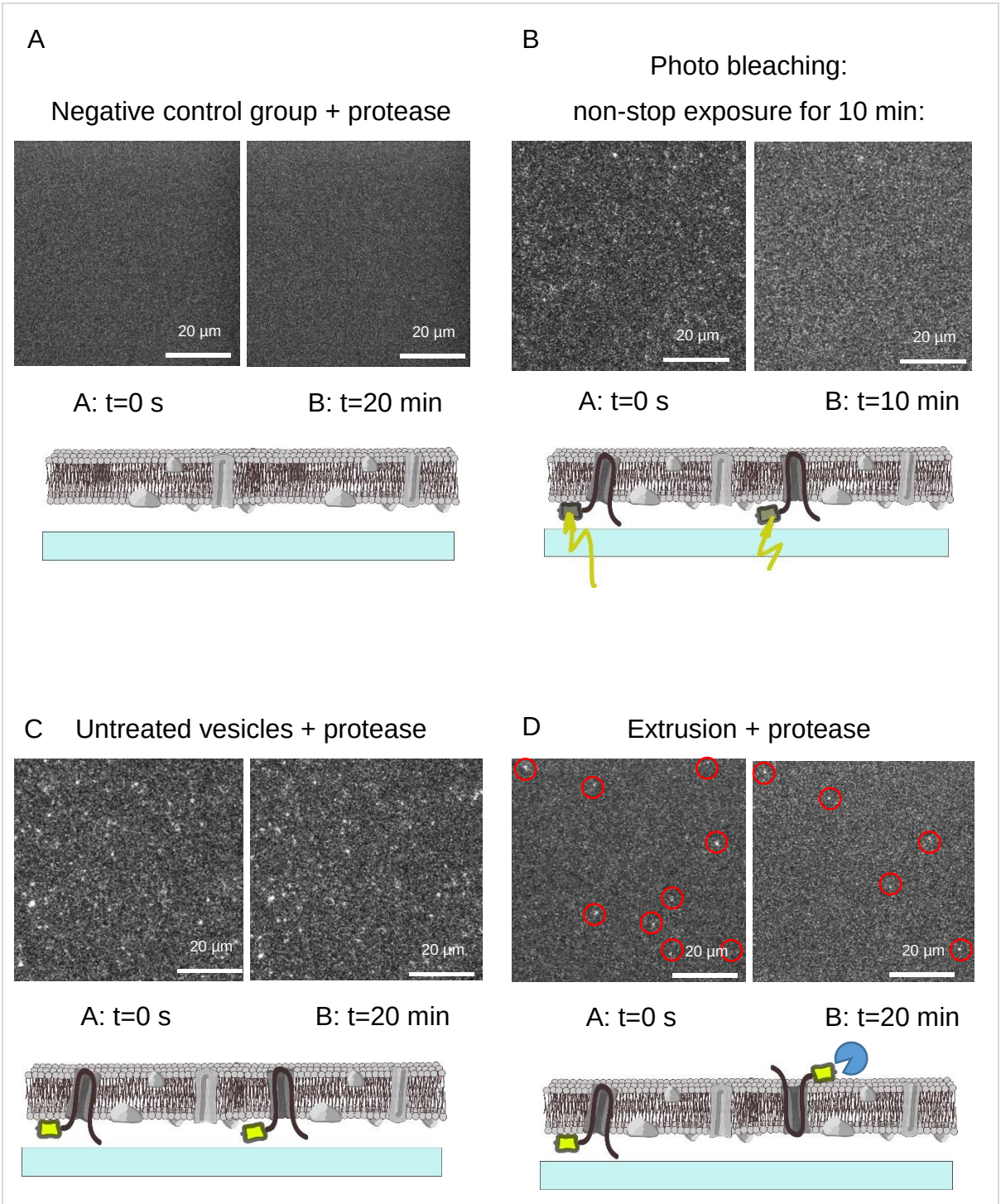

Figure 27: Confirmation of protein orientation using RCI2A: (A): Negative control group (B): Photobleaching (C): Untreated vesicles (D): Extruded vesicles. The extrusion process leads to a random rearrangement after the nylon membrane was passed. Unfortunately this step also leads to a loss in protein resulting in less particles to count for the experiment.

3.11 Single protein tracking in SLBs

After confirming bilayer formation the protein mobility in the membrane was determined by single particle tracking. The mobility of proteins is essential for a biomimetic bilayer and currently one of the major obstacles in the production of a biomimetic platform. Different approaches, from PEGylated liposomes to PEG cushions were used to address this problem. It was tried to rupture all three native PM-vesicles without the use of rupture vesicles which worked a few times for bubbles (data not shown, as not reproducible) but not for blebs and MF-vesicles. A mobile particle was defined as the movement of the molecule in an area larger than the maximum displacement of the fluorescently labeled domain. Or in other words a protein was considered mobile if the radius of movement was bigger than the size of the fluorescent protein plus link sequence. If the movement of a particle is exceeding this minimal radius the molecule was considered mobile and the mean squared displacement (MSD) was used to determine its diffusivity. Moment scaling spectrum (MSS) analysis was use to reveal the confinement of GPI-YFP and heterogeneity of the plasma membrane (Sbalzarini & Koumoutsakos 2005). Several protein qualities such as size, structure and orientation are possible explanations for the observed protein mobility, diffusivity, and confinement. For the chemically induced blebs the FA/DTT concentrations, crosslinking and aggregation of protein were thought to impact the bilayer properties but has been shown to have negligible influence at these low concentrations (Liu et al. 2018) on the SLB. Protein confinement can also result from unruptured vesicles attached to the surface which are integrated into the membrane but not mobile due to their spherical structure. For the naturally derived bubbles the broad distribution of size which has been shown to range from 100nm up to 1000nm (see Figure 10) plays an important role and makes a homogeneous rupture not as straightforward as for blebs. This is also supported by the fact that vesicles from membrane fraction isolation processes which is by its nature selective for a specific size of vesicles lead to the highest rates of mobility. The isolation of a membrane fraction is not selective for plasma membrane derived vesicles but rather a mixture of vesicles derived from Vacuole, ER and Golgi. Due to the diffusion limitations closer to the silica substrate caused by mass transport limitation it is also possible to assume a bigger fraction of smaller particles leading to a faster rupture process.

Brij® 58 (Sigma) might provide a good alternative by turning the vesicles inside out providing several advantages. First it can be used to remove soluble proteins present inside the vesicles as well as loosely attached cytoskeleton or microtubules what are still hanging on the inside of the PM-vesicles (Delphine Pflieger 2008). Second the rearrangement of the vesicle would provide a second platform showing not only the cell PM-exterior but also a model for the cell cytosolic membrane and third it would reduce the potential risk of a fluorescence domain to attach to the substrate. The fact that all proteins assessed by (Martiniere et al. 2012) are mobile in the native whole cell system including the cell wall is very promising for the cell mimetic platform. But it was also observed, that some proteins in the plant PM are easily immobilized against the cell wall even under native conditions (Martiniere et al. 2012). This might be a regulatory mechanism for plants, that proteins involved in stress response e.g. for water or salt stress are activated in their function after lowering the cell turgor during a beginning wilting reacting to these environmental conditions. After taking a look at the size distribution of the individual membrane factions it became obvious, that all these fractions contained a broad variety of vesicle diameters ranging from 100 nm up to 1 µm resulting in a different susceptibility to rupture by fusogenic liposomes. What might also influence protein mobility is the presence of so called micro domains. Our current understanding of the cell PM suggests a patchwork structure composed of different lipids and proteins that are not all freely diffusing (Li-beisson 2016). Some lipids as well as some proteins have a higher affinity towards one partner and rather arrange themselves than with any other fraction of the membrane. Self-arrangement within a micro-domain not only co-localizes multiple components but might also be involved in the regulation of that unit's activity (Hsia et al. 2015). To our surprise big differences were observed between the vesicle types. Highest diffusion coefficient was obtained with MF followed by blebs and the least mobility was achieved with bubble derived SLBs. This could be explained by the protein content varying greatly within the different fractions as well as the size distribution of the vesicle itself. With the majority of vesicles around 500 nm. I hypothesize that the size difference between PM-vesicle and fusogenic vesicles should not be more than 3x as it might lead to an unaffected native vesicle when the comparably smaller fusogenic vesicle ruptures. A major improvement of mobility was achieved by using 100 nm rupture vesicles instead of 50 nm ones. By doubling the size of the fusogenic liposomes even bigger PM-

vesicles could be ruptured. And ruptured vesicles are immediately resulting in mobile protein. When looking at the diffusion coefficient obtained by FRAP measurements and the values obtained by the SPT measurements we cannot compare them, as they are measuring a two completely different things. The FRAP diffusion coefficient is measuring the R18 dye whereas the SPT measurement is not looking at the diffusion coefficient of the fluorescently labeled proteins.

Potential improvements to increase the protein diffusion coefficient could still be applied to silica substrate in future experiments would be the immersion of leaf tissue in 25 µM Latrunculin B (Calbiochem) (60 min) (Martiniere et al. 2012) to remove the actin cytoskeleton which is probably still attached to the PM after budding off the cell. It might also help to add 20 µM Oryzalin (60 min) to remove microtubules which are also potential obstacles for the formation of a continuous SLB. Additionally incubation in 100µM filipin III (Sigma-Aldrich) (30 min) is able to disrupt sterols in the plasma membrane enabling a higher mobile fraction (Martiniere et al. 2012). None of these techniques were used in our experiments which tried to mimic the cell surface as closely as possible to the native system but could improve future experiments.

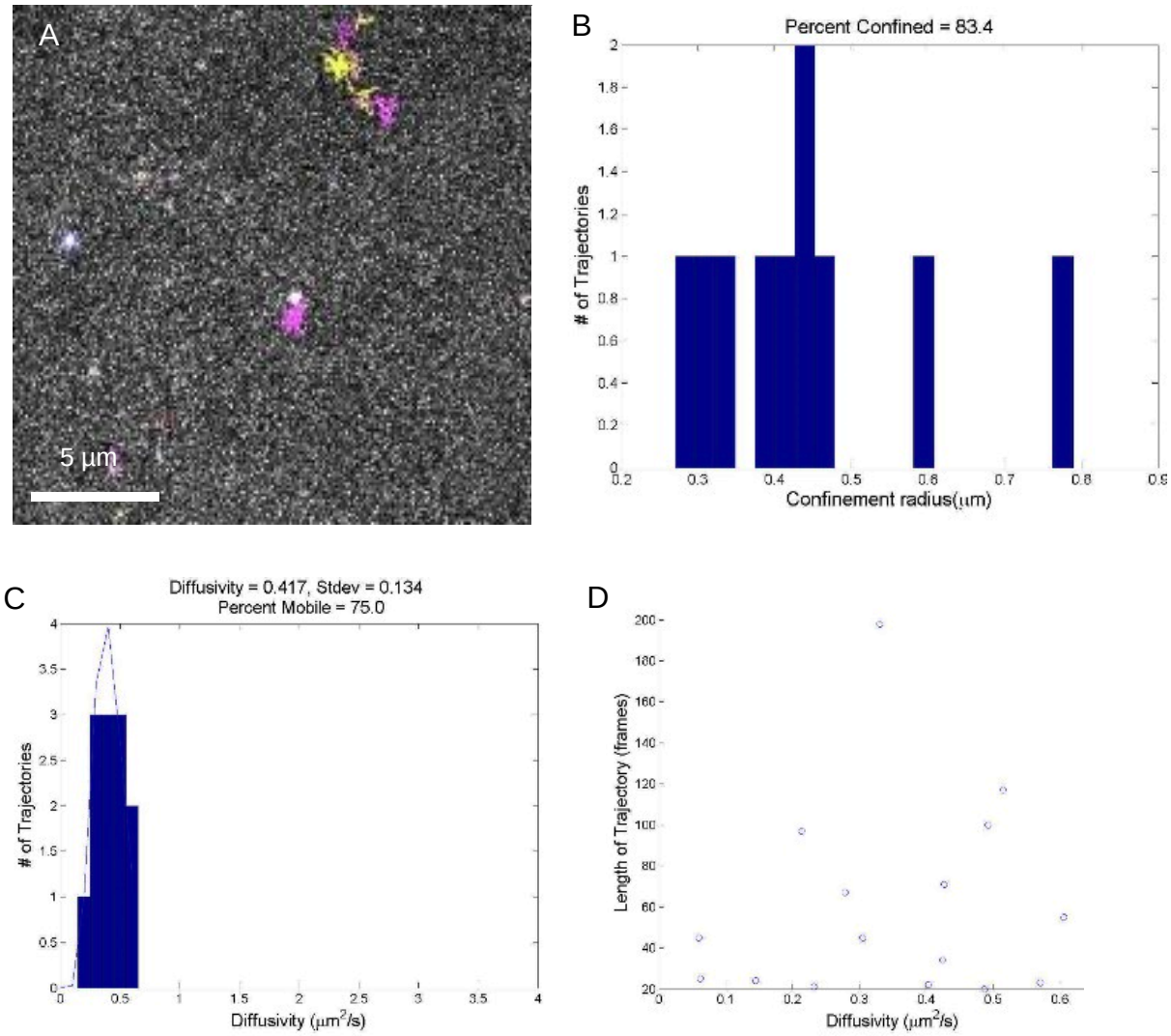

Figure 28: Single particle tracking of Pin1 stable expressed in Zea mays, produced from blebs and fusogenic vesicles. (A) Trajectories of tracked fluorescent proteins (B) Confinement radium, particles with a radius greater than 0.4 are considered mobile, this data cannot be compared to the mobility coefficient obtained by the FRAP experiments (C) The measurement of the diffusivity show 0.41 µm²/s which is in the range of the FRAP results ranging around 0.35 µm²/s for Zea mays. Mobile fraction of 75%. (D) Most diffusivity events are taking place around 0.45 µm²/s to 0.5 µm²/s (E) The particle is considered as confined if the value of parameter β is less than 0.4 µm²/s, (F) Length of the trajectory shows a broad distribution of short length trajectories over a broad diffusivity range. More than 40% of all tracks were present for more than 100 frames.

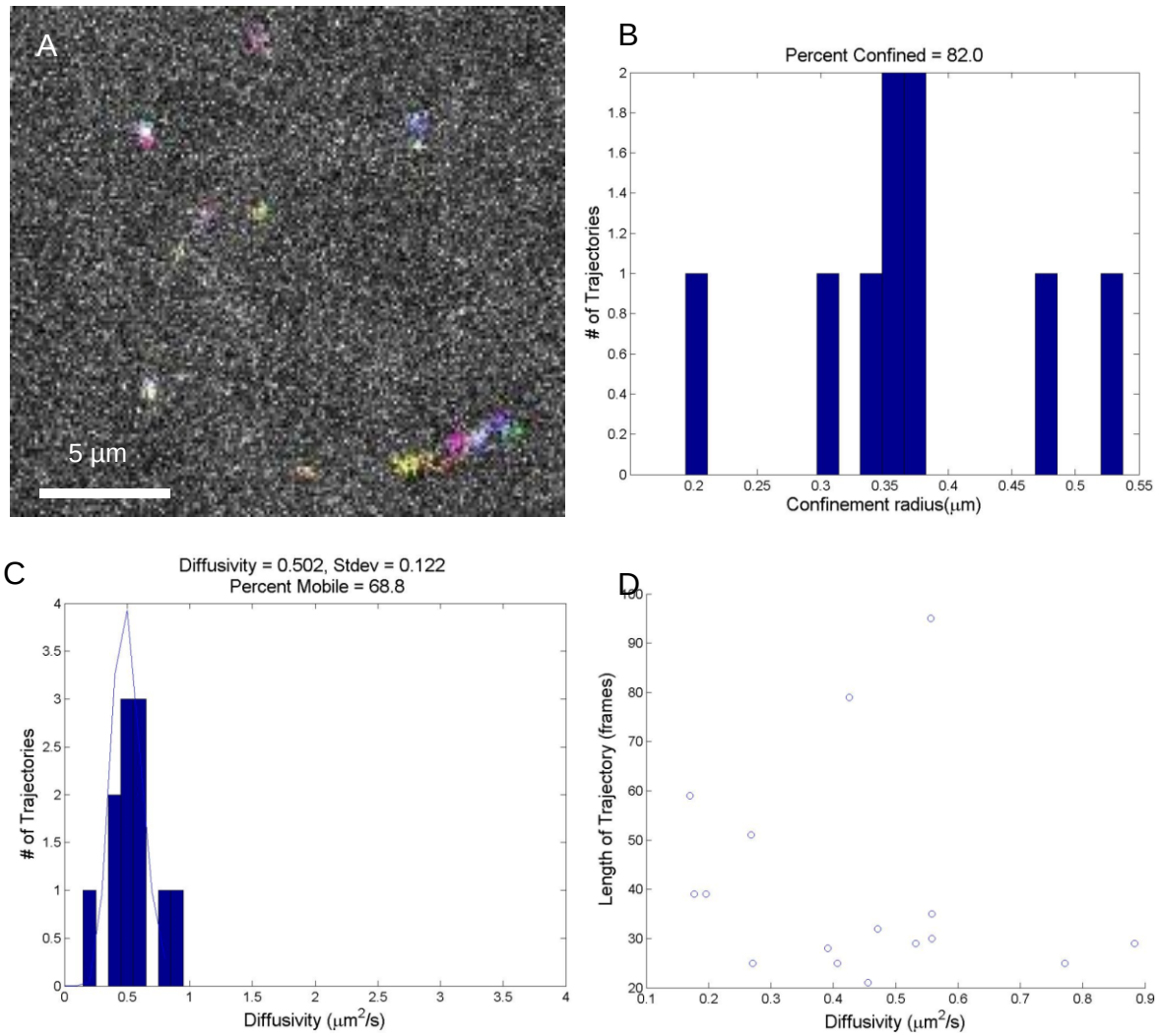

Figure 29: Single protein tracking results for SbMate transiently expressed in Nicotiana benthamiana, produced from blebs and fusogenic vesicles. (A) Trajectories of tracked fluorescent proteins, each protein trajectory was marked in a different color. (B) Confinement radium, showing a total confinement of 82% (C) The measurement of the diffusivity show 0.5 which is higher than the FRAP results ranging around 0.33 µm²/s for the average FRAP diffusivity. Mobile fraction of 68%. (D)) Length of the trajectory is comparably lower than for the Arabidopsis blebs with only one trajectory being recorded for almost 100 frames.

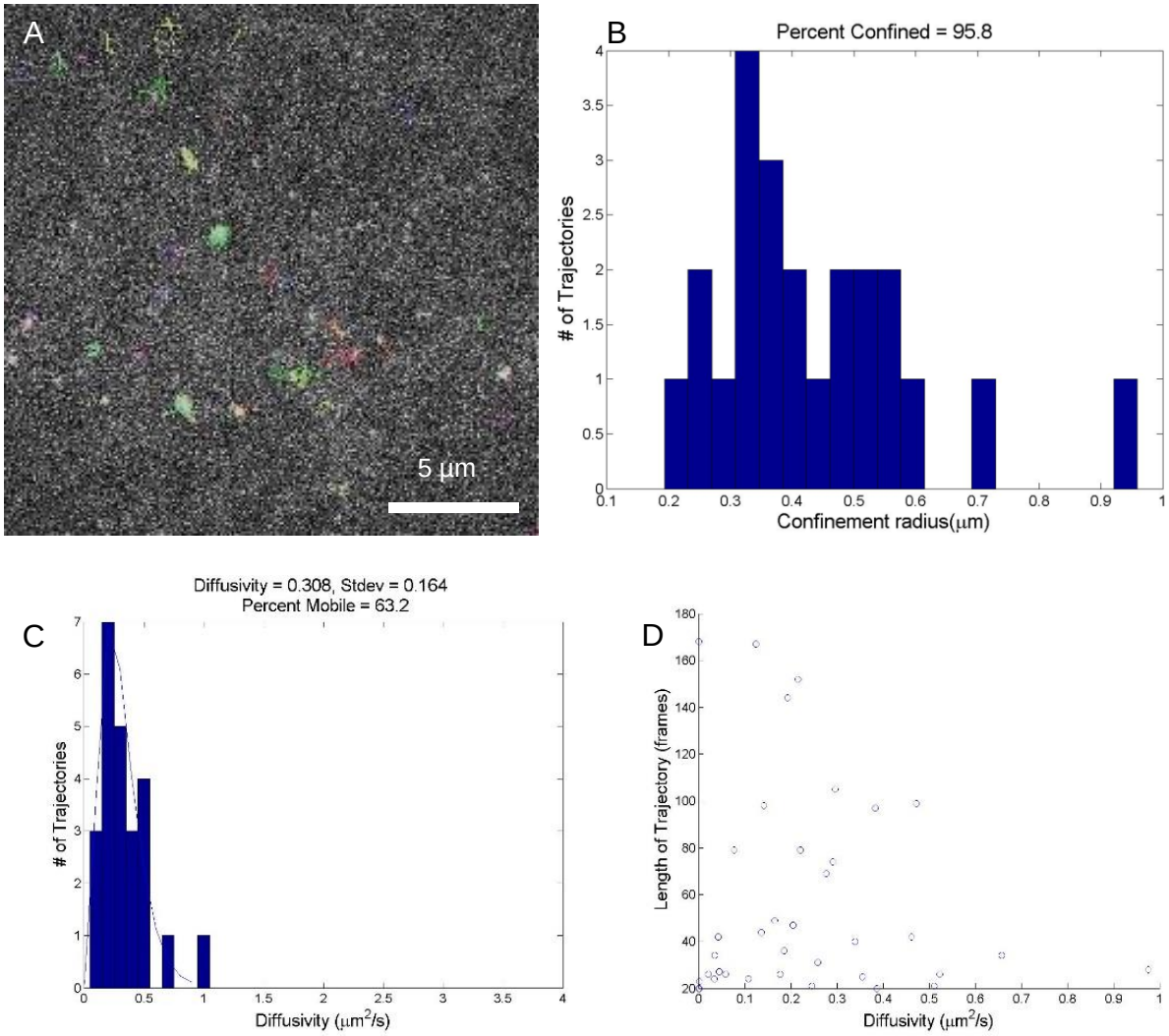

Figure 30: Single protein tracking results for RCI2A transiently expressed in Arabidopsis thaliana, produced from blebs and fusogenic vesicles. (A) Trajectories of tracked fluorescent proteins (B) Confinement radium, showing a total confinement of 95.8% (C) The measurement of the diffusivity shows 0.3 which is very close to the average diffusivity over all FRAP experiments of 0.33 µm²/s. Mobile fraction of 63%. (D) Length of the trajectory is comparably higher than for example for the Pin1 showing here more than eight recorded for more than 100 frames.

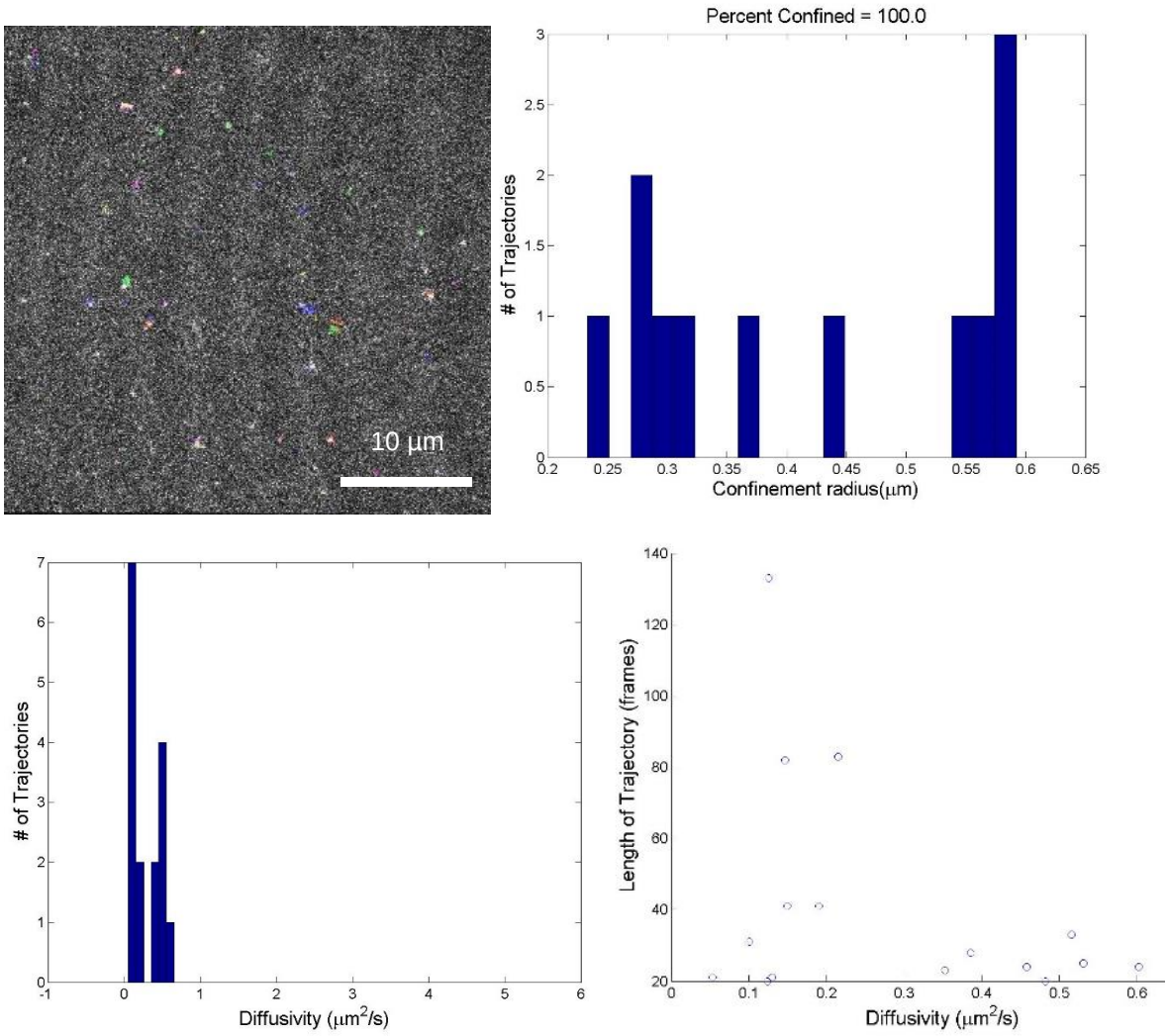

Figure 31: Single protein tracking results for RCI2A transiently expressed in Arabidopsis thaliana, produced from MF. (A) Trajectories of tracked fluorescent proteins (B) Confinement radium, showing a total confinement of 100% and the greatest confinement radius of all recorded events having more than 4 trajectories with a confinement radius greater than 0.5 µm (C) The measurement of the diffusivity shows 0.35 µm²/s which is very close to the average diffusivity over all FRAP experiments of 0.33 µm²/s. Mobile fraction of 93%. (D) Length of the trajectory is comparably smaller than for other bleb experiments with only one trajectory above 100 frames.

4 Conclusions and Implications

In summary, I have confirmed that it is possible to produce supported lipid bilayers from plant cell derived vesicles. It was possible to demonstrate this by using common monocotyledon and dicotyledonous model organisms. Three different vesicle types can be generated and used according to the experiment requirements. With each vesicle type providing certain advantages and drawbacks. Plant cell blebs generated from intact protoplasts are representing the most reliable way of vesicle production. We showed with the enzymatic cleavage, that they rupture in an inside up (parachute mode) manner in analogy with similar results reported in the literature for mammalian blebs. The osmotically induced bubbles represent a method to produce vesicles without inducing them chemically This simple approach comes with certain drawbacks such as inhomogeneous size distribution and contamination with other membrane fractions such as vacuolar and ER membrane. Despite the potential for improvement this method paves the way for various membrane characterization techniques which could not be applied to the plant PM such as various microscopy techniques confocal microscopy, TIRF microscopy) and other methods such as QCM-D, SPR and AFM to investigate physical plant plasma membrane properties. These techniques can now be applied to generate novel assays and approaches to characterize the plant plasma membrane essential for nutrient uptake, environmental sensing, pathogen interaction, and temperature and drought adaptation, which were previously not available. Although several limitations have been overcome, some remain such as protein mobility which is not as high as expected for a membrane protein of this size. Another point of improvement is protein concentration as well as high enough ratio of native vesicles to rupture vesicles. A last point to discuss would be the dilution of native PM-vesicles during the rupture process which is well known (Hsia et al. 2016) and a problem of unknown impact. The major problem is the dilution of the native PM-vesicles by the fusogenic vesicles. It is hard to quantify the amount of fusogenic vesicles that are incorporated into the SLB. As the native PM-vesicles are also composed of POPC (Angus S. Murphy, Wendy Peer 2011) the lipid ratio is shifting but no new lipid is introduced into the system.

To enumerate, the conclusions we can draw from this study are as follows:

(1) Protoplasts are behaving very similar to chemically induced blebs and are capable of producing microscale proteoliposomes after a treatment with formaldehyde and DTT.
(2) These proteoliposomes can be used to create a supported lipid bilayer with the assistance of fusogenic liposomes.
(3) This rupture method is capable of creating a cell PM mimicking platform with as the cytosolic domain of the protein down as confirmed by protein orientation assays.
(4) A new proteoliposome type the so called bubbles was found to be a byproduct of the cell wall digestion process. These proteoliposomes called bubbles are probably induced by an osmotic pressure gradient between the cytosol and the digestion buffer. They are varying in size and range from sizes half of a protoplasts down to the size of several hundred nanometers
(5) Nanometer sized structures were also obtained by membrane fraction isolation which is a suitable method to produce several hundred nanometer sized structures for the creation of supported lipid bilayers and particularly interesting when requiring an enriched protein fraction.

The findings of this thesis are applicable to the broad field of plant science. We think, that planar plant plasma membrane bilayers are a suitable platform to study membrane characteristics. This is a novel approach for all cells using blebs or bubbles and membrane fractions form Z. mays, N. tabacum and A. thaliana as an intermediate to form SLBs. This platform is intended to function as a new tool to study plant membrane properties and could be used to gain new insights into protein-protein interaction, stress tolerance, temperature adaptation, transport phenomena and host pathogen interaction on a subcellular level.

4.1 Future perspective:

This work is trying to help establish the new field of plant SLBs. A field that might open up many new options for the characterization of plant membranes. Designed as an initial attempt for this new method this work tries to lay the foundation by establishing the necessary protocols as well as characterizing this platform as far as possible. We know now, that protoplasts behave very similar to mammalian cells and produce blebs after chemical induction. But there are still many open questions, such as, how can we obtain a more uniform blebbing procedure. This question is crucial for a complete rupture as too big vesicles might not rupture at all and maintain their spherical form on the chip. We have demonstrated the formation of bubbles during the initial digestion process but there are still many open questions why bubbles have a much longer shelf life (data not shown) which can exceed blebs two-fold and reach up to three weeks at 4° C. When looking at future applications for this platform then we are ultimately confronted with the characterization of protein diffusion and protein–protein interaction of plant yield relevant proteins such as membrane transporters. Taking this idea further the colocalization of two interacting membrane proteins during transport or two membrane proteins involved in a signaling step might be a potential target. Local changes in the composition of lipid bilayers so called lipid rafts (Angus S. Murphy, Wendy Peer 2011) are involved in membrane deformation and signal transduction. The characterization of these PM lipid rafts on the other hand would benefit from the 2D planar bilayer which is conveniently accessible with state-of-the-art microscopy techniques. When applying the idea of supported lipid plant bilayers to another specific plant organelle the thylakoid membrane embedded in the chloroplast might potentially yield a photosynthetic SLB doped with functional photosynthetic centers such as photosystem 2, cytochrome b6f and photosystem 2 which would yield 4 H+ ions per successfully absorbed light photon as well as 4 H+ from photo biological water splitting. This electrochemical gradient would last as long as the ATP-synthase and other H+ driven ports and symports would be closed and could be used to generate electricity. The total efficiency of such a system would be probably less than the average 5% of a whole plant photosynthetic efficiency but could be a first attempt towards a leaf on a chip platform.

4.2 Acknowledgements

The authors would like to thank the DeLisa working group for generously providing facilities and support. I would like to thank the Jander Group at BTI for providing the PIN1 line together with the necessary facilities for upscale and protoplast isolation. As well as the Piñeros laboratory for generously providing multiple plasmids for fluorescently labeled plasma membrane proteins as well as for producing most of the raw material for protoplast transformation.
Thank you for the support and help from all the members of the Roeder working group at Cornell University for providing their facilities and plant material for all the stable expressing plant lines and Organelle marker lines.
As well as all the helpful members of the Daniel working group, first and foremost Han-Yuan Liu, Rohit Singh, Zachery Manzer, Zeinab Mohamed and Tiffany Tang.

This work was supported in part by

National Science Foundation (CAREER grant CBET-1149452);
National Science Foundation (CBET-1263701);
National Science Foundation (NSF DMR- 1719875);
Marshall Plan Scholarship (MPS Vertragsnummer: 850)
Robert F. Smith School of Chemical and Biomolecular Engineering, (tuition waver)

5 References

Abas, L. & Luschnig, C., 2010. Maximum yields of microsomal-type membranes from small amounts of plant material without requiring ultracentrifugation. *Analytical Biochemistry*, 401(2), pp.217–227. Available at: http://dx.doi.org/10.1016/j.ab.2010.02.030.

Andree, H.A.M. et al., 1992. Clustering of lipid-bound annexin V may explain its anticoagulant effect. *Journal of Biological Chemistry*, 267(25), pp.17907–17912.

Angus S. Murphy, Wendy Peer, B.S., 2011. *The Plant Plasma Membrane*, Springer.

Axelrod, D. et al., 1976. Mobility measurement by analysis of fluorescence photobleaching recovery kinetics. *Biophysical Journal*, 16(9), pp.1055–1069. Available at: http://dx.doi.org/10.1016/S0006-3495(76)85755-4.

Boss, J., 1955. Mitosis in cultures of newt tissues. III. Cleavage and chromosome movements in anaphase. *Experimental Cell Research*, 7(2), pp.443–456.

Brian, A.A. & McConnell, H.M., 1984. Allogeneic stimulation of cytotoxic T cells by supported planar membranes. *Proceedings of the National Academy of Sciences of the United States of America*, 81(19), pp.6159–63. Available at: http://www.ncbi.nlm.nih.gov/pubmed/6333027%0Ahttp://www.pubmedcentral.nih.gov/articlerender.fcgi?artid=PMC391879.

Champion-Lapalu, L. et al., 2002. Cryo-scanning electron microscopy: A new tool for interpretation of fracture studies in bitumen/polymer blends. *Energy and Fuels*, 16(1), pp.143–147.

Charras, G.T., 2008. A short history of blebbing. *Journal of Microscopy*, 231(3), pp.466–478.

Chiantia, S. et al., 2006. Combined AFM and two-focus SFCS study of raft-exhibiting

model membranes. *ChemPhysChem*, 7(11), pp.2409–2418.

Cho, N.-J. et al., 2010. Quartz crystal microbalance with dissipation monitoring of supported lipid bilayers on various substrates. *Nature Protocols*, 5(6), pp.1096–1106. Available at: http://www.nature.com/doifinder/10.1038/nprot.2010.65.

Costello, D.A. et al., 2013. Membrane fusion-competent virus-like proteoliposomes and proteinaceous supported bilayers made directly from cell plasma membranes. *Langmuir*, 29(21), pp.6409–6419.

Delmar, J.A. et al., 2015. Crystallization of membrane proteins by vapor diffusion. *Methods in Enzymology*, 557, pp.363–392.

Delphine Pflieger, J.R., 2008. *Organelle Proteomics*, Paris: Humana Press.

DePierre, J. W., Karnovsky, M.L., 1973. A Review of Methods for Their Characterization and Isolation The Hoagland Medical Library. *Journal of Cell Biology*, 56(November 1971), pp.275–303.

Diaz et al., 2008. Double Cushions Preserve Transmembrane Protein Mobility in Supported Bilayer Systems. *Langmuir*, 24(1), pp.1–23.

Dong, W.H. et al., 2011. Simple, time-saving dye staining of proteins for sodium dodecyl sulfate-polyacrylamide gel electrophoresis using coomassie blue. *PLoS ONE*, 6(8), pp.6–8.

Ekeroth, J., Konradsson, P. & Höök, F., 2002. Bivalent-ion-mediated vesicle adsorption and controlled supported phospholipid bilayer formation on molecular phosphate and sulfate layers on gold. *Langmuir*, 18(21), pp.7923–7929.

Erisman, J.W. et al., 2008. How a century of ammonia synthesis changed the world. *Nature Geoscience*, 1(10), pp.636–639.

Fackler, O.T. & Grosse, R., 2008. Cell motility through plasma membrane blebbing. *Journal of Cell Biology*, 181(6), pp.879–884.

Faulkner, C., 2013. Receptor-mediated signaling at plasmodesmata. *Frontiers in Plant Science*, 4(December), pp.1–6. Available at: http://journal.frontiersin.org/article/10.3389/fpls.2013.00521/abstract.

Ferrari, R., Manfroi, A.J. & Young, W.R., 2001. Strongly and weakly self-similar diffusion. *Physica D: Nonlinear Phenomena*, 154(1–2), pp.111–137.

Fraenkel-Conrat, H. & Olcott, H.S., 1948. The Reaction of Formaldehyde with Proteins. V. Cross-linking between Amino and Primary Amide or Guanidyl Groups. *Journal of the American Chemical Society*, 70(8), pp.2673–2684.

Fuhrmans, M. & Mueller, M., 2013. Mechanisms of vesicle spreading on surfaces: Coarse-grained simulations. *Langmuir*, 29(13), pp.4335–4349.

Fuller, J.E. & Grandjean, B.D., 2001. Economy and religion in the neolithic revolution: Material surplus and the proto-religious ethic. *Cross-Cultural Research*, 35(4), pp.370–399.

Gamper, N. & Shapiro, M.S., 2007. Regulation of ion transport proteins by membrane phosphoinositides. *Nature Reviews Neuroscience*, 8(12), pp.921–934.

Grandbois, M., Clausen-Schaumann, H. & Gaub, H., 1998. Atomic force microscope imaging of phospholipid bilayer degradation by phospholipase A2. *Biophysical journal*, 74(5), pp.2398–2404. Available at: http://dx.doi.org/10.1016/S0006-3495(98)77948-2.

Harlan, J.R., 1971. Agricultural origins: centres and noncenters. *Science*, 174(4008), pp.468–474.

Helenius, A.R.I. & Simons, K.A.I., 1975. BY DETERGENTS membrane structure and function it is usually necessary to dissociate the membrane into its components . The techniques for extraction and analysis of the membrane lipids are well worked out , and are mainly based on the use of organic solve. , 415, pp.29–79.

Henriques, R. & Mhlanga, M.M., 2009. PALM and STORM: What hides beyond the Rayleigh limit? *Biotechnology Journal*, 4(6), pp.846–857.

Hoekenga, O.A. et al., 2006. AtALMT1, which encodes a malate transporter, is identified as one of several genes critical for aluminum tolerance in Arabidopsis. *Proceedings of the National Academy of Sciences*, 103(25), pp.9738–9743. Available at: http://www.pnas.org/cgi/doi/10.1073/pnas.0602868103.

Hopwood, D., 1969. A comparison of the crosslinking abilities of glutaraldehyde, formaldehyde and ??-hydroxyadipaldehyde with bovine serum albumin and casein. *Histochemie*, 17(2), pp.151–161.

Hsia, C.-Y., Richards, M.J. & Daniel, S., 2015. A review of traditional and emerging methods to characterize lipid–protein interactions in biological membranes. *Anal. Methods*, 7(17), pp.7076–7094. Available at: http://xlink.rsc.org/?DOI=C5AY00599J.

Hsia, C.Y. et al., 2016. A Molecularly Complete Planar Bacterial Outer Membrane Platform. *Scientific Reports*, 6(August), pp.1–14. Available at: http://dx.doi.org/10.1038/srep32715.

Hsu, H.L. et al., 2016. Viral fusion efficacy of specific H3N2 influenza virus reassortant combinations at single-particle level. *Scientific Reports*, 6(October), pp.1–12.

Jones, A.D. & Ejeta, G., 2016. A new global agenda for nutrition and health: the importance of agriculture and food systems. *Bulletin World Health Organization*, 94(December 2015), pp.228–229.

Kankare, J., 2002. Sauerbrey equation of quartz crystal microbalance in liquid medium. *Langmuir*, 18(18), pp.7092–7094.

Kellner, R.R. et al., 2007. Nanoscale organization of nicotinic acetylcholine receptors revealed by stimulated emission depletion microscopy. *Neuroscience*, 144(1),

pp.135–143.

Komatsu, S., Konishi, H. & Hashimoto, M., 2007. The proteomics of plant cell membranes. *Journal of Experimental Botany*, 58(1), pp.103–112.

Koppel, D.E. et al., 1976. Dynamics of fluorescence marker CONCENTRATION AS A PROBE OF MOBILITY. *Biophysical Journal*, 16, pp.1315–1329.

Kusumi, A. et al., 2005. Single-molecule tracking of membrane molecules: Plasma membrane compartmentalization and dynamic assembly of raft-philic signaling molecules. *Seminars in Immunology*, 17(1), pp.3–21.

Kusumi, A., Sako, Y. & Yamamoto, M., 1993. Confined Lateral Diffusion of Membrane-Receptors as Studied by Single-Particle Tracking (Nanovid Microscopy) - Effects of Calcium-Induced Differentiation in Cultured Epithelial-Cells. *Biophysical Journal*, 65(5), pp.2021–2040.

Lee, A.G., 2004. How lipids affect the activities of integral membrane proteins. *Biochimica et Biophysica Acta - Biomembranes*, 1666(1–2), pp.62–87.

Levental, I. et al., 2010. Palmitoylation regulates raft affinity for the majority of integral raft proteins. *Proceedings of the National Academy of Sciences*, 107(51), pp.22050–22054. Available at: http://www.pnas.org/cgi/doi/10.1073/pnas.1016184107.

Leyser, O., 2017. Auxin Signaling. *Plant Physiology*, 176(January), p.pp.00765.2017. Available at: http://www.plantphysiol.org/lookup/doi/10.1104/pp.17.00765.

Li-beisson, Y.N.Y., 2016. *Lipids in Plant and Algae Development*, Available at: http://link.springer.com/10.1007/978-3-319-25979-6.

Li, L., Zhang, Q. & Huang, D., 2014. A review of imaging techniques for plant phenotyping. *Sensors (Switzerland)*, 14(11), pp.20078–20111.

Ligaba, A. et al., 2013. Functional, structural and phylogenetic analysis of domains

underlying the Al sensitivity of the aluminum-activated malate/anion transporter, TaALMT1. *Plant Journal*, 76(5), pp.766–780.

Liu, H.Y. et al., 2018. Biologically Complex Planar Cell Plasma Membranes Supported on Polyelectrolyte Cushions Enhance Transmembrane Protein Mobility and Retain Native Orientation. *Langmuir*, 34(3), pp.1061–1072.

Liu, H.Y. et al., 2017. Supported Planar Mammalian Membranes as Models of in Vivo Cell Surface Architectures. *ACS Applied Materials and Interfaces*, 9(41), pp.35526–35538.

Májek, P. et al., 2013. Improved coomassie blue dye-based fast staining protocol for proteins separated by SDS-PAGE. *PLoS ONE*, 8(11), pp.2–7.

Martiniere, A. et al., 2012. Cell wall constrains lateral diffusion of plant plasma-membrane proteins. *Proceedings of the National Academy of Sciences*, 109(31), pp.12805–12810. Available at: http://www.pnas.org/cgi/doi/10.1073/pnas.1202040109.

McConnell, H.M. et al., 1986. Supported planar membranes in studies of cell-cell recognition in the immune system. *BBA - Reviews on Biomembranes*, 864(1), pp.95–106.

Melnik, S. et al., 2018. Cloning and plant-based production of antibody MC10E7 for a lateral flow immunoassay to detect [4-arginine]microcystin in freshwater. *Plant Biotechnology Journal*, 16(1), pp.27–38.

Mengel, K. & Kirkby, 2001. *Principles of plant nutrition. 5th edn.*, Available at: http://aob.oxfordjournals.org/content/93/4/479.full.pdf+html.

Milhiet, P.E. et al., 2002. Spontaneous insertion and partitioning of alkaline phosphatase into model lipid rafts. *EMBO Reports*, 3(5), pp.485–490.

Mueller, V. et al., 2011. STED nanoscopy reveals molecular details of cholesterol- and

cytoskeleton-modulated lipid interactions in living cells. *Biophysical Journal*, 101(7), pp.1651–1660. Available at: http://dx.doi.org/10.1016/j.bpj.2011.09.006.

Owen, D.M. et al., 2010. PALM imaging and cluster analysis of protein heterogeneity at the cell surface. *Journal of Biophotonics*, 3(7), pp.446–454.

Parker, J.L. & Newstead, S., 2016. The Next Generation in Membrane Protein Structure Determination. , 922, pp.61–72. Available at: http://link.springer.com/10.1007/978-3-319-35072-1.

Rajendran, L., 2005. Lipid rafts and membrane dynamics. *Journal of Cell Science*, 118(6), pp.1099–1102. Available at: http://jcs.biologists.org/cgi/doi/10.1242/jcs.01681.

Reimhult, E., Höök, F. & Kasemo, B., 2003. Intact vesicle adsorption and supported biomembrane formation from vesicles in solution: Influence of surface chemistry, vesicle size, temperature, and osmotic pressure. *Langmuir*, 19(5), pp.1681–1691.

Reimhult, E., Höök, F. & Kasemo, B., 2002. Temperature dependence of formation of a supported phospholipid bilayer from vesicles on [formula presented]. *Physical Review E - Statistical Physics, Plasmas, Fluids, and Related Interdisciplinary Topics*, 66(5), p.4.

Reimhult, E., Höök, F. & Kasemo, B., 2002. Vesicle adsorption on SiO2and TiO2: Dependence on vesicle size. *Journal of Chemical Physics*, 117(16), pp.7401–7404.

Reimhult, E., Kasemo, B. & Höök, F., 2009. Rupture pathway of phosphatidylcholine liposomes on silicon dioxide. *International Journal of Molecular Sciences*, 10(4), pp.1683–1696.

Richards, M.J. et al., 2016. Membrane Protein Mobility and Orientation Preserved in Supported Bilayers Created Directlfile:///C:/Users/marti/Downloads/Chao &

Daniel JACS 2011.pdfy from Cell Plasma Membrane Blebs. *Langmuir*, 32(12), pp.2963–2974.

Richter, A. et al., 2016. Characterization of Biosynthetic Pathways for the Production of the Volatile Homoterpenes DMNT and TMTT in *Zea mays*. *The Plant Cell*, 28(10), pp.2651–2665. Available at: http://www.plantcell.org/lookup/doi/10.1105/tpc.15.00919.

Richter, R.P., Him, J.L.K. & Brisson, A., 2003. Supported lipid membranes. *Materials Today*, 6(11), pp.32–37.

Sbalzarini, I.F. & Koumoutsakos, P., 2005. Feature point tracking and trajectory analysis for video imaging in cell biology. *Journal of Structural Biology*, 151(2), pp.182–195.

Scholthof, K.B.G. et al., 2011. Top 10 plant viruses in molecular plant pathology. *Molecular Plant Pathology*, 12(9), pp.938–954.

Seddon, A.M., Curnow, P. & Booth, P.J., 2004. Membrane proteins, lipids and detergents: Not just a soap opera. *Biochimica et Biophysica Acta - Biomembranes*, 1666(1–2), pp.105–117.

Sezgin, E. et al., 2012. Elucidating membrane structure and protein behavior using giant plasma membrane vesicles. *Nature Protocols*, 7(6), pp.1042–1051. Available at: http://www.nature.com/doifinder/10.1038/nprot.2012.059.

Silin, V.I. et al., 2002. The role of surface free energy on the formation of hybrid bilayer membranes. *Journal of the American Chemical Society*, 124(49), pp.14676–14683. Available at: http://www.ncbi.nlm.nih.gov/pubmed/12465979.

Simons, K. & Toomre, D., 2000. Lipid rafts and signal transduction. *Nature Reviews Molecular Cell Biology*, 1(1), pp.31–39.

Smil, V., 1999. Detonator of the population explosion. *Nature*, 400(6743), p.415.

Smith, M.B. et al., 2011. Interactive, computer-assisted tracking of speckle trajectories in fluorescence microscopy: Application to actin polymerization and membrane fusion. *Biophysical Journal*, 101(7), pp.1794–1804. Available at: http://dx.doi.org/10.1016/j.bpj.2011.09.007.

Smith, P.R. et al., 1999. Anomalous Diffusion of Major Histocompatibility Complex Class I Molecules on HeLa Cells Determined by Single Particle Tracking. , 76(June).

Sonnleitner, A., Schütz, G.J. & Schmidt, T., 1999. Free Brownian motion of individual lipid molecules in biomembranes. *Biophysical Journal*, 77(5), pp.2638–2642.

Soumpasis, D.M., 1983. Theoretical analysis of fluorescence photobleaching recovery experiments. *Biophysical Journal*, 41(1), pp.95–97. Available at: http://dx.doi.org/10.1016/S0006-3495(83)84410-5.

Steinem, C. et al., 1996. Impedance analysis of supported lipid biayer membranes: a scrutiny of different preparation techniques. *Biochimica et Biophysica Acta*, 1279(2), pp.169–180.

Storrie, B. & Madden, A., 1990. Isolation of Subcellular Organelles By. *Methods Enzymol*, 182(1987), pp.203–225.

Svizzero, S. & Tisdell, C.A., 2014. The neolithic revolution and human societies: Diverse origins and development paths. *Economics, ecology and the environment working paper*, no. 192(192), p.38 TS-WorldCat. Available at: d:%5CPromotion%5CCitavi%5CSicker Women at the Dawn of Agriculture%5CCitaviFiles%5CSvizzero and Tisdell 2014 - The Neolithic Revolution and Human Societies. Diverse Origins and development paths.pdf.

Terrettaz, S. et al., 1993. Protain Binding to Supported Lipid membranes: Investigation of the Cholera Toxin-Ganglioside Interaction by Simulataneous Impedance

Spectroscopy and Surface Plasmon Resonance. *Langmuir*, 9(6), p.1361.

Thompson, M. V. & Wolniak, S.M., 2008. A Plasma Membrane-Anchored Fluorescent Protein Fusion Illuminates Sieve Element Plasma Membranes in Arabidopsis and Tobacco. *Plant Physiology*, 146(4), pp.1599–1610. Available at: http://www.plantphysiol.org/cgi/doi/10.1104/pp.107.113274.

Tilman, D., 1998. The greening of the green revolution. *Nature*, 396(6708), pp.211–212.

Waadt, R. & Kudla, J., 2008. In plant visualization of protein interactions using bimolecular fluorescence complementation (BiFC). *Cold Spring Harbor Protocols*, 3(4).

Wang, L. & Tonggu, L., 2015. Membrane protein reconstitution for functional and structural studies. *Science China Life Sciences*, 58(1), pp.66–74. Available at: http://link.springer.com/10.1007/s11427-014-4769-0.

Watts, T.H., Gaub, H.E. & Mcconnell, H.M., 1986. T-cell-mediated association of peptide antigen and major histocompatibility complex protein detected by energy transfer in an evanescent wave-field. *Nature*, 320(6058), pp.179–181.

Whitfield, A.E., Ullman, D.E. & German, T.L., 2005. Tospovirus-Thrips Interactions. *Annual Review of Phytopathology*, 43(1), pp.459–489. Available at: http://www.annualreviews.org/doi/10.1146/annurev.phyto.43.040204.140017.

Wu, J. et al., 2013. High-efficiency localization of Na+-K+ATPases on the cytoplasmic side by direct stochastic optical reconstruction microscopy. *Nanoscale*, 5(23), pp.11582–11586.

Yip, C.M., Darabie, A.A. & McLaurin, J.A., 2002. Aβ42-peptide assembly on lipid bilayers. *Journal of Molecular Biology*, 318(1), pp.97–107.

Yoo, S.D., Cho, Y.H. & Sheen, J., 2007. Arabidopsis mesophyll protoplasts: A versatile

cell system for transient gene expression analysis. *Nature Protocols*, 2(7), pp.1565–1572.

Zhang, Y., Zhang, C. & Li, W., 2012. The nucleocapsid protein of an enveloped plant virus, Tomato spotted wilt virus, facilitates long-distance movement of Tobacco mosaic virus hybrids. *Virus Research*, 163(1), pp.246–253.

6 APPENDIX A: LIST OF ACRONYMS

PM	Plasma membrane
SLB	Supported lipid bilayer
CW	Cell wall
ER	Endoplasmatic reticulum
MF	Membrane Fraction
FA	Formaldehyde
TIRF	Total internal reflection microscopy
FRAP	Fluorescent recovery after photo-bleaching
M.F.	Mobile fraction
DTT	1,4-Dithiothreitol
EDTA	Ethylenediaminetetraacetic
RuBisCo	Ribulose-1,5-bisphosphate carboxylase/oxygenase
QCM-D	Quartz crystal Microbalance with Dissipation
TSWV	Tomato spotted wilt virus
CHO	Chinese Hamster ovary
AA	Amino Acid
AFM	Atomic force microscope
SPR	Surface plasmon resonance
PALM	Phtoactivation localization microscopy
STORM	Stochastic optical reconstruction microscopy
R18	rhodamine dye Octadecyl Rhodamine B Chloride
Δf	Change in frequency
ΔD	Change in dissipation
PEG	polyethylene-glycol
POPC	1-oleoyl-2-palmitoyl-sn-glycero-3-phosphocholine
POPC-PEG-5000	1-oleoyl-2-palmitoyl-sn-glycero-3-phosphocholine-polyethylene glycol
SPT	Single protein tracking
MSS	moment scaling spectrum
MSD	mean squared displacement
SSA	Sub-Saharan-Africa

7 List of figures

Figure 1: (A) plant cell with CW showing the membrane of interest in false color yellow and the chloroplasts in green. The ducts interconnecting all cytoplasts are shown in yellow. There are several thousand such ducts interconnecting all individual cells. (B) Healthy chloroplast after cell wall digestion and closing of the plasmodesmata. Depicted right after the digestion and before the centrifugation step the chloroplasts are moved to one side due to centrifugal forces after the centrifugation. .....- 7 -
Figure 2: Native plant lipid bilayer including membrnae proteins, transmembrnae proteins, spingolipids, sterolipids, cholesterol shielding their hydrophobic parts in the inside of the about 4 nm thick lipid doublelayer. .....- 11 -
Figure 3: Cell PM mimicking models .....- 13 -
Figure 4: Production of PM-vesicles: (A) plant material, (B) Cross section of an undigested leaf, (C) Extraction of a MF from the whole leaf material, (D) Cross section of the leaf material after digestion with enzymes, ((E) plant cell during the digestion process, partially digested CW with emanating cytosol after the plasmodesmata channels have been closed, (F) Bubble after cytosolic budding, (G) Final healthy protoplast only encapsulated by the PM, (H) protoplast during blebbing and vesicle budding, (I) Plant PM-bleb......- 18 -
Figure 5: (A) Vesicle derived from the plant PM with native lipid and protein ratio and orientation. (B) Fusogenic vesicle equippe dwith PEG-5000 in a molar ratio of 0,5%. (C) SLB after rupture and spred out, leaving most of the proteins sitting on the glass substrate. (D) SLB with included PEG-5000 brushes fused with the bilayer during the rupture process and supporting the SLB at a hight of about 5 nm above the glass substrate. .....- 19 -
Figure 6: Overview rupture process of plant PM-vesicles. (A) Attached PM-vesicles on silica substrate in GPMV buffer. (B) Autorupture of the fusogenic vesicles triggering the rupture of PM-vesicles (C) Fully ruptured SLB after about 30 min. .....- 56 -
Figure 7: Material preparation for protoplast digestion: (A) Middle section is used for the digestion. Leaf tip and base are removed from the whole plant, (B) Plant material removed from the leafs and the cut leaf stripes of about 1 mm, (C) Leaf material in digestion buffer after the application of the vacuum when the leaf stripes appear darker, (D) Protoplast after the first washing step and spin down. .....- 34 -
Figure 8: Protoplasts: (A) Arabidopsis thaliana protoplasts after the second washing step. Visible in the upper right corner are free Chloroplasts which are removed after the washing steps, (B), N. benthamiana protoplasts after the first washing step. Visible is already the clear shift of chloroplasts to one side by the centrifugal forces (C) Zea mays protoplasts after the second washing step. Compared to unwashed protoplasts the size distribution is much more homogeneous and all protoplasts with a higher or lower relative density are removed. The relative density is predominantly determined by the chloroplast content. One reason why the Zea Mays plants yielded more protoplasts after two days in the dark prior to the digestion process, which leads to a degradation of excessive chloroplasts......- 35 -
Figure 9: Zeta potential of all the plants and all vesicle types: The data was obtained from more than 30 individual measurements from six independent isolation experiment shows the zeta potential (ZP) for three plants and three different types of vesicles. The

surface charge density is similar for all three plants with no significant difference between bubbles and blebs ranging from -10 mV to -5 mV. And a significantly higher charge for the MF around -20 mV. These results indicate that the origin of plant material has less influence on the zeta potential than the method of production. Impact on the surface charge density by the blebbing buffer and the associated chemicals seems to influence on the charge of the particles raising the average ZP between 25% for A. thaliana and 50% for N. benthamiana...... - 39 -
Figure 10: Particle size distribution: The size distribution obtained from more than 30 individual measurements from six independent isolation experiment shows the vesicle size distribution for three plants. Differences for vesicle types between the plant species are not significant. As the 95% quantile whiskers indicate, there is no significant difference between the individual vesicles with blebs (average 500 nm) as the smallest fraction. Bubbles (average 750 nm) as the second smallest fraction but a much higher dispersity grade which can be explained by the uncontrolled inflation during the osmotically driven production of vesicles. Membrane fraction (average 1000 nm) was produced the biggest vesicles with the highest heterogeneity. ..... - 39 -
*Figure 11: Particle concentration: The concentrations of PM-vesicles isolated from blebs and bubbles was constantly around 5*10^7 vesicles/ml. Due to the ultracentrifugation concentration step the particle concentration was considerably higher for the MF. Blank experiments showed a buffer concentration of 2* 10^5 for the GPMV buffer. Particle concentration for blebs was significantly lower from blebs for mammalian cells 1*10^9 (Liu et al. 2017) which was only achieved for plant vesicles with a MF isolation.:*..... - 40 -
Figure 12: Particle size distribution over time: (A) The fresh bleb sample showed three peaks at 10nm, 200nm and 800nm. The smallest peak bight be cell debris which couldn't be cleared from the buffer due to its relative density. The other two peaks are probably cell blebs, it couldn't be clarified if both peaks are cell blebs. Over time the article distribution shifts towards a medium fraction around 400 nm and a big fraction of around 8000 nm which might be explained by auto vesicle fusion. (B) To evaluate the accuracy of the dynamic light scattering measurements of the Zetasizer the fusogenic liposomes extruded with a 100 nm nylon membrane were measured and showed the expected Gaussian distribution profile around 100nm. ..... - 41 -
Figure 13: SEM images of spherical objects addressed in the following as bubbles: (A) Bubbles images in a natural crack next to a Chloroplast. The majority of spherical objects seems to be around 200nm to 400nm. (B) Bubbles on the cell surface next to holes where they might have been produced (C) Bubbles imaged here show a slightly deformed structure which could be explained by the cryo conservation process. - 42 -
Figure 14 Cryo SEM images of spherical objects addressed in the following as blebs: (A) Four blebs of about 400 nm diameter next to each other monitored in a crack, (B) Blebs on the surface of the cryo sample, (C) Blebs imaged in a crack where they seem to peel out of the fractionated sample. ..... - 43 -
Figure 15: Cryo SEM images of whole plant cells during digestion: (A) Two semi digested parenchyma cell walls bordering each other with the lumen already released, next there is an intact spherical chloroplast. This picture was taken 30 min post digestion start. (B) Detail of the secondary cell wall with clearly visible plasmodesmata channels. The CW is already empty as there is no protoplast inside the cell. (C) Detail of the plasmodesmata tubes connecting the individual plant cells. ..... - 42 -
Figure 16: Characterization of RCI2A protein from Arabidopsis thaliana: (A) The RCI2A::YFP (~34 kDa) construct stably expressed in Arabidopsis showing a homogeneous and very strong expression all over the PM. (B) Detail of the CW shows

a clear separation of the two PM's and indicates that the construct doesn't get secreted into the apoplastic space and is detached from the PM. (C) Negative control (D) Coomassie staining showing a band at around 34 kDa which is the molecular weight of RCI2A......- 44 -
Figure 17: Characterization of SbMate protein from Arabidopsis thaliana: (A) The SbMate::GFP (~55 kDa) construct transiently expressed in Nicotiana benthamiana protoplasts (B) strong expression of SbMate after the protoplast digestion visible around the PM (C) Negative control with an untransformed protoplasts. (D) Coomassie staining showing a band at around 55 kDa which is the molecular weight of SbMate. - 44 -
Figure 18: Characterization of Pin1 protein in Zea mays: (A) The Pin1::YFP (~18 kDa) construct stable expressed in Zea mays (B) strong expression of Pin1::YFP in the leaf tissue (C) Closer look at the abaxial side of the Zea mays leaf (D) Coomassie staining showing a band at around 18 kDa which is the molecular weight of Pin1::YFP. ..- 45 -
Figure 19: QCM profile of Nicotiana benthamiana blebs: (A) <depiction of QCM workflow (I) flow in on PM-vesicles, (II) Injection of rupture vesicles (III) Auto rupture of fusogenic vesicles, (IV) Self assembles SLB, (B) Change in the third frequency overtone (C) Calculated mass deposition on the quartz sensor, as the upshift is only 50 ng from deposition to final rupture the blebs might have been ruptured or not, but when looking at the dissipation a clear tendency towards successful rupture is shown (D) Dissipation profile during the rupture process shows an upshift in ΔD from the firs deposition of PM-vesicles to the final dissipation indicating a successfully formed bilayer......- 46 -
Figure 20: QCM profile of: QCM profile of Nicotiana benthamiana blebs: (A) Depiction of QCM workflow (I) flow in on PM-vesicles, (II) Injection of fusogenic vesicles (III) Auto rupture of fusogenic vesicles, (IV) Self assembled SLB, (B) Change in the third frequency overtone indicating a mass deposition (C) Calculated mass deposition on the quartz sensor, as the upshift is about 400 ng less than the pure vesicles themselves. This downshift in mass can be explained by the release of water from the vesicles into the buffer. When looking at the dissipation a clear tendency towards successful rupture is shown (D) Dissipation profile during the rupture process shows a slightly higher upshift than for the blebs. This indicates, that something has bound to the sensor and then become more compact probably due to the release of water. - 47 -
Figure 21: Summarized changes in frequency and dissipation: (A) toal changes in frequency of (N=6) experiments, (B) Total change in dissipation (N=6) indicating that bubbles lead to a bigger mass deposition than blebs......- 48 -
Figure 22: Rupture process induced by fusogenic vesicles at bubbles from three different plants. Blebs and MF ruptured identical and was put into the supplemental Appendix A: (A) Simplified rupture comic, (B) Rupture and dequenching of Arabidopsis bubbles, (C) Rupture and dequenching of Nicotiana benthamiana bubbles, (D) Rupture and dequenching of Zea mays bubbles......- 50 -
Figure 23: FRAP profie of bubbles, blebs and MF: (A) Bubbles, Arabidopsis thaliana, (I) raw data and soumpasis fit to calculate the diffusivity, (II) Area of interest (AOI) with the scratch mark in the corner, (III) cross section of the recovery profile to demonstrate recovery due to mobility and not by photo bleaching, (IV) Close up of the frap spot at time zero, (V) Close up of the FRAP spot after 30 seconds, (VI) Close up of the FRAP spot after 2000s showing a complete reovery (B) Blebs, Arabidopsis thaliana (C) MF, Arabidopsis thaliana.....- 52 -

Figure 24: FRAP profile of bubbles, blebs and MF: (A) Bubbles, Nicotiana Benthamiana, (I) raw data and Soumpasis fit to calculate the diffusivity, (II) Area of interest (AOI) with the scratch mark in the corner, (III) cross section of the recovery profile to demonstrate recovery due to mobility and not by photo bleaching, (IV) Close up of the frap spot at time zero, (V) Close up of the FRAP spot after 30 seconds, (VI) Close up of the FRAP spot after 2000s showing a complete recovery (B) Blebs, Nicotiana Benthamiana (C) MF, Nicotiana Benthamiana. .....- 53 -
Figure 25: FRAP profile of bubbles, blebs and MF of Zea mays: (A) Bubbles, Zea mays, (I) raw data and Soumpasis fit to calculate the diffusivity, (II) Area of interest (AOI) with the scratch mark in the corner, (III) cross section of the recovery profile to demonstrate recovery due to mobility and not by photo bleaching, (IV) Close up of the frap spot at time zero, (V) Close up of the FRAP spot after 30 seconds, (VI) Close up of the FRAP spot after 2000s showing a complete recovery (B) Blebs, Zea mays (C) MF, Zea mays. .....- 54 -
Figure 26: Summary of Diffusivity and Mobile fraction of all FRAP experiments (N=30): (A) Total diffusivity ranges around 0.3 for all three fractions with a broader distribution for the blebs and MF (B) Summarized MF for all three fractions showing an average mobile fraction between 90% and 95%. The best recovery was obtained using the MF. .....- 55 -
Figure 27: Confirmation of protein orientation using RCI2A: (A): Negative control group (B): Photobleaching (C): Untreated vesicles (D): Extruded vesicles. The extrusion process leads to a random rearrangement after the nylon membrane was passed. Unfortunately this step also leads to a loss in protein resulting in less particles to count for the experiment. .....- 59 -

8 List of tables

Table 1: Osmotic conditions for protoplast and bubble generation.....- 24 -
Table 2: Digestion buffer .....- 25 -
Table 3: Blebbing buffer .....- 25 -
Table 4: Membrane fraction extraction buffer.....- 26 -